

A. BÖNCÜ

STRUCTURAL FIRE SAFETY  
OF  
STANDARD CIRCULAR RAILROAD TUNNELS  
UNDER DIFFERENT SOIL CONDITIONS

ALTAN BÖNCÜ

METU  
2008

MAY 2008

STRUCTURAL FIRE SAFETY  
OF  
STANDARD CIRCULAR RAILROAD TUNNELS  
UNDER DIFFERENT SOIL CONDITIONS

A THESIS SUBMITTED TO  
THE GRADUATE SCHOOL OF NATURAL AND APPLIED SCIENCES  
OF  
MIDDLE EAST TECHNICAL UNIVERSITY

BY

ALTAN BÖNCÜ

IN PARTIAL FULFILLMENT OF THE REQUIREMENTS  
FOR  
THE DEGREE OF MASTER OF SCIENCE  
IN  
CIVIL ENGINEERING

MAY 2008

Approval of the Thesis

**“STRUCTURAL FIRE SAFETY OF STANDARD CIRCULAR RAILROAD  
TUNNELS UNDER DIFFERENT SOIL CONDITIONS”**

Submitted by **ALTAN BÖNCÜ** in partial fulfillment of the requirements for the degree of **Master of Science in Civil Engineering Department, Middle East Technical University** by,

Prof. Dr. Canan Özgen  
Dean, Graduate School of **Natural and Applied Sciences** \_\_\_\_\_

Prof. Dr. Güney Özcebe  
Head of Department, **Civil Engineering** \_\_\_\_\_

Asst. Prof. Dr. Alp Caner  
Supervisor, **Civil Engineering Dept., METU** \_\_\_\_\_

**Examining Committee Members:**

Dr. Erhan Karaesmen (\*)  
Civil Engineering Dept., METU \_\_\_\_\_

Asst. Prof. Dr. Alp Caner (\*\*)  
Civil Engineering Dept., METU \_\_\_\_\_

Prof. Dr. Osman Cahit Eralp  
Mechanical Engineering Dept., METU \_\_\_\_\_

Assoc. Prof. Dr. İsmail Özgür Yaman  
Civil Engineering Dept., METU \_\_\_\_\_

Dr. Kartal Toker  
Civil Engineering Dept., METU \_\_\_\_\_

**Date:** \_\_\_\_\_ 27.05.2008

(\*) Head of Examining Committee

(\*\*) Supervisor

**I hereby declare that all information in this document has been obtained and presented in accordance with academic rules and ethical conduct. I also declare that, as required by these rules and conduct, I have fully cited and referenced all material and results that are not original to this work.**

Name, Last name : Altan BÖNCÜ

Signature :

## **ABSTRACT**

### **STRUCTURAL FIRE SAFETY OF STANDARD CIRCULAR RAILROAD TUNNELS UNDER DIFFERENT SOIL CONDITIONS**

Böncü, Altan

M.S, Department of Civil Engineering

Supervisor: Asst. Prof. Dr. Alp CANER

May 2008, 140 pages

In many tunnel designs, reinforced concrete tunnel lining design is selected based on construction requirements rather than design loads. A constant cross-section is typically used along a tunnel even if the design loads change from one location to another, especially for tunnels constructed by tunnel boring machines (TBM). Factor of safety against failure is not constant along the length of tunnel and is typically high at shallow depth regions. Factor of safety during a rare event is usually much less than the ones set for service load states. Rare events such as earthquake, train derailment, explosion and long duration fires do not happen daily and generally a minor reparable damage is targeted at the structure during those types of events. The focus of this study is to analytically investigate structural fire safety of reinforced concrete circular tunnel linings in terms of reduction in service load safety and to develop recommendations for preliminary assessment of structural fire endurance of circular tunnel linings. Analytical methods accounting for thermal non-

linearity, material degradation, tunnel lining-ground interaction and fire time stages are available to assess the structural fire safety of the concrete tunnel linings. Analytical results are determined to be in good agreement with tunnel key segment hydrocarbon fire test.

**Keywords:** Tunnel linings, fire resistance, fire test, spalling, fibers, structural safety, rehabilitation.

## ÖZ

### FARKLI ZEMİN KOŞULLARINDAKİ STANDART YUVARLAK KESİTLİ DEMİRYOLU TÜNELLERİNİN YAPISAL YANGIN GÜVENLİĞİ

Böncü, Altan

Yüksek Lisans, İnşaat Mühendisliği Bölümü

Tez Yöneticisi: Y. Doç. Dr. Alp CANER

Mayıs 2008, 140 sayfa

Tünel tasarımlarının büyük çoğunluğunda kesit seçimi yapımsal gereksinimler göz önünde tutularak yapılır. Tünel delme makinaları (TBM) ile yapılan tüneller başta olmak üzere, tasarım yükü tünel boyunca değişmesine karşın, tek bir kesit kullanılır. Dolayısıyla, göçmeye karşı güvenlik katsayısı tünel boyunca sabit değildir ve yüzeysel bölgelerde daha yüksektir. Nadir görülen durumlarda bu katsayı, servis yüklerindeki duruma göre çok daha düşük seviyelere iner. Deprem, raydan çıkma, patlama ve uzun süreli yangınlar gibi sıradışı olaylar günlük olarak yaşanmaz ve bu tür olaylar ardından yapıda, küçük tamirler ile atlatılan hasarlar hedeflenir. Bu çalışmanın amacı, yuvarlak kesitli tünellerin yapısal yangın güvenliğini servis yükleri altındaki güvenlik katsayısındaki azalma ile incelemek ve yuvarlak kesitli tünel yapılarının yapısal yangın dayanımına ilişkin ön değerlendirmeler geliştirmektir. Tünellerde yapısal

yangın güvenliğini, doğrusal olmayan ısı, malzeme bozulması, tünel-zemin etkileşimi ve artımsal yangın seviyeleri ile analitik olarak değerlendiren methodlar mevcuttur. Analitik sonuçlar, tünel anahtar segmentinin hidrokarbon test sonuçları ile yakın uyum göstermektedir.

**Anahtar kelimeler:** Tünel yapıları, yangın dayanımı, yangın testi, dökülme, silikon, yapısal güvenlik, güçlendirme.

To My Family

## ACKNOWLEDGEMENTS

I wish to express my special thanks to Assistant Prof. Dr. Alp CANER for his continuous help, friendly and kind guidance throughout this study.

I would also like to express my appreciation to Dr. Erhan KARAESMEN and Gülay ÖZDEMİR (B.S, Civil Eng.) for their encouragement and support to do such a study.

I would also like to thank to Barbaros SARICI (M.Eng, Civil Eng.) from RUA Engineering, Assoc. Prof. Dr. İsmail Özgür YAMAN and Serkan KAYILI (M.S, Mechanical Eng.) from Mechanical Engineering Department of METU for their advice, orientation, and help in both analytical and experimental steps throughout the study. I would like to expand my thanks to Turkish Chamber of Civil Engineers (TMMOB İnşaat Mühendisleri Odası, İMO) for their friendly attitude.

I would present my sincere thanks to my friends Murat IŞILDAK (B.S, Civil Eng.), Taner KARAGÖZ (M.S, Mechanical Eng.), my lovely uncle Ruhi İLHAN, and my office mate Müjdat KILINÇ and Mehmet ÖKMEN for their invaluable suggestions and all kind of support.

Finally, special thanks to my sister Demet İLHAN and my family for all their love, patience and support during all my life.

## TABLE OF CONTENTS

ABSTRACT.....	iv
ÖZ.....	vi
DEDICATION.....	viii
ACKNOWLEDGEMENTS .....	ix
TABLE OF CONTENTS.....	x
LIST OF TABLES.....	xv
LIST OF FIGURES .....	xvii
LIST OF SYMBOLS AND ABBREVIATIONS.....	xxv
CHAPTER	
1. INTRODUCTION .....	1
1.1 Background .....	1
1.2 Extreme Events for Tunnels .....	2
1.3 Fire Safety of Tunnels .....	3
1.4 Tunnel Boring Machine (TBM) and TBM Tunnels .....	5
1.5 Objective .....	9

1.6 Scope .....	10
2. LITERATURE REVIEW.....	11
3. 2007-2008 METU EXPERIMENTAL STUDIES.....	20
3.1 Introduction.....	20
3.2 Fire Test Specimen Geometry and Properties .....	20
3.2.1 Measured Compressive Strength of Cores Taken from Reference Segment.....	21
3.2.2 Measured Tensile Strength of Reinforcement Taken from Reference Segment.....	23
3.2.3 Determination of Moisture Content and Water Absorption Capacity of Specimens .....	24
3.3 Fire Test Equipment Setup and Description.....	25
3.4 Fire Tests of Segments .....	28
3.4.1 Test of Specimen at Ambient Conditions for 1 Hour Fire (Test 1) .....	28
3.4.2 Test of Specimen at Ambient Conditions for 4 Hour Fire (Test 2) .....	28
3.4.3 Test of Fully Saturated Specimen for 4 Hour Fire (Test 3) .....	30

3.5 Post Fire Evaluations .....	33
3.5.1 Concrete Spalling and Colorization.....	33
3.5.2 Concrete Strain Distribution.....	36
3.5.3 Concrete Compressive Strength and Reinforcement Tensile Strength at the Damaged Sections.....	38
3.6 Micro Level Investigation of Concrete Before and After Fire .....	40
4. PARAMETRIC ANALYSES AND NUMERICAL RESULTS.....	46
4.1 Introduction.....	46
4.2 Heat Transfer Analysis .....	47
4.3 Computation of Primary, Equilibrating and Creep Strains .....	50
4.4 Structural Analysis and Computation of Secondary Strains .....	52
4.5 Computation of Total Strain Distribution.....	59
4.6 Computation of Capacity and Demand.....	60
4.7 Recommendations for Preliminary Structural Fire Safety Assessment of Circular Tunnel Linings .....	61
5. RESULTS AND FINDINGS.....	69
6. CONCLUSION .....	72

6.1 Conclusion .....	72
6.2 Recommendations for Future Work.....	73
REFERENCES .....	74
APPENDICES	
A. INTERACTION DIAGRAMS AT THE END OF HYDROCARBON FIRE FOR SPRING LINE AND CROWN .....	80
B. INTERACTION DIAGRAMS AT THE END OF RWS FIRE FOR SPRING LINE AND CROWN .....	93
C AXIAL LOAD DEMAND AND CAPACITY DURING HYDROCARBON FIRE FOR SPRING LINE AND CROWN.....	106
D. AXIAL LOAD DEMAND AND CAPACITY DURING RWS FIRE FOR SPRING LINE AND CROWN .....	113
E. AXIAL LOAD DEMAND AND CAPACITY VERSUS SUBGRADE REACTION MODULUS DURING HYDROCARBON FIRE FOR SPRING LINE .....	120
F. BENDING MOMENT VERSUS SUBGRADE REACTION MODULUS AT THE END OF HYDROCARBON FIRE FOR CROWN .....	123
G. RATIO OF CROWN DEFLECTION TO TUNNEL RADIUS DURING HYDROCARBON FIRE .....	126

H. RATIO OF CROWN DEFLECTION TO TUNNEL RADIUS DURING RWS FIRE .....	133
I. COMPUTER PROGRAMS USED IN THE ANALYSES .....	140
I.1 Larsa 4D.....	140
I.2 Radtherm .....	140
I.3 Firecap .....	140

## LIST OF TABLES

### TABLES

Table 1.1 Recent Tunnel Accidents .....	4
Table 1.2 Selective TBM Machines for Railway Tunnels around the World [9] .....	9
Table 2.1 Heat Release and Smoke Flow Rates of Vehicles [32, 34].....	14
Table 3.1 Compressive Strength Test Results of Concrete Prior to Fire Test .....	22
Table 3.2 Tensile Strength Test Results of Reinforcement Prior to Fire Test .....	24
Table 3.3 Moisture Content Test Results of Reference Segment Specimens .....	25
Table 3.4 Moisture Contents of Specimens before Fire Test .....	33
Table 3.5 Summary of Depth of Damaged and Spalled Concrete .....	38
Table 3.6 Compressive Strength Test Results of Fire Exposed Concrete .....	39
Table 3.7 Tensile Strength Test Results of Fire Exposed Reinforcement .....	40
Table 4.1 Investigated Tunnel Sections .....	54
Table 4.2 Axial Load Capacity-Demand ( $P_{CAP}-P_{DEM}$ ) and $\alpha$ Values .....	65

Table 5.1 Summary of Depth of Concrete Needs to be Repaired ..... 70

## LIST OF FIGURES

### FIGURES

Figure 1.1 Opening (Entrance) of a Highway Tunnel [2].....	2
Figure 1.2 Fire-Air Temperature Curves for Tunnels [4] .....	5
Figure 1.3 Modern Tunnel Boring Machine (a) Photograph of a TBM Designed for Rock, (b) Schematic of TBM Designed for Soft Ground [6, 7].....	6
Figure 1.4 TBM Cutting Head [8] .....	7
Figure 1.5 Rapid Transition TBM Tunnel [8] .....	8
Figure 2.1 Large Extreme Tunnel Fire (Trucks Carrying Missiles Caught Fire and Melted, No Signs of Concrete Spalling), South Korea: November 2005.....	15
Figure 2.2 Large Extreme Tunnel Fire (No Explosive Spall, Even though the Tunnel Lining is Directly Exposed to Flames), Santa Clara, USA: October 2007 .....	15
Figure 3.1 Precast TBM Key Segments.....	21
Figure 3.2 Compressive Strength Tests of Reference Segment Core Samples .....	22
Figure 3.3 Tensile Strength Tests of Reference Segment Reinforcement Samples .....	23
Figure 3.4 Fire Test Furnace.....	26

Figure 3.5 “K” (Chromel–Alumel) Type Thermocouples [38].....	26
Figure 3.6 Placements of Thermocouples and Inside of Furnace.....	27
Figure 3.7 Data Acquisition System.....	27
Figure 3.8 Placements of Thermocouples in Plan View (Test 2) .....	29
Figure 3.9 Temperature Records (Test 2).....	30
Figure 3.10 Concrete Face and Inside of Furnace (Test 3) .....	31
Figure 3.11 Placements of Thermocouples in Plan View (Test 3).....	32
Figure 3.12 Temperature Records (Test 3).....	32
Figure 3.13 Spalling of Specimen (Test 1).....	34
Figure 3.14 Spalling of Specimen (Test 2).....	34
Figure 3.15 Spalling of Specimen (Test 3).....	34
Figure 3.16 Colorization after Test 1 .....	35
Figure 3.17 Colorization after Test 2 and Test 3.....	35
Figure 3.18 Concrete Strain Distributions within First Hour .....	36
Figure 3.19 Concrete Strain Distribution at the End of Fourth Hour.....	37
Figure 3.20 Calcium Silicate Hydrate Gels (C-S-H) .....	41
Figure 3.21 Calcium Hydroxide Gels (C-H).....	41
Figure 3.22 Reference Segment Chemical Compounds (C-S-H and C-H Gels) .....	42
Figure 3.23 Chemical Decomposition of C-S-H Gels (Test 1).....	43
Figure 3.24 Chemical Decomposition of C-S-H Gels (Test 2).....	43
Figure 3.25 Decomposed C-H Gels (Test 3).....	44
Figure 3.26 Cracked Concrete Textures (Test 3).....	44

Figure 3.27 Micro Crack Opening (Test 3).....	45
Figure 4.1 Algorithm of Fire Analysis .....	47
Figure 4.2 Heat Transfer Analysis Model.....	49
Figure 4.3 Induced Hydrocarbon and RWS Fire Curves.....	49
Figure 4.4 Temperature Penetrations into Concrete Lining	
(a) Harmonized Hydrocarbon Fire for 4 Hour Rating,	
(b) Rijkswaterstaat Hydrocarbon Fire for 2 Hour Rating.....	51
Figure 4.5 Long Cylindrical Body Representing Plane Strain	
Conditions [39] .....	53
Figure 4.6 Typical Service Loads on a TBM Tunnel .....	56
Figure 4.7 2D Beam-Spring Model of a TBM Tunnel Lining.....	56
Figure 4.8 Deformed Shape of S3.30.010 (a) t = 0 min., (b) t = 10 min.,	
(c) t = 30 min., (d) t = 60 min., (e) t = 90 min., (f) t = 120 min.,	
(g) t = 150 min., (h) t = 180 min., (i) t = 240 min.....	57-58
Figure 4.9 Total Strain Distribution [4].....	59
Figure 4.10 Hydrocarbon Fire R/t vs. $P_{CAP}/P_{DEM}$ @ SL at 240 <sup>th</sup> Minute ...	62
Figure 4.11 Hydrocarbon Fire R/t vs. $P_{CAP}/P_{DEM}$ @ Cr at 240 <sup>th</sup> Minute ....	62
Figure 4.12 RWS Fire R/t vs. $P_{CAP}/P_{DEM}$ @ SL at 240 <sup>th</sup> Minute.....	64
Figure 4.13 RWS Fire R/t vs. $P_{CAP}/P_{DEM}$ @ SL at 240 <sup>th</sup> Minute.....	64
Figure 4.14 Hydrocarbon Fire R/t vs. $M_{CAP}/M_{DEM}$ @ SL at 240 <sup>th</sup> Minute ..	67
Figure 4.15 Hydrocarbon Fire R/t vs. $M_{CAP}/M_{DEM}$ @ Cr at 240 <sup>th</sup> Minute...	67
Figure 4.16 RWS Fire R/t vs. $M_{CAP}/M_{DEM}$ @ SL at 120 <sup>th</sup> Minute .....	68
Figure 4.17 RWS Fire R/t vs. $M_{CAP}/M_{DEM}$ @ Cr at 120 <sup>th</sup> Minute .....	68

Figure A.1 M-P @ SL: (a) S3.30.010, (b) S3.30.125, (c) S3.30.240, (d) S3.36.010, (e) S3.36.125, (f) S3.36.240 .....	80-81
Figure A.2 M-P @ SL: (a) S4.30.010, (b) S4.30.125, (c) S4.30.240, (d) S4.36.010, (e) S4.36.125, (f) S4.36.240 .....	82
Figure A.3 M-P @ SL: (a) M3.30.010, (b) M3.30.125, (c) M3.30.240, (d) M3.36.010, (e) M3.36.125, (f) M3.36.240 .....	83
Figure A.4 M-P @ SL: (a) M4.30.010, (b) M4.30.125, (c) M4.30.240, (d) M4.36.010, (e) M4.36.125, (f) M4.36.240 .....	84
Figure A.5 M-P @ SL: (a) D3.30.010, (b) D3.30.125, (c) D3.30.240, (d) D3.36.010, (e) D3.36.125, (f) D3.36.240.....	85
Figure A.6 M-P @ SL: (a) D4.30.010, (b) D4.30.125, (c) D4.30.240, (d) D4.36.010, (e) D4.36.125, (f) D4.36.240.....	86
Figure A.7 M-P @ Cr: (a) S3.30.010, (b) S3.30.125, (c) S3.30.240, (d) S3.36.010, (e) S3.36.125, (f) S3.36.240 .....	87
Figure A.8 M-P @ Cr: (a) S4.30.010, (b) S4.30.125, (c) S4.30.240, (d) S4.36.010, (e) S4.36.125, (f) S4.36.240 .....	88
Figure A.9 M-P @ Cr: (a) M3.30.010, (b) M3.30.125, (c) M3.30.240, (d) M3.36.010, (e) M3.36.125, (f) M3.36.240 .....	89
Figure A.10 M-P @ Cr: (a) M4.30.010, (b) M4.30.125, (c) M4.30.240, (d) M4.36.010, (e) M4.36.125, (f) M4.36.240 .....	90
Figure A.11 M-P @ Cr: (a) D3.30.010, (b) D3.30.125, (c) D3.30.240, (d) D3.36.010, (e) D3.36.125, (f) D3.36.240.....	91

Figure A.12 M-P @ Cr: (a) D4.30.010, (b) D4.30.125, (c) D4.30.240, (d) D4.36.010, (e) D4.36.125, (f) D4.36.240.....	92
Figure B.1 M-P @ SL: (a) S3.30.010, (b) S3.30.125, (c) S3.30.240, (d) S3.36.010, (e) S3.36.125, (f) S3.36.240 .....	93-94
Figure B.2 M-P @ SL: (a) S4.30.010, (b) S4.30.125, (c) S4.30.240, (d) S4.36.010, (e) S4.36.125, (f) S4.36.240 .....	95
Figure B.3 M-P @ SL: (a) M3.30.010, (b) M3.30.125, (c) M3.30.240, (d) M3.36.010, (e) M3.36.125, (f) M3.36.240 .....	96
Figure B.4 M-P @ SL: (a) M4.30.010, (b) M4.30.125, (c) M4.30.240, (d) M4.36.010, (e) M4.36.125, (f) M4.36.240 .....	97
Figure B.5 M-P @ SL: (a) D3.30.010, (b) D3.30.125, (c) D3.30.240, (d) D3.36.010, (e) D3.36.125, (f) D3.36.240.....	98
Figure B.6 M-P @ SL: (a) D4.30.010, (b) D4.30.125, (c) D4.30.240, (d) D4.36.010, (e) D4.36.125, (f) D4.36.240.....	99
Figure B.7 M-P @ Cr: (a) S3.30.010, (b) S3.30.125, (c) S3.30.240, (d) S3.36.010, (e) S3.36.125, (f) S3.36.240 .....	100
Figure B.8 M-P @ Cr: (a) S4.30.010, (b) S4.30.125, (c) S4.30.240, (d) S4.36.010, (e) S4.36.125, (f) S4.36.240 .....	101
Figure B.9 M-P @ Cr: (a) M3.30.010, (b) M3.30.125, (c) M3.30.240, (d) M3.36.010, (e) M3.36.125, (f) M3.36.240 .....	102
Figure B.10 M-P @ Cr: (a) M4.30.010, (b) M4.30.125, (c) M4.30.240, (d) M4.36.010, (e) M4.36.125, (f) M4.36.240 .....	103

Figure B.11 M-P @ Cr: (a) D3.30.010, (b) D3.30.125, (c) D3.30.240, (d) D3.36.010, (e) D3.36.125, (f) D3.36.240.....	104
Figure B.12 M-P @ Cr: (a) D4.30.010, (b) D4.30.125, (c) D4.30.240, (d) D4.36.010, (e) D4.36.125, (f) D4.36.240.....	105
Figure C.1 P <sub>CAP</sub> -P <sub>DEM</sub> : (a) S3.30.010, (b) S3.30.125, (c) S3.30.240, (d) S3.36.010, (e) S3.36.125, (f) S3.36.240 .....	106-107
Figure C.2 P <sub>CAP</sub> -P <sub>DEM</sub> : (a) S4.30.010, (b) S4.30.125, (c) S4.30.240, (d) S4.36.010, (e) S4.36.125, (f) S4.36.240 .....	108
Figure C.3 P <sub>CAP</sub> -P <sub>DEM</sub> : (a) M3.30.010, (b) M3.30.125, (c) M3.30.240, (d) M3.36.010, (e) M3.36.125, (f) M3.36.240 .....	109
Figure C.4 P <sub>CAP</sub> -P <sub>DEM</sub> : (a) M4.30.010, (b) M4.30.125, (c) M4.30.240, (d) M4.36.010, (e) M4.36.125, (f) M4.36.240 .....	110
Figure C.5 P <sub>CAP</sub> -P <sub>DEM</sub> : (a) D3.30.010, (b) D3.30.125, (c) D3.30.240, (d) D3.36.010, (e) D3.36.125, (f) D3.36.240.....	111
Figure C.6 P <sub>CAP</sub> -P <sub>DEM</sub> : (a) D4.30.010, (b) D4.30.125, (c) D4.30.240, (d) D4.36.010, (e) D4.36.125, (f) D4.36.240.....	112
Figure D.1 P <sub>CAP</sub> -P <sub>DEM</sub> : (a) S3.30.010, (b) S3.30.125, (c) S3.30.240, (d) S3.36.010, (e) S3.36.125, (f) S3.36.240 .....	113-114
Figure D.2 P <sub>CAP</sub> -P <sub>DEM</sub> : (a) S4.30.010, (b) S4.30.125, (c) S4.30.240, (d) S4.36.010, (e) S4.36.125, (f) S4.36.240 .....	115
Figure D.3 P <sub>CAP</sub> -P <sub>DEM</sub> : (a) M3.30.010, (b) M3.30.125, (c) M3.30.240, (d) M3.36.010, (e) M3.36.125, (f) M3.36.240 .....	116

Figure D.4 $P_{CAP}-P_{DEM}$ : (a) M4.30.010, (b) M4.30.125, (c) M4.30.240, (d) M4.36.010, (e) M4.36.125, (f) M4.36.240 .....	117
Figure D.5 $P_{CAP}-P_{DEM}$ : (a) D3.30.010, (b) D3.30.125, (c) D3.30.240, (d) D3.36.010, (e) D3.36.125, (f) D3.36.240.....	118
Figure D.6 $P_{CAP}-P_{DEM}$ : (a) D4.30.010, (b) D4.30.125, (c) D4.30.240, (d) D4.36.010, (e) D4.36.125, (f) D4.36.240.....	119
Figure E.1 $P-k_s$ : (a) S3.30, (b) S3.36, (c) S4.30, (d) S4.36, (e) M3.30, (f) M3.36 .....	120-121
Figure E.2 $P-k_s$ : (a) M4.30, (b) M4.36, (c) D3.30, (d) D3.36, (e) D4.30, (f) D4.36 .....	122
Figure F.1 $M-k_s$ : (a) S3.30, (b) S3.36, (c) S4.30, (d) S4.36, (e) M3.30, (f) M3.36 .....	123-124
Figure F.2 $M-k_s$ : (a) M4.30, (b) M4.36, (c) D3.30, (d) D3.36, (e) D4.30, (f) D4.36 .....	125
Figure G.1 $\delta_{CR}/R-t$ : (a) S3.30.010, (b) S3.30.125, (c) S3.30.240, (d) S3.36.010, (e) S3.36.125, (f) S3.36.240 .....	126-127
Figure G.2 $\delta_{CR}/R-t$ : (a) S4.30.010, (b) S4.30.125, (c) S4.30.240, (d) S4.36.010, (e) S4.36.125, (f) S4.36.240 .....	128
Figure G.3 $\delta_{CR}/R-t$ : (a) M3.30.010, (b) M3.30.125, (c) M3.30.240, (d) M3.36.010, (e) M3.36.125, (f) M3.36.240 .....	129
Figure G.4 $\delta_{CR}/R-t$ : (a) M4.30.010, (b) M4.30.125, (c) M4.30.240, (d) M4.36.010, (e) M4.36.125, (f) M4.36.240 .....	130

Figure G.5 $\delta_{CR}/R-t$ : (a) D3.30.010, (b) D3.30.125, (c) D3.30.240, (d) D3.36.010, (e) D3.36.125, (f) D3.36.240.....	131
Figure G.6 $\delta_{CR}/R-t$ : (a) D4.30.010, (b) D4.30.125, (c) D4.30.240, (d) D4.36.010, (e) D4.36.125, (f) D4.36.240.....	132
Figure H.1 $\delta_{CR}/R-t$ : (a) S3.30.010, (b) S3.30.125, (c) S3.30.240, (d) S3.36.010, (e) S3.36.125, (f) S3.36.240 .....	133-134
Figure H.2 $\delta_{CR}/R-t$ : (a) S4.30.010, (b) S4.30.125, (c) S4.30.240, (d) S4.36.010, (e) S4.36.125, (f) S4.36.240 .....	135
Figure H.3 $\delta_{CR}/R-t$ : (a) M3.30.010, (b) M3.30.125, (c) M3.30.240, (d) M3.36.010, (e) M3.36.125, (f) M3.36.240 .....	136
Figure H.4 $\delta_{CR}/R-t$ : (a) M4.30.010, (b) M4.30.125, (c) M4.30.240, (d) M4.36.010, (e) M4.36.125, (f) M4.36.240 .....	137
Figure H.5 $\delta_{CR}/R-t$ : (a) D3.30.010, (b) D3.30.125, (c) D3.30.240, (d) D3.36.010, (e) D3.36.125, (f) D3.36.240.....	138
Figure H.6 $\delta_{CR}/R-t$ : (a) D4.30.010, (b) D4.30.125, (c) D4.30.240, (d) D4.36.010, (e) D4.36.125, (f) D4.36.240.....	139

## LIST OF SYMBOLS AND ABBREVIATIONS

### SYMBOLS

$A_c$	: Cross Sectional Area of Concrete ( $\text{mm}^2$ )
Al	: Aluminum
$A_{ti}$	: Reduced Area of $i^{\text{th}}$ Layer at Time $t$ ( $\text{mm}^2$ )
C	: Carbon
Ca	: Calcium
$c$	: Specific Heat ( $\text{J/KgK}$ )
D	: Tunnel at Deep Region
DL	: Dead Load ( $\text{kN/m}$ )
$E_c$	: Elastic Modulus of Concrete (MPa)
$E_s$	: Elastic Modulus of Steel (MPa)
$F_d$	: Correction Factor Accounting for Core Drilling Damage
Fe	: Iron
$F_{dia}$	: Correction Factor Accounting for Core Diameter
$F_{l/d}$	: Correction Factor Accounting for Length to Diameter Ratio of Core
$F_{mc}$	: Correction Factor Accounting for Core Moisture Content
$F_r$	: Correction Factor Accounting for Core Reinforcement
FL( $t$ )	: Fire Induced Structural Load at the Investigated Fire Time
$FS_{to}$	: Factor of Safety at the Start of Fire
$FS_{t\_end}$	: Factor of Safety at the End of Fire
$f_c$	: Concrete Strength (MPa)
$f_c'$	: Design Strength of Concrete (MPa)
$f_{c_{ti}}$	: Reduced Compressive Strength of Concrete at $i^{\text{th}}$ Layer (MPa)
J	: Joule

H	: Overburden Depth of Tunnel from the Crown Level (m)
HL	: Hydrostatic Load (kN/m)
H <sub>w</sub>	: Water Head (m)
K	: Kelvin
k	: Thermal Conductivity (W/mK)
k <sub>s</sub>	: Subgrade Reaction Modulus (kN/m <sup>3</sup> )
kg	: Kilogram
M	: Tunnel at Medium Depth Region
M <sub>CAP</sub>	: Bending Moment Capacity (kNm)
M <sub>DEM</sub>	: Bending Moment Demand (kNm)
Mo	: Molybdenum
m	: Meter
O	: Oxygen
P	: Axial Load (kN)
P <sub>CAP</sub>	: Axial Load Capacity (kN)
P <sub>DEM</sub>	: Axial Load Demand (kN)
PL	: Earth Pressure (kN/m)
P <sub>lb</sub>	: Lateral Earth Pressure at Bottom of the Tunnel (kN/m)
P <sub>lt</sub>	: Lateral Earth Pressure at Top of the Tunnel (kN/m)
P <sub>n(t)</sub>	: Reduced Axial Load Capacity (kN)
P <sub>v</sub>	: Vertical Earth Pressure at Crown Level (kN/m)
P <sub>vb</sub>	: Vertical Earth Pressure at Bottom Level (kN/m)
P <sub>wsl</sub>	: Water Pressure at Spring Line Level (kN/m)
q	: Surcharge Load (kN/m)
R	: Radius of Tunnel Lining (m)
R <sub>nr(t)</sub>	: Reduced Capacity due to Material Degradation at the Investigated Fire Time
S	: Tunnel at Shallow Region
Si	: Silicon
T	: Temperature (°C)
t	: Thickness of Tunnel Lining (m)

$u$	: Displacement in x Direction
$V$	: Shear Force
$v$	: Displacement in y Direction
$W$	: Watt
$w$	: Displacement in z Direction
$\alpha$	: Lump Sum Factor of Change Parameter
$\alpha_T$	: Thermal Expansion Coefficient
$\delta_{CR}$	: Crown Deflection (mm)
$\sigma_{ck}$	: Characteristic Compressive Strength of Concrete (MPa)
$\phi_r$	: Resistance Factor
$\emptyset$	: Diameter of Concrete Core Specimen (cm)
$\sigma_y$	: Tensile Yield Strength of Steel (MPa)

## ABBREVIATIONS

ACI	: American Concrete Institute
ALARP	: As Low As Reasonably Practicable
ATC	: Applied Technology Council
C-H	: Calcium Hydroxide
C-S-H	: Calcium Silicate Hydrate
Cr	: Crown of Tunnel Lining
EPB	: Earth Pressure Balance
FEMA	: Federal Emergency Management Agency
HSC	: High Strength Concrete
MW	: Mega Watt
RMP	: Rock Mass Properties
RWS	: Rijkswaterstaat Hydrocarbon Curve
SI	: System of Units
SL	: Spring Line of Tunnel Lining
SSD	: Saturated Surface Dry
TBM	: Tunnel Boring Machine
2-D	: Two Dimensional
3-D	: Three Dimensional

# CHAPTER 1

## INTRODUCTION

### 1.1 Background

Tunnels, underground passages, are one of the major parts of various transportation network systems such as highways, rail roads, rapid transit artery; pedestrian passageway; fresh water conveyance, cooling water supply, waste water collector or transport; and hydropower generator, or utility corridor [1]. Immersed tube, cut and cover, bored or mined, and air rights structure tunnels are constructed with different techniques [3].

Highway or railroad tunnels are constructed to reduce adverse topological conditions on the route of transportation route if economically feasible, Figure 1.1. Construction technique and type is selected after topological and geotechnical studies. Construction time and cost is a function of selected tunnel system.

Circular, multicurve, horseshoe, cathedral arch, or flat roofed are some of the cross sectional shapes for a tunnel. The geometrical features such as diameter and length of a tunnel with a circular cross-section are typically decided based on clearance and service requirements. Diameter of a tunnel can range from 1 meter to 15 meters, and length can range from 30 meters to 50 kilometers [1].

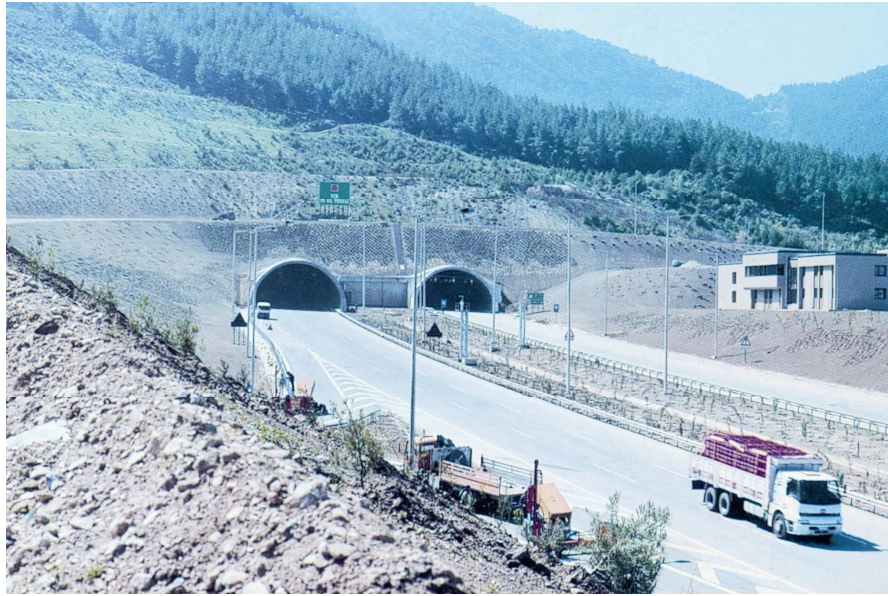


Figure 1.1 Opening (Entrance) of a Highway Tunnel [2]

## 1.2 Extreme Events for Tunnels

Safety is important in tunnels since it is a fully closed medium with very limited access to exits. There might be various sources of extreme events such as earthquakes, train derailments, explosions and long duration fires. Some of these can result in interruption of service with economic losses and sometimes even more severe results like casualties and loss of human lives. Recent tunnel accidents, probable cause, casualties and a damage measure spalling levels are listed in Table 1.1. As seen in that table, accidents that cause fire are mainly the most dangerous cases that can occur in a tunnel.

Tunnels have different structural response to extreme events compared to above ground civil engineering structures because of four facts: (1) high ratio of longitudinal length to cross sectional dimension, (2) complete confinement by the surrounding soils and rocks, (3) reflected pressures developed from

the tunnel boundaries when an internal explosion occurs, or reflection of heat due to radiation during a fire, and (4) coupled behavior of air blast inside the tunnel and wave propagation through the surrounding soil [3].

### **1.3 Fire Safety of Tunnels**

Life safety in case of fire needs a special attention both in design and operation of a tunnel. The important items of tunnel fire life safety are detection, alarm, incident location, communications, planned response, personnel evacuation, smoke control, and power supplies [1].

In literature there are some fire endurance design methods for buildings. However, there is not a specific design code for tunnel fire in special. The main reason for this can be tunnel fires having different heat release rates, peak temperatures, boundary conditions and design details compared to above ground structures [4].

There are four main fire curves, Figure 1.2, defined and used for underground structures to simulate different fire scenarios [1, 5]. Curve 1, the cellulosic curve, stands for burning of general building content. Curve 2, the hydrocarbon curve, is used for representing the fires that may include some small amount of petroleum. Curve 3, the ZTV curve which has been developed in Germany, stands for the fires that have a sharp temperature increase at the beginning i.e. 1200 °C in 5 minutes. Curve 4, the RWS (Rijkswaterstaat hydrocarbon) curve which has been developed in Netherlands, stands for burning of a fuel tanker with a fire load of 300 MW [4, 17].

Table 1.1 Recent Tunnel Accidents

Location/ Accident Year	Tunnel Type	Probable Cause	Casualties	Concrete Spalling (mm)
Caldecot Tunnel, USA, 1982	Roadway	Fuel Tanker	7 fatalities, 2 injuries	450
Gotthard Tunnel Switzerland, 1984	Roadway	Truck	None	300
Beaune, Germany, 1995	Roadway	Collision	40 fatalities	300
Pfander, Germany, 1995	Roadway	Collision	3 fatalities	>300
Baku, Azerbaijan, 1995	Railway	-	300 fatalities, 270 injuries	Significant
Channel Tunnel, England, 1996	Railway	Cargo Fire	30 injuries	450
Palermo, Italy, 1996	Roadway	-	5 fatalities	Not Reported
Mont Blanc, France-Italy, 1999	Roadway	Truck	41 fatalities	400
Gottingen, Germany, 1999	Railway	Cargo Fire	None	200
Tauern, Australia, 1999	Roadway	Truck	12 fatalities, 21 injuries	350
Cable Railway, Switzerland, 2000	Cable Track	Electric Fire	159 fatalities	300
Gotthard Tunnel, Switzerland, 2001	Roadway	Collision	10 fatalities	300
S. Korea, 2005	Roadway	Truck	None	Not Reported
USA, 2007	Roadway	Truck	None	Not Reported

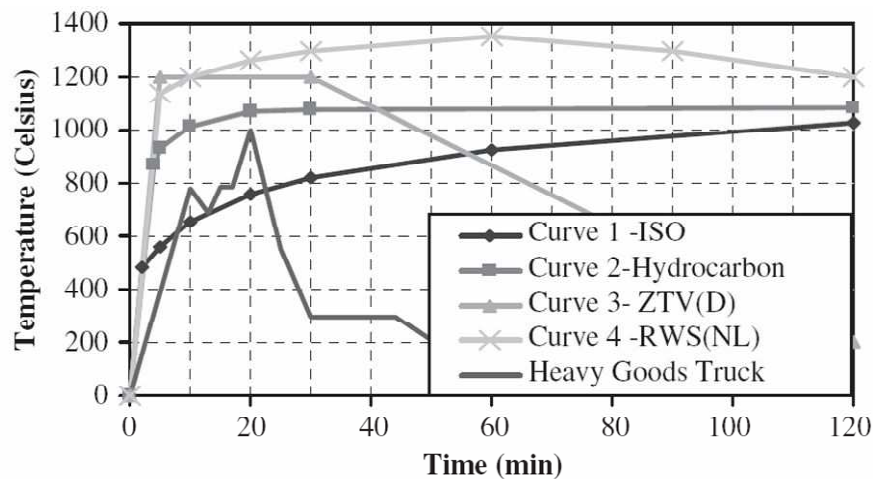
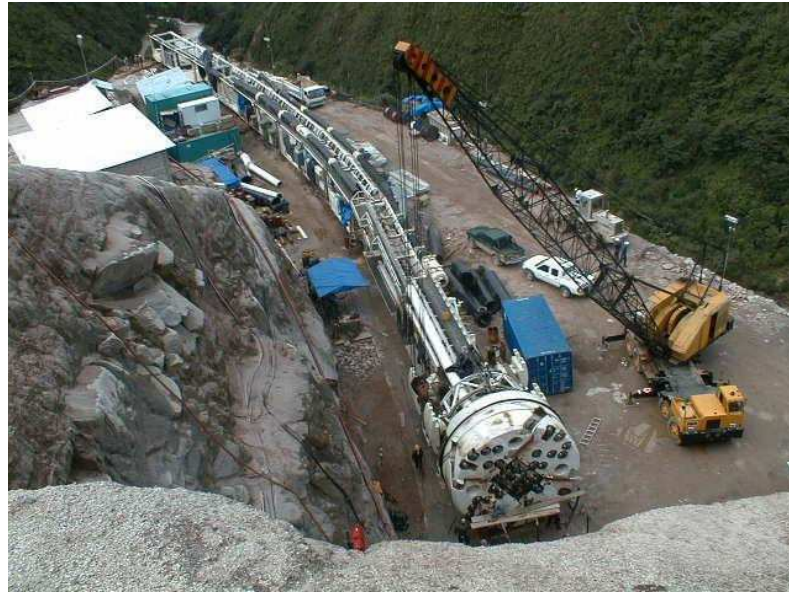


Figure 1.2 Fire-Air Temperature Curves for Tunnels [4]

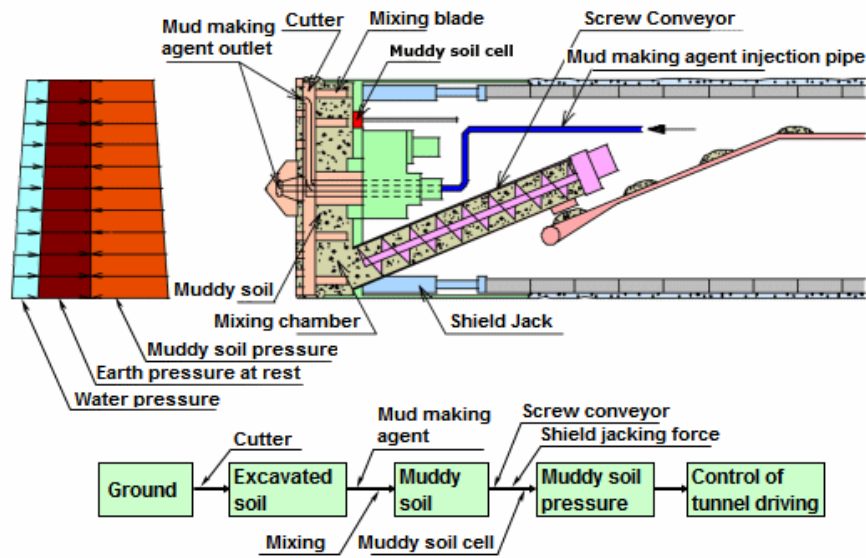
In practice, vertical shafts are needed when the tunnel length is more than 3000 meters for ease of construction and fire safety purposes. For those tunnels that have a shorter length than this limit horizontal ventilations with jet fans can provide a stable solution. Providing horizontal ventilation for tunnels longer than 3000 meters can create large air pressures for vehicles that can endanger the driving safety.

#### 1.4 Tunnel Boring Machine (TBM) and TBM Tunnels

TBM is complex moving earth grater machine which is designed according to soil conditions (like soft ground or hard rock), and the desired tunnel diameter. Like other modern and well developed machines, TBM had prototype much before today's version. Those were developed in the early 1800's, mostly in United States and Great Britain [1]. In time, many design imposed challenges were overcome with addition of new parts with new features. A modern TBM, shown in Figure 1.3, consists of mainly ten interdependent parts.



(a)



(b)

Figure 1.3 Modern Tunnel Boring Machine (a) Photograph of a TBM Designed for Rock, (b) Schematic of a TBM Designed for Soft Ground [6, 7]

First and the most important part of a TBM is its cutting head. The cutting head has mainly two parts: teeth and cutting wheels operating under pressure as shown in Figure 1.4. It has a limited operation life. Main bearings are located just behind the cutting head and are designed to carry the full thrust of the machine.



Figure 1.4 TBM Cutting Head [8]

Motors and gear boxes drive the cutting head. In a TBM that is designed to work under external water pressure, these parts are assembled in a water tight bulkhead to operate properly. Steering shoes, grippers, and shoe jacks are hydraulically operated parts just behind the cutting head. They bear against the soil surface radially to keep the TBM on desired project alignment and grade, and to prevent rotation of the whole system due to the moving head.

Ground support equipment is just behind the main bearings for precast liner erection, relatively simple rock bolting drillings, steel rib erection or shotcreting depending on the ground and the necessary process. Conveyor belts are another part which is relatively long and used for hauling the cut material to the rear of the machine for a train to carry the waste material out of the tunnel.

Back up facilities are located at the rear of the machine. They include high-voltage electrical cable reel, ventilation duct, track-laying equipment and catenary, and water and drainage lines if necessary [1].

All these parts of a TBM are designed and assembled on project basis. TBM tunnels are mostly constructed within the railway projects as shown in Figure 1.5, and diameter of the tunnel and therefore the TBM has a relatively wide range. Selective TBM machine types and bore diameters for railway tunnels around the world are listed in Table 1.2.



Figure 1.5 Rapid Transition TBM Tunnel [8]

Table 1.2 Selective TBM Machines for Railway Tunnels around the World [9]

Tunnel	Diameter	Used TBM Type
St. Clair River Tunnel (Canada)	9.53 m.	Mixed Face EPB
Port Headland Harbor Tunnel (Australia)	5.08 m.	Mixed Face EPB
Edmonton South LRT Extension (Canada)	6.53 m.	Mixed Face EPB
Jonction Cenrale Chateler-Gra De Lyon Metro Line C (France)	7.06 m.	Single Shield Rock
Metropolitano di Milano (Italy)	6.50 m.	Mixed Face EPB
Vale de Chekas (Portugal)	9.80 m.	Mixed Face EPB
Moscow Metro Extension (Russia)	6.15 m.	Mixed Face EPB
Northeast Line (Singapore)	6.50 m.	Mixed Face EPB
Metro Madrid (Spain)	7.20 m.	RMP SE
Metro Taipei (Taiwan)	6.15 m.	Mixed Face EPB
Marmaray (Turkey)	7.98 m.	Mixed Face EPB
Congress Neights Metro (USA)	6.45 m.	Soft Ground EPB
Channel Tunnel Rail Link (UK)	8.13 m.	Mixed Face EPB
Metro de Valencia (Venezuela)	9.53 m.	Soft Ground EPB
İzmir Metro (Turkey)	6.56 m.	Mixed Face EPB

### 1.5 Objective

Limited research is available on structural tunnel fire safety. The focus of this study is to analytically investigate structural fire safety of circular tunnel linings under different soil conditions in terms of reduction in service load safety, and to develop recommendations for preliminary assessment of structural fire endurance of circular tunnel linings.

## 1.6 Scope

In Chapter 4, for the structural fire safety analysis of circular tunnel linings, as the first step, the temperature profile inside the concrete lining is analytically predicted by utilizing software package RADTHERM which is a non-linear heat-transfer analysis program. A series of hydrocarbon fire tests of tunnel segments are used to verify the analytical results.

As the second step, the capacity of the reinforced concrete lining is determined by utilizing FIRECAP. This software has been developed for analyzing the axial force-moment interaction taking into account material degradation due to temperature increase in the section (considering both concrete and steel).

Finally, structural analysis including three parameters, i.e. tunnel radius ( $R$ ), subgrade reaction modulus ( $k_s$ ), and tunnel lining thickness ( $t$ ) are performed to calculate sectional demand forces by utilizing LARSA 4D. The nonlinear analysis is done for two different fire scenarios: Harmonized hydrocarbon fire for 4 hour rating, and Rijkswaterstaat hydrocarbon fire (RWS) for 2 hour rating.

In Chapter 2, the detailed literature review is presented related to the studies on fire. Behavior of heated concrete and steel, spalling mechanism of concrete and residual material strength after fires are the main topics of the past research.

In Chapter 3, related to the analytical calculations presented in Chapter 4, experimental studies conducted with cooperation and collaboration between Mechanical and Civil Engineering Departments of Middle East Technical University in December 2007-January 2008 are presented.

## CHAPTER 2

### LITERATURE REVIEW

Structural concrete modeling and understanding the mechanical behavior of concrete at high temperatures are rather important issues in fire design of concrete structures in general, and tunnel linings in specific. In stress calculations, elastic theory yields results different from experimental findings at high temperatures. An unloaded and restrained concrete member would fail at about 350 °C during heating if the elastic theory is applied which is not the real case [10]. Extensive research on mechanical behavior of concrete that has been exposed to high temperatures was done for the first time in Sweden [5, 11] and Germany [12] in 1970's. Following these studies, Anderberg [13] developed the first complete constitutive model of fire-exposed concrete for structural computations in 1976, and it provided realistic results confirmed by several number of statically indeterminate fire exposed concrete member tests. This study has great contributions in understanding the behavior of structures under fire effects and developing new design methods and codes [10].

Most of the past research deals with physical and mechanical properties of concrete at high temperatures and relies on experimental observations rather than analytical solutions. Loading history at high temperatures significantly affects the physical and mechanical properties of concrete. The modulus of elasticity decreases by a higher percentage compared to the percent decrease in compressive strength of an unloaded test member subjected to 700 °C per tests of Anderberg [10]. Furthermore, the reduction rates for both parameters decrease as the concrete is tested under loading.

Similar to Anderberg [10], ACI 216 [30] specifications also indicate that an axially loaded specimen will have a smaller reduction in compressive strength due to heat compared to an unloaded specimen. This proves that loading history has a considerable effect on the mechanical properties of concrete at high temperatures [10, 30].

Cheng et al. [14] performed experiments to determine change in strength and stress-strain curve of high strength concrete (HSC) at temperatures of 20 °C (as room temperature), 100 °C, 200 °C, 400 °C, 600 °C, and 800 °C. Concrete strength, type of aggregate, and addition of steel fibers were variables in experiments. Specimens of four types of HSC, (siliceous aggregate concrete, carbonate aggregate concrete, with and without steel fiber reinforcement) were tested. Specimens were 100 mm in diameter and 200 mm in height. In all investigated types, similar strength reduction pattern was observed. At 200 °C the strength loss was about 20% of the initial values. The strength loss was even sharper between 400 and 800 °C, and only 45% was left at 600 °C. At 800 °C strength loss was about 80% of its initial value. The reason for this decreasing trend was stated as the dehydration of cement paste and shrinkage of the paste whereas the expansion demand of the heated aggregate resulting in disintegration in the concrete [14].

In the same research study, it was observed that the presence of steel fibers had little influence on the compressive strength but they increased the ductility of HSC around 400 °C relative to other specimens that contain no steel fibers. The reduction in elastic modulus was 50% at 400 °C. Aggregate type used in concrete had moderate influence on the elastic modulus variation. Ultimate strain values were measured as 0.02 at 800 °C being increased from 0.003 at room temperature and the increase in ultimate strain was higher in carbonate aggregate HSC than that of siliceous aggregate HSC [14].

Similar experiments were carried out by Guerrini et al. [15] to investigate the HSC microstructure at high temperatures. Within that study, HSC containing crushed limestone or dolomitic aggregates, synthetic fibers, white cement, marble, and quartz aggregates, and hybrid fiber reinforcement were tested after heating the specimens up to 250 °C, 500 °C, and 750 °C to determine residual properties. A comparison of porosity of HSC with crushed limestone and dolomitic aggregates were made to understand damage mechanism with respect to residual strength. Consequently, it was observed that limestone aggregate might prevent the explosive failure even without fibers. However, mix design including dolomitic aggregate needed addition of fibers to keep the integrity of concrete at high temperatures. A progressive micro cracking due to temperature rise was observed as well.

Total response under uniaxial compression and bending tests were conducted on HSC containing quartz aggregate and hybrid fibers (polypropylene and micro steel fibers). Crack propagation due to applied load was monitored with laser interferometry, which is a highly accurate nondestructive technique for monitoring of shape and size of damage zone [16]. Loss in mechanical behavior, oxidation, and partial melting of steel fibers were some of the observations and results of the tests. It was concluded that the residual behavior of HSC is greatly affected by mix design, constituents, and heat induced chemo-physical transformations [15].

Spalling, defined as loss of concrete itself, is the most significant and undesirable effect that can occur within the concrete lining during a tunnel fire that influences the structural performance and integrity. A reinforced concrete element subjected to sudden extreme fires such as the ones selected for design of tunnels can spall in two different ways. The first type of spalling is usually called explosive spalling of concrete and the second type is typically called gradual spalling of concrete during the fire. At the early stages of tunnel fires with high heat release rates and high temperatures, moisture in

the concrete can rapidly turn into steam; in concrete with low permeability and high moisture content, the steam pressure can produce explosive-like spalling. Aggregate type and moisture content are important factors influencing the explosive spalling tendency of concrete [17, 18].

Spalling is a complex mechanism that depends on different excitations. In the recent catastrophic tunnel fires in South Korea and USA, as shown in Figure 2.1 and Figure 2.2, the explosive spalling was not reported. In those fires, trucks which can generate design fire curves melted. However, the combination of high strength, high moisture content and low permeability makes the concrete vulnerable to the explosive spalling as in the case of Channel Tunnel fire. Heat release and smoke flow rates of some type of vehicles for a possible fire scenario are presented in Table 2.1.

Table 2.1 Heat Release and Smoke Flow Rates of Vehicles [32, 34]

Type and Number of Vehicles	Heat Release Rate (MW)	Smoke Flow (m <sup>3</sup> /s)
1 Small Passenger Car	2.5	20
1 Large Passenger Car	5	30
2-3 Passenger Cars	8-15	50
1 Van / 1 Bus	15-20	60-80
1 Lorry with Burning Goods	20-30	20
Gasoline Tank	100	Not Reported
Maintenance Car	12.5	Not Reported



Figure 2.1 Large Extreme Tunnel Fire (Trucks Carrying Missiles Caught Fire and Melted, No Signs of Concrete Spalling),  
South Korea: November 2005



Figure 2.2 Large Extreme Tunnel Fire (No Explosive Spall, Even though the Tunnel Lining is Directly Exposed to Flames),  
Santa Clara, USA: October 2007

Msaad and Bonnet [19] worked on the latter mechanism and created thermochemoplastic analytical models for Channel Tunnel fire to assess the thermal softening (stiffness reduction) and thermal decohesion (strength reduction) due to compressive stresses generated by restrained thermal dilation. With the help of this basic model, the mechanical variables were defined as stresses and strains on the heated face of concrete. Accordingly, plastification temperature and depth were determined where the spalling caused by restrained thermal dilation occurred. It was stated that the prediction of thermal decohesion is enough to forecast the probable thermal spalling [19].

Pichler et al. [20] made analytical assessment of structural performance of Lainzer Tunnel (between Vienna and Salzburg) against dehydration in concrete at high temperatures. A certain amount of polypropylene fibers has been used in the design of the tunnel liner in order to minimize the spalling effect. And the dehydration of concrete, resulting in both stiffness and strength reduction, became the main fire assessment criterion. Deformation of the lining was investigated with increasing load level during fire stage. The analysis was performed for only one cross section of the tunnel as a 2-D model where tunnel cross section and soil were modeled. The performance analysis made it possible to determine the state of dehydration in concrete due to fire. Despite the fact that the existence of polypropylene fibers prevented the spalling by increasing the pore volume in the concrete, the dehydration that occurred at elevated temperatures made repair of the lining necessary. The critical depth for the replacement was determined as 14 cm.

Tajima et al. [21] conducted fire tests on real TBM sections to investigate the deformation and load bearing capacity of TBM shield tunnel lining in case of fire. They tried to reproduce analytical approximations in order to express the real behavior of the specimens. The specimens were loaded up to the design values and heated according to RABT curve which represents a maximum of

1200 °C temperature and has a duration of 170 minutes. During the tests, concrete and rebar temperatures were measured separately. The analytical model which was set to represent the time history of deformation and load bearing capacity of the tested members consists of two main parts: (1) heat conduction analysis and (2) nonlinear thermal stress analysis. No spalling was observed in the members containing polypropylene fibers. However, there was carbonation effect due to high temperature reaching 1200 °C on the surface of the concrete without any insulation. The carbonation effect was observed only in the layers where temperature went up to 500 °C. It has been also stated that the foundation reactions were not taken into consideration which constitutes the further investigation steps of the study.

Since tunnel fires are rare events, the importance of statistical methods and investigations increases while designing a tunnel lining and its components against fire accidents. In the paper by Richards et al. [22], the optimization criteria in a risk based methodology for optimum tunnel configuration has been evaluated in terms of operational safety, construction cost and schedule, and environmental impact. The risk assessment was performed for three tunnel configurations: (1) twin tube tunnels with single track, (2) monotube tunnels with two tracks, and (3) monotube with two tracks and central dividing wall. The risk concept was based on one of the described principle ALARP (As Low As Reasonably Practicable) which is considered for collective risks. In this approach all risks concerning the users of the system and the environment are taken into account. Risks that are above a certain limit are defined intolerable and those below that limit are within the range of ALARP. According to probability of occurrence and severity the risk was modeled as the product of frequency of occurrence times magnitude of consequences. Major risks were stated as design, construction, and operational risks and mitigation measures were determined according to ALARP category. It was also stated that these mitigation measures should be included in the design state of a certain tunnel project.

In their study Caner et al. [4] developed an approach to evaluate the fire induced damage on tunnel linings. In the paper, fire safety evaluation calculations based on mainly two stages: (1) heat transfer analysis, and (2) nonlinear structural analysis. Time dependent behavior of concrete under fire effect, liner and ground interaction and material degradation have been also taken into account in the analytical models. The capacity and demand curves of a certain tunnel section were plotted under the fire loading together with service loads. It was stated that special care should be paid in the mix design of concrete in order to prevent spalling which is one of the main reason for the strength degradation of the liner. Some suggestions were introduced and techniques stated for the repair procedures of concrete sections, reinforcement, waterproofing, micro-polypropylene fibers, and insulation materials after a tunnel fire. In this thesis, these procedures and analytical techniques will be handled in a broader and more detailed way to suggest on TBM tunnels under certain fire effects.

Bamonte et al. [23] studied thermo-mechanical characterization of concrete mixes suitable for the rehabilitation of fire damaged tunnel linings. The effect of fire on elastic modulus and compressive strength was the main concern of the investigation. Within this frame, three types of concrete specimen, having a strength range between 40 to 75 MPa, containing siliceous, calcareous, and basalt aggregate with three different cement types (limestone, blast furnace, and Portland cement) were tested by heating up to 600 °C in order to evaluate the temperature sensitivity of the samples. Measurements were taken at 20 °C, 200 °C, 400 °C, and 600 °C respectively. It was observed that for all three types of cement the basalt aggregates have contributed to improve concrete residual behavior as compared to other two. The strength loss of concrete made by basalt aggregate was about 50% at 600 °C whereas the strength loss for those made by siliceous and calcareous aggregates were around 65%. It was noted that the concrete grade was also a reason for the change in strength reduction ratios. Normal strength ( $f_c=41-47$  MPa) and

high performance ( $f_c=57-66$  Mpa) concrete samples lost about 60% of their initial compressive strength, while the strength loss in HSC sample ( $f_c=69-75$  MPa) was around 70%. Performed tests revealed that the blended cement provided a better resistance for concrete at high temperatures as compared to Portland cement. As far as the modulus of elasticity was concerned, it was mentioned that siliceous concrete samples lost 84%, calcareous concrete samples lost 78%, and basalt concrete samples lost 73% of their initial values.

As far as the structural fire safety is concerned, use of micro-polypropylene fibers, which will melt during the fire, will increase the permeability of the concrete at temperatures above  $130^\circ\text{C}$ , and will minimize or eliminate the explosive spalling by releasing steam [17, 18, 24, and 25]. One of the disadvantages of the use of micro-polypropylene fibers in concrete mix design may be a reduction in the workability of the concrete [4].

Alternatively, fire-proofing material can be used as well. However, it considerably increases the cost of construction. There are two main concerns with fire-proofing materials: (1) they need maintenance from time to time which brings closure of the tunnel to traffic and (2) vulnerability to moisture content and cyclic wind pressures that develop in tunnel. There are significant durability concerns on the long-term performance of the fire proofing materials [26].

In the light of the studies reviewed and considerations mentioned above, there is a special need for a detailed study and/or method for fire safety evaluations on tunnel liners in general and TBM tunnels in specific.

## **CHAPTER 3**

### **2007-2008 METU EXPERIMENTAL STUDIES**

#### **3.1 Introduction**

Tunnel key segments made of high strength concrete were subjected to 4 hour long hydrocarbon fire. Heat transfer and temperature distribution in a reinforced concrete tunnel segment, and consequent effects of fire as spalling, material degradation, and creep are the main parameters to investigate. Finally, those are compared with the results of analytical calculations presented in Chapter 4.

Three different specimens were tested without load. The tests, including design and construction of special fire test furnace, were conducted with the cooperation and collaboration between Civil Engineering and Mechanical Engineering Departments of METU. The tests were conducted in December 2007 and January 2008 at METU.

#### **3.2 Fire Test Specimen Geometry and Properties**

Three TBM tunnel key segments out of six segments were fire tested. At each test only one parameter (either fire duration or moisture content) was changed. Dimensions of a specimen were measured to be 32 cm high, 150 cm long and maximum 112 cm wide. Approximate weight of the test specimens was 1100 kg. Two of the segments are shown in Figure 3.1. The specified 28 day concrete compressive strength of the specimens was 50 MPa, and minimum tensile strength of reinforcement was 420 MPa. Three

segments were kept as reference specimens which were not subjected to fire and were used to determine the material and strength properties.



Figure 3.1 Precast TBM Key Segments

### **3.2.1 Measured Compressive Strength of Cores Taken from Reference Segment**

Cylindrical concrete cores were taken from reference segments prior to fire test to determine the concrete compressive strength. Cores were measured to have a height of 32 centimeters. Cores were cut into two parts and each part was capped for compression test as shown in Figure 3.2. It shall be noted that the segments were heavily reinforced and most of the tested cores had reinforcement inside them. The results of the core strength tests were corrected according to ATC-33 “NEHRP Commentary on the Guidelines for the Seismic Rehabilitation of Buildings (FEMA Publication 274)” [27] and are shown in Table 3.1.



Figure 3.2 Compressive Strength Tests of Reference Segment Core Samples

Table 3.1 Compressive Strength Test Results of Concrete Prior to Fire Test

Reference Specimens									
Spec. No.	Ø (cm)	H (cm)	Strength (MPa)	Correction Factors [27, 35]					f <sub>c</sub> (MPa)
				F <sub>l/d</sub>	F <sub>dia</sub>	F <sub>r</sub>	F <sub>mc</sub>	F <sub>d</sub>	
1	9.3	17.0	74.2	1.00	1.01	1.00	0.96	1.06	75.7
2	9.3	12.5	72.3	0.95	1.01	1.00	0.96	1.06	70.4
3	9.3	16.0	79.5	0.99	1.01	1.00	0.96	1.06	80.7
Average									75.6

Average compressive strength for the cores was determined to be around 75.6 MPa. This determined value was about 50% higher than the minimum required concrete compressive strength at 28 days, i.e. the selected design value.

### 3.2.2 Measured Tensile Strength of Reinforcement Taken from Reference Segment

Reinforcements (rebar) were extracted from the body of the reference segment by crushing the cover concrete and cutting the reinforcement. There were two different sizes of reinforcements. The reference rebars were determined to have a ductile failure as shown in Figure 3.3. The reference rebars geometric properties and tensile test results are presented in Table 3.2.

As shown in Table 3.2, the average yield strength was determined to be around 462 MPa, which was around 10% higher than the minimum required reinforcement yield strength. For specimen No.4, elongation percentage could not be determined since fracture developed outside the marked range.



Figure 3.3 Tensile Strength Tests of Reference Segment  
Reinforcement Samples

Table 3.2 Tensile Strength Test Results of Reinforcement Prior to Fire Test

Reference Specimens				
Specimen No.	1	2	3	4
Diameter (mm)	10.2	10.2	12.1	12.1
Yield Strength (MPa)	490	479	436	445
Ultimate Strength (MPa)	638	638	602	602
% Elongation	15.5	16.0	16.0	-

### 3.2.3 Determination of Moisture Content and Water Absorption Capacity of Specimens

The moisture content of the reference segment was determined from moisture tests of four different specimens, which were obtained from the reference segment.

The specimens were taken out of the segment immediately after the shipment to the Materials Laboratory of Civil Engineering Department of METU. It was observed that reference segment had around 3.2% moisture content by weight.

The same specimens were tested for water absorption capacity, which was determined to be 3.9% on average. It was concluded that the segments already had high moisture content initially at the shipment. The test results are shown in Table 3.3.

Table 3.3 Moisture Content Test Results of Reference Segment Specimens

Reference Specimens					
Spec. No.	1	2	3	4	Average
Moisture Content (%)	3.30	3.09	3.18	3.09	3.2
Water Absorption (%)	3.76	3.85	4.05	3.77	3.9
Dry Unit Weight (kg/m <sup>3</sup> )	2355	2345	2392	2362	2363
SSD Unit Weight (kg/m <sup>3</sup> )	2444	2435	2489	2451	2455

### 3.3 Fire Test Equipment Setup and Description

A special furnace was designed, and constructed next to Fluid Mechanics Laboratory of Mechanical Engineering Department of METU for the TBM key segment hydrocarbon fire tests. The main structure of the furnace was made of steel beams. The inner face walls of the furnace were insulated by ceramic fiber and rock wool covers. Two inspection windows were placed on the burner side of the furnace and three inspection windows on the front side. The combustion products were exhausted from the chimney at the opposite side of the burner. Also, a flow adjustment device was attached inside the chimney to control and achieve the desired medium temperature to simulate the hydrocarbon fire.

The inner dimensions of the furnace were 130 cm in width, 250 cm in length and 100 cm in height. As for the fire source, an Alarko Lamborghini natural gas burner was used. The test setup is shown in Figure 3.4. The temperature measurements were conducted by means of “K” (chromel–alumel) type thermocouples as shown in Figure 3.5. The nominal temperature ranges of the thermocouples were -270 and 1372 °C [33].



Figure 3.4 Fire Test Furnace



Figure 3.5 “K” (Chromel–Alumel) Type Thermocouples [38]

Placement of the specimen in the furnace and five thermocouples at different depths are shown in Figure 3.6. Continuous data transfer and record from thermocouples to computer were achieved through Elimko E680 Data Logger device and software. The schematic description of the data acquisition system is shown in Figure 3.7.



Figure 3.6 Placements of Thermocouples and Inside of Furnace

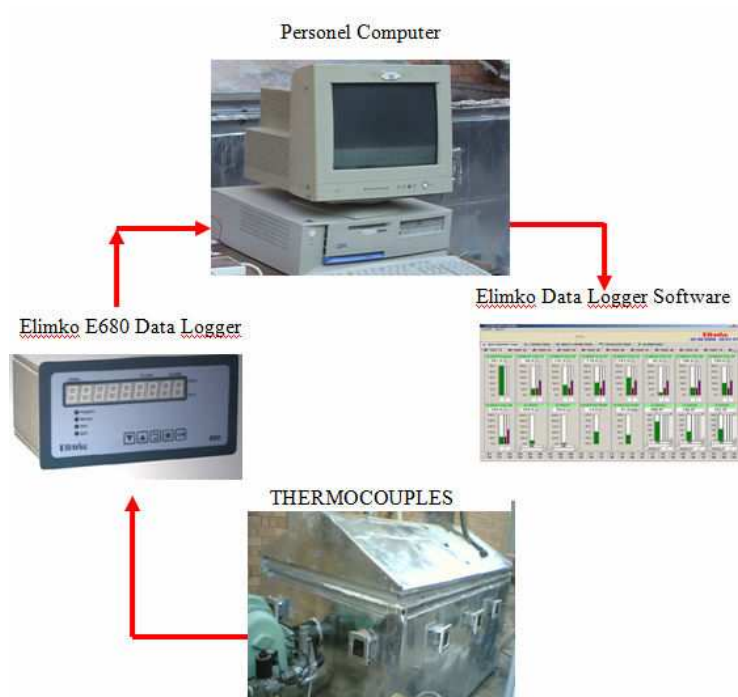


Figure 3.7 Data Acquisition System

### **3.4 Fire Tests of Segments**

As mentioned in the introduction, three fire tests conducted. First test was performed for one hour to check the system and to ensure that the furnace can withstand suspected explosive spalling effects. The second one was tested in a similar way for four hours. The third test was for the water soaked specimen. Segment was fully saturated to increase the probability of explosive spalling. Third test was conducted for four hour hydrocarbon fire. All tests were conducted without external loading, which represent the worst case scenario of tunnel fires.

#### **3.4.1 Test of Specimen at Ambient Conditions for 1 Hour Fire (Test 1)**

The first test fire duration was one hour. Three probes were placed at the top surface of the segment. Two probes were placed at the side about 5 centimeters from the bottom. It was observed that the test set up worked without any problem and very minor explosive spillings were observed during the first 30 minute of Test 1.

#### **3.4.2 Test of Specimen at Ambient Conditions for 4 Hour Fire (Test 2)**

The second hydrocarbon fire test was performed for four hours. The thermocouple probes were placed as shown in Figure 3.8 schematically. The surface temperature of the concrete block was measured at different points and the temperature variation measured at these points was almost identical, except for small variations due to thermal cracks. The temperature variation near the bottom side of the concrete block was also measured. The low thermal conductivity of the concrete made the concrete block a good insulator and high temperature on the flame exposed surface could not penetrate into the concrete significantly. Concrete surface temperature

reached steady state in an hour as shown in Figure 3.9. General behavior of the temperature variation was close to hydrocarbon curve.

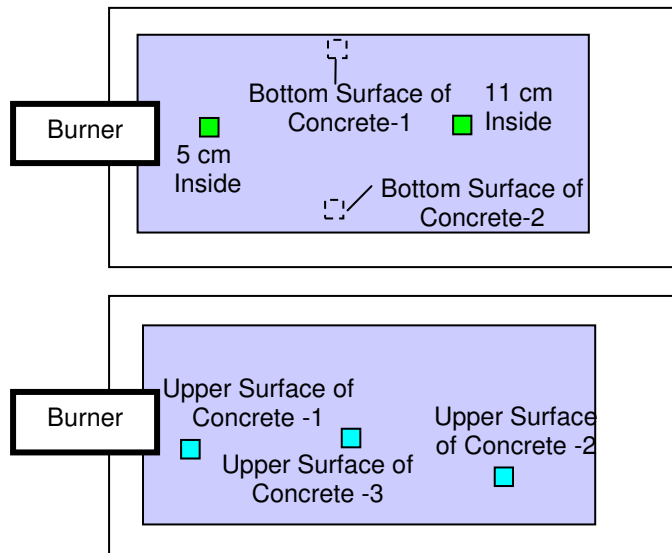


Figure 3.8 Placements of Thermocouples in Plan View (Test 2)

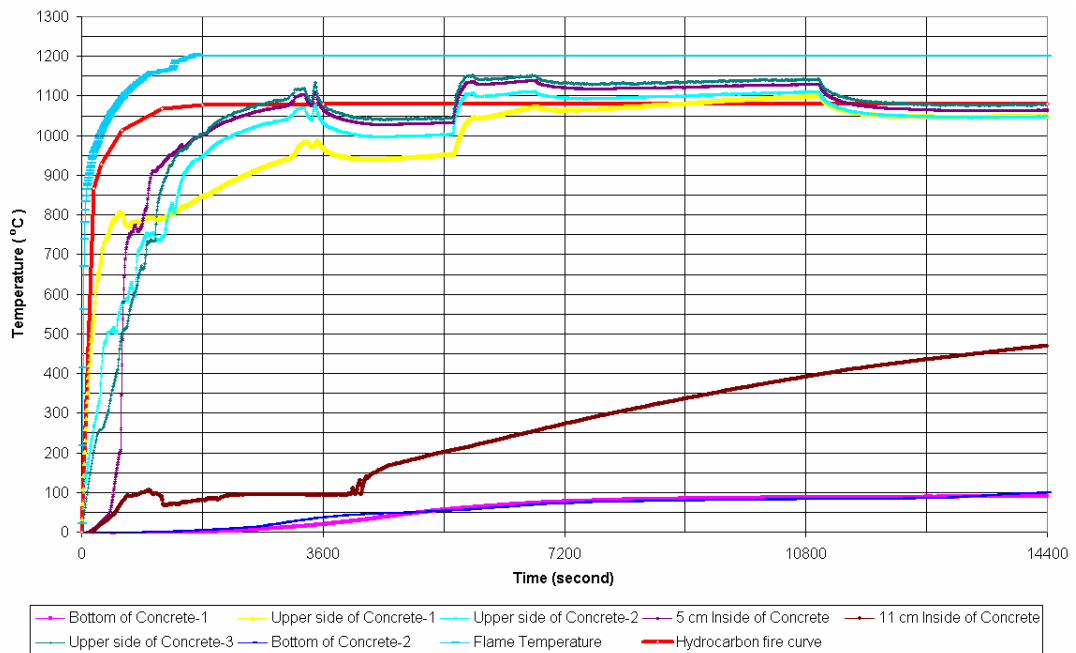


Figure 3.9 Temperature Records (Test 2)

### 3.4.3 Test of Fully Saturated Specimen for 4 Hour Fire (Test 3)

The third test was performed for fully saturated specimen under hydrocarbon fire again. Inside view of the furnace and concrete surface during Test 3 is shown in Figure 3.10. The thermocouple locations are shown in Figure 3.11. Surface temperature of the concrete block reached steady state around ninety minutes which was slightly longer than the experiment results as depicted in Figure 3.9. Unlike Test 2 results, lower temperatures were obtained for fully saturated concrete block.



Figure 3.10 Concrete Face and Inside of Furnace (Test 3)

Temperatures were slightly higher than 1080 °C, which was around the maximum value for hydrocarbon fire: 1100 °C. The general behavior of the temperature variation of the concrete block was close to the hydrocarbon fire curve. The top and bottom surface temperature of the concrete block was measured at various points in the same way as Test 2. During this test, the 11 cm probe came out of its original position and started to read surface temperatures at the early stages of the fire as depicted in Figure 3.12.

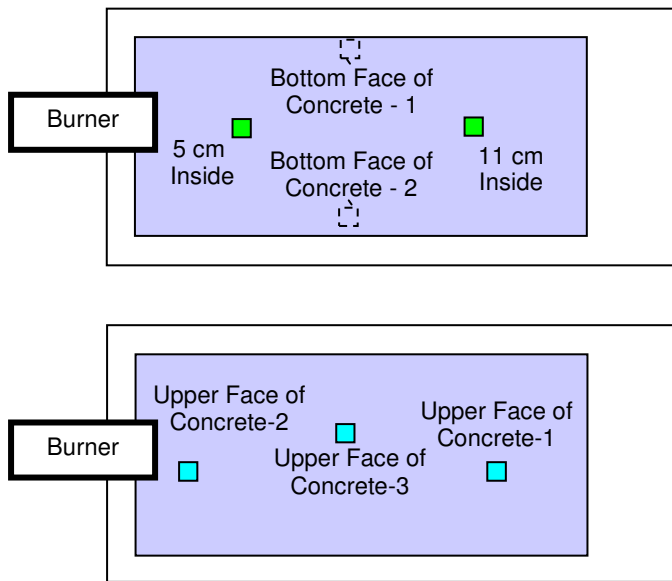


Figure 3.11 Placements of Thermocouples in Plan View (Test 3)

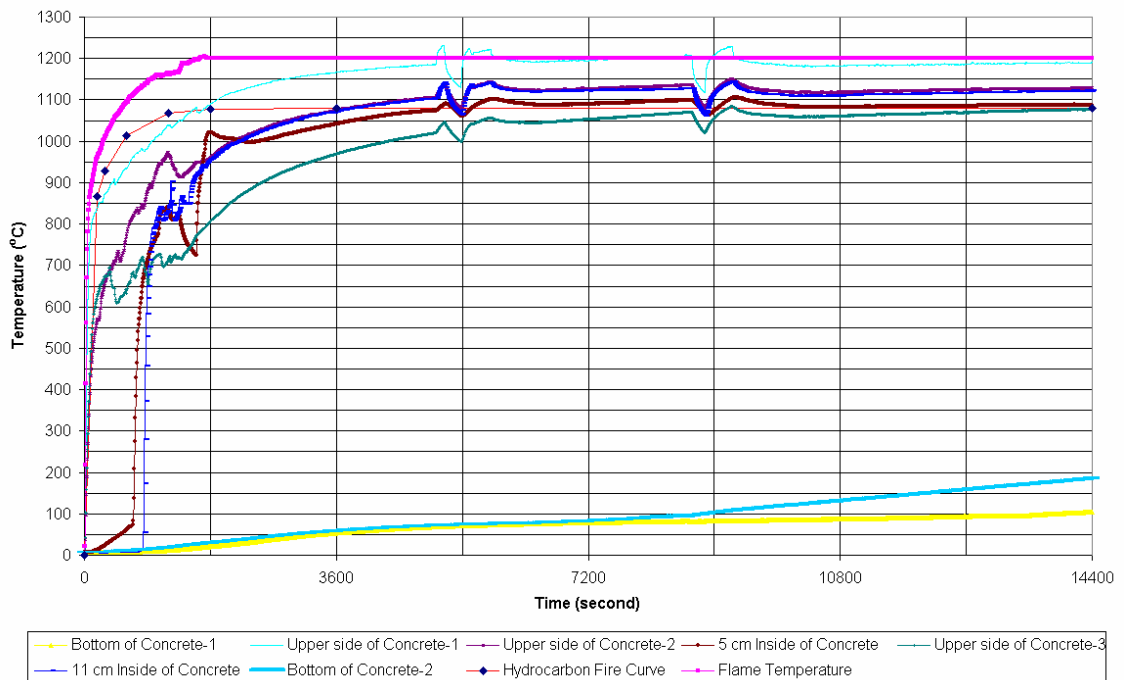


Figure 3.12 Temperature Records (Test 3)

### 3.5. Post Fire Evaluations

In post fire evaluation, concrete spalling, colorization at height of cores, fire touched rebar strength tests and concrete strain distribution were studied.

#### 3.5.1 Concrete Spalling and Colorization

Surface of segments were examined to determine the level of spalling. Spalling mostly developed at locations that were touched by flames. For Test 1, the spalling was around 1 to 2 centimeters on the surface as shown in Figure 3.13. Reinforcement was not exposed and no surface cracking was observed.

For both four hour fire test segments with different moisture contents presented in Table 3.4, similar concrete spalling of maximum range of 2 to 4 centimeters was observed locally. On average, spalling was 2 centimeters as shown in Figures 3.14 and 3.15. The clear cover was lost at a couple of locations and about 10% of reinforcements were exposed. Again no surface cracking was observed for either test.

Table 3.4 Moisture Contents of Specimens before Fire Test

Specimen No.	Fire Duration	Moisture Content
1 (Test 1)	1 hr	3.2%
2 (Test 2)	4 hr	3.2%
3 (Test 3)	4 hr	3.5%



Figure 3.13 Spalling of Specimen (Test 1)



Figure 3.14 Spalling of Specimen (Test 2)



Figure 3.15 Spalling of Specimen (Test 3)

The concrete cores taken from segments indicated that the colorization happened within the first 3 to 4 centimeters for one hour tested segment and within the first 5 to 6 centimeters for four hour tested segments as shown in Figure 3.16 and 3.17.



Figure 3.16 Colorization after Test 1



Figure 3.17 Colorization after Test 2 and Test 3

### 3.5.2 Concrete Strain Distribution

Sample cores were taken from the fire damaged segments. It was observed that the cores had internal cracking. The FIRECAP analyses were in good agreement with test observations as shown in Figure 3.18. The particular reason for cracking can be explained as follows: The hot surface layers want to expand more than the cooler layers inside the concrete at the early stages of the fire. The cooler layers try to restrain the expansion of the layers close to the hot surface. In such a case, cooler internal layers are under tension and crack internally. However, at the later stages of the fire, visually observed cracks, as can be seen from the Figure 3.19, are minimized in the internal layers subject to compression.

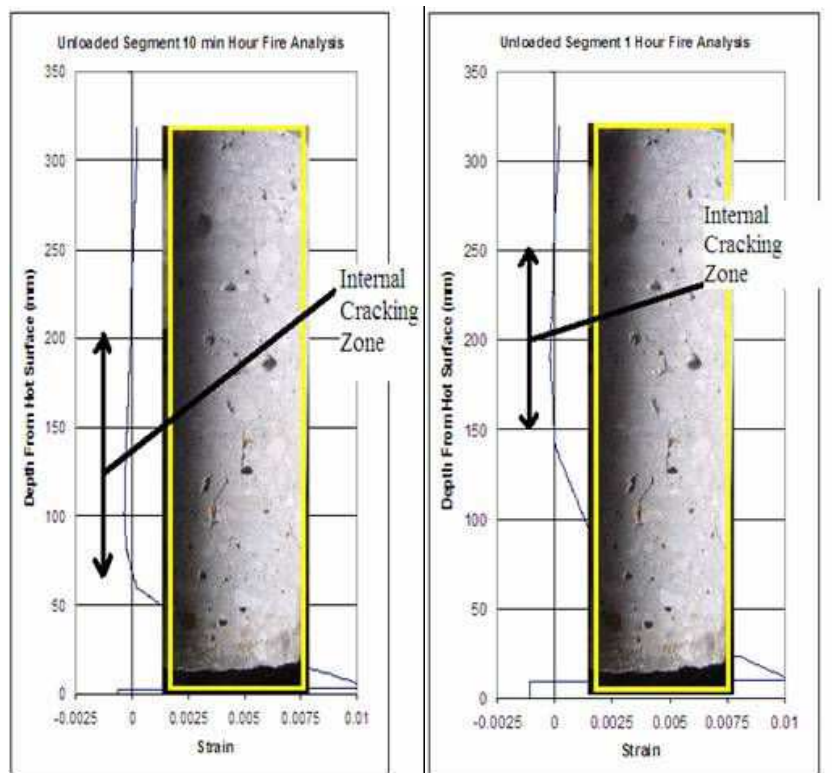


Figure 3.18 Concrete Strain Distributions within First Hour

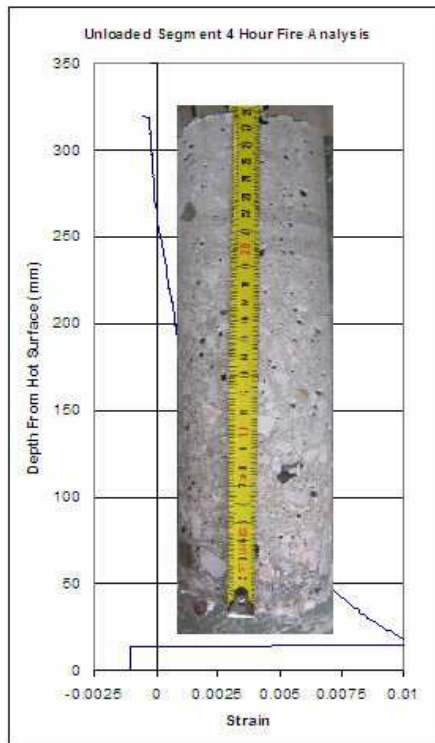


Figure 3.19 Concrete Strain Distributions at the End of Fourth Hour

Such internal cracking will be minimized or eliminated in case of an axially loaded segment. The segments of TBM rings have all initial compressive stresses due to external loads such as earth pressure and hydrostatic pressure at their existing locations. The FIRECAP analysis of loaded segments indicated that the internal cracking is minimized or eliminated in most of the cases when the segments have initial compressive stresses as in the real life case. Both et al. (2003) observed similar results in their study [31]. The fire tests were done in an unloaded state with no initial compressive stresses applied to the key segment which represent the worst case for internal cracking.

At high temperatures concrete can develop 0.011 compressive crushing strain [10, 30]. About this limit concrete is going to spall. Externally applied loads develop on average 0.001 compressive strain, which is only 9% of ultimate strain capacity. The external loads will increase the depth of spalling just slightly, in the order of 2 mm on average for the tests conducted at METU.

### **3.5.3 Concrete Compressive Strength and Reinforcement Tensile Strength at the Damaged Sections**

Cores taken from Test 1, Test 2, and Test 3 segments were tested under compression. The cores were cut into two parts as top and bottom. Top-1 core was taken from the section close to the hot surface and Bottom-1 from cooler part of Test 1 segment. Top-2 and Bottom-2 can be defined in the same way for Test 2.

For top cores, damaged and colorized depths indicated in Table 3.5 were separated from the top part. The compressive strength test results of fire exposed concrete are presented in Table 3.6. According to the tests, the top cores were weaker than the bottom cores as expected.

Table 3.5 Summary of Depth of Damaged and Spalled Concrete

Fire Duration	Depth of Damaged and Spalled Concrete
1 Hour Fire	~4 cm
4 Hour Fire	~11 cm

Per ACI 216, repair limit for concrete cooled from 380 °C, are those parts having less than 50% of initial  $f_c'$ . It is necessary to replace the concrete layer below this compressive strength value. Compressive strength tests of specimens showed that in any case the concrete compressive strength were much higher than the target concrete strength of 37 MPa., based on initially measured compressive strength of concrete ( $f_c'$ ): 75 MPa. However, the design specified concrete strength, 50 MPa, was allowed to degrade down to 25 MPa not to have any repairs per ACI 216.

Table 3.6 Compressive Strength Test Results of Fire Exposed Concrete

Cores from Fire Damaged Segments									
Spec No	Ø (cm)	H (cm)	Strength (MPa)	Correction Factor [27, 35]					$f_c$ (MPa)
				$F_{l/d}$	$F_{dia}$	$F_r$	$F_{mc}$	$F_d$	
Bottom 1	9.3	12.0	69.1	0.94	1.01	1.08	0.96	1.06	72.0
Bottom 2	9.3	11.0	54.1	0.92	1.01	1.08	0.96	1.06	54.9
Top 1	9.3	8.5	55.4	0.86	1.01	1.08	0.96	1.06	52.6
Top 2	9.3	9.5	48.3	0.88	1.01	1.13	0.96	1.06	49.3

It shall be noted that cores had visible internal cracks at only mid height as predicted analytically also. The segments were tested in a very undesirable condition at an unloaded state with flames touching its surface for four hours. The flame temperatures were about 10% higher than the hydrocarbon fire temperatures.

The reinforcement taken from the fire-tested segments were adversely affected from the fire but did not lose their ductility. The related test results of reinforcements are presented in Table 3.7. For specimens 2 and 3,

elongation percentages could not be determined since fracture developed outside the marked range.

Table 3.7 Tensile Strength Test Results of Fire Exposed Reinforcement

Samples Taken From Fire Tested Specimens			
Specimen No.	1	2	3
Diameter (mm)	9.9	9.9	12.1
Yield Strength (MPa)	455	446	455
Ultimate Strength (MPa)	728	734	595
% Elongation	15.0	-	-

### 3.6 Micro Level Investigation of Concrete Before and After Fire

Concrete pieces taken from fire tested and reference segments were also investigated on micro level. There were four main samples on investigation: (1) reference segment pieces, (2) one hour fire segment pieces, Test 1, (3) four hour fire segment pieces, Test 2, and (4) four hour fire segment pieces, Test 3. Fire tested segment samples were taken from the fire damaged surface zones, but not from cooler inner parts.

General views of the reference sample by electron microscope and the chemical compounds are presented in Figure 3.20, 3.21, and 3.22. Calcium silicate hydrate gels (C-S-H), the main cementitious compound, and calcium hydroxide gels (C-H) are clearly visible in Figure 3.20 and 3.21 respectively.

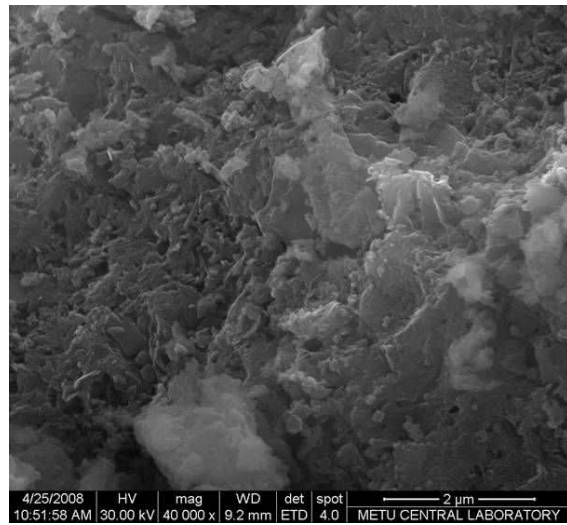


Figure 3.20 Calcium Silicate Hydrate Gels (C-S-H)

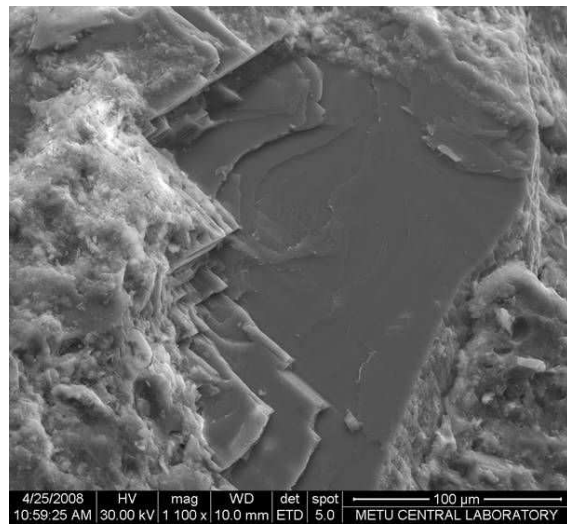


Figure 3.21 Calcium Hydroxide Gels (C-H)

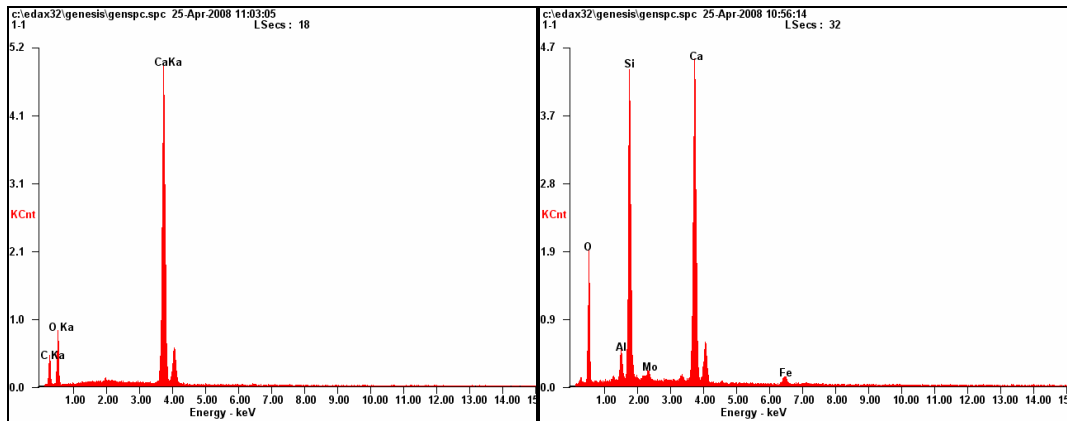


Figure 3.22 Reference Segment Chemical Compounds  
(C-S-H and C-H Gels)

For the one hour and four hour fire concrete specimen (Test 1 and 2), the surface texture of the microstructure deteriorated as presented in Figure 3.23 and 3.24. Chemically bound water of C-S-H and C-H gels decreased or even disappeared after 300 °C. Beyond this limit, deterioration in the chemical form of concrete and decomposition of C-S-H gels occur [37]. For the four hour fire test of saturated specimen (Test 3) C-H gel formations were also severely affected by fire as can be seen in Figure 3.25. After 530 °C, decomposition of C-H gels take place in the concrete and consecutive volumetric contraction becomes more dominant and effective [37].

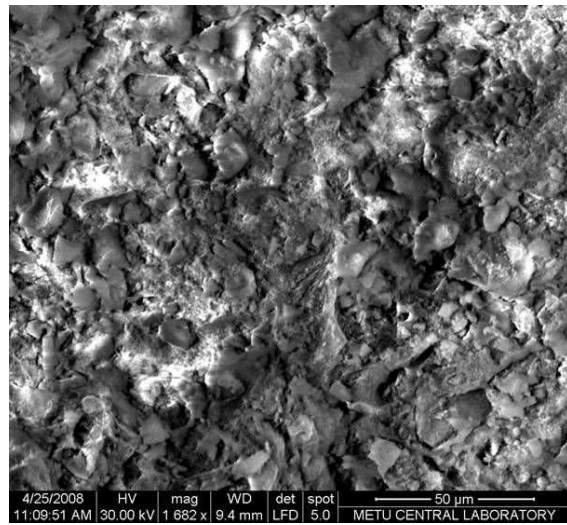


Figure 3.23 Chemical Decomposition of C-S-H Gels (Test 1)

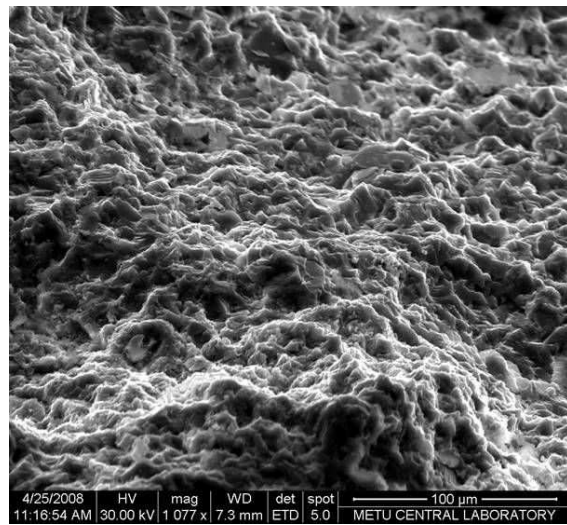


Figure 3.24 Chemical Decomposition of C-S-H Gels (Test 2)

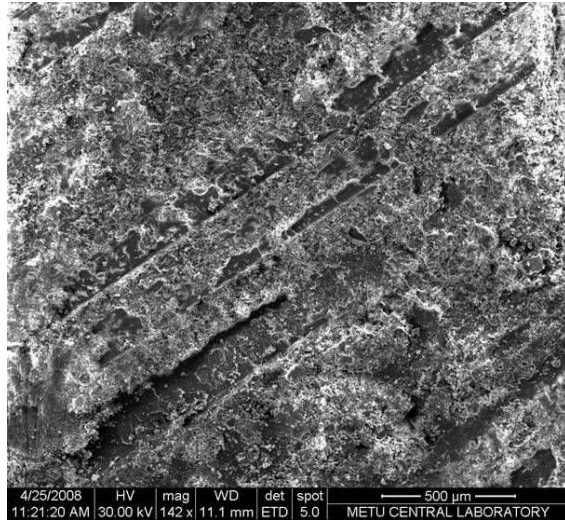


Figure 3.25 Decomposed C-H Gels (Test 3)

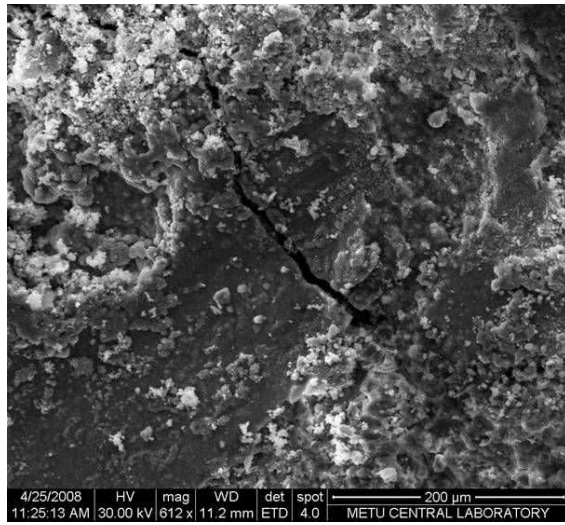


Figure 3.26 Cracked Concrete Textures (Test 3)

Beyond 530 °C, volumetric contraction due to decomposed C-H gels may go up to 33% [37]. As can be seen in Figure 3.26 and 3.27, micro cracks were apparent within fire tested segments. Crack widths were measured between to be 5 to 9 μm after fire.

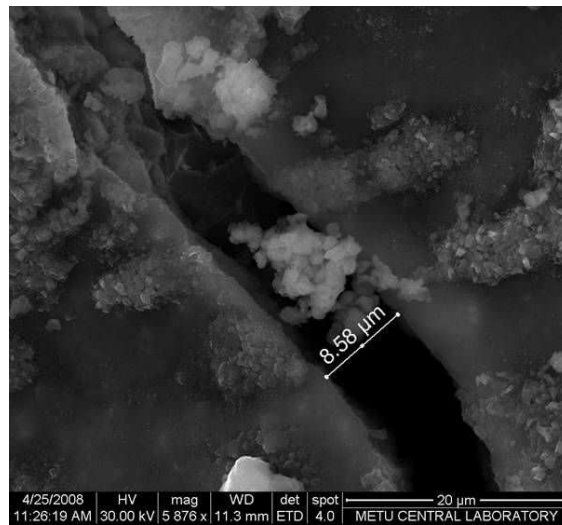


Figure 3.27 Micro Crack Opening (Test 3)

## CHAPTER 4

### PARAMETRIC ANALYSES AND NUMERICAL RESULTS

#### 4.1 Introduction

TBM tunnels are analytically investigated under two different fire scenarios: Harmonized Hydrocarbon Fire for four hour rating, and Rijkswaterstaat Hydrocarbon Fire (RWS) for two hour rating. The selected sections represent the typical TBM tunnel properties.

Heat transfer analysis is used to determine temperature penetration into concrete utilizing RADTHERM software. Non-linear strain distribution computation including material nonlinearity, degradation and creep effects are performed using FIRECAP program. Nonlinear time dependent structural analysis including material degradation and ground-lining interaction is performed using LARSA 4D software. Algorithm of the structural fire analysis is presented in Figure 4.1.

Thirty six different rings are investigated within the body of this section. Subgrade reaction modulus,  $k_s$ , ratio of lining radius to thickness,  $R/t$ , and depth of lining,  $h$ , are the main variables. The structural analysis is performed at different stages of the fire on thirty-six different models for two fire scenarios, totaling seventy-two analyses with four hundred and sixty eight time stages.

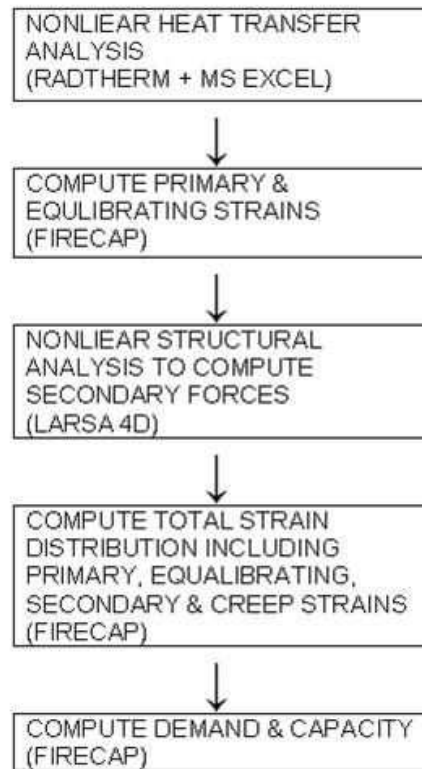


Figure 4.1 Algorithm of Fire Analysis

Characteristic compressive strength of concrete,  $\sigma_{ck}$ , at 28-days is 50 MPa, elastic modulus of concrete,  $E_c$  is 18,500 MPa; and tensile yield strength of steel,  $\sigma_y$ , is 420 MPa and elastic modulus of steel,  $E_s$ , is 200,000 MPa. Concrete mix design mainly has calcium carbonate as aggregate.

#### 4.2 Heat Transfer Analysis

The first step in the fire evaluation is non-linear heat transfer analysis. The concrete lining and soil are modeled to simulate a one dimensional heat transfer analysis utilizing RADTHERM software. The model is shown in

Figure 4.2. The surrounding soil layer serves as a heat sink in the calculations.

The source of an extreme tunnel fire is mostly represented by two different curves, a harmonized hydrocarbon curve for a four hour fire rating with a peak temperature of 1100 °C and a RWS curve for a two hour fire rating with a peak temperature of 1350 °C. These curves show unventilated state of the tunnel [4]. Hydrocarbon and RWS fire curves are presented in Figure 4.3.

Non-linear heat transfer analysis includes temperature dependent thermal properties of concrete: thermal conductivity ( $k$ ) measured in  $W * m^{-1} * K^{-1}$  (SI units), specific heat ( $c$ ) measured in  $J * Kg^{-1} * K^{-1}$  (SI units), and thermal expansion coefficient ( $\alpha_T$ ), a dimensionless quantity. These parameters are a function of temperature, aggregate type and/or composition of concrete mix design [28, 29, and 30].

Calculation of thermal conductivity is performed according to Equations 4.1 and 4.2. For temperatures between  $1000 < T < 1300$  °C, thermal conductivity is assumed decreasing linearly from 0.21 to 0.07 due to poor material properties. For this range concrete loses its conductive property and becomes poor conductor.

$$0 < T < 300 \text{ } ^\circ\text{C} \quad \longrightarrow \quad k = 2.0 - 0.0013 * T \quad (4.1)$$

$$300 < T < 1000 \text{ } ^\circ\text{C} \quad \longrightarrow \quad k = 2.21 - 0.002 * T \quad (4.2)$$

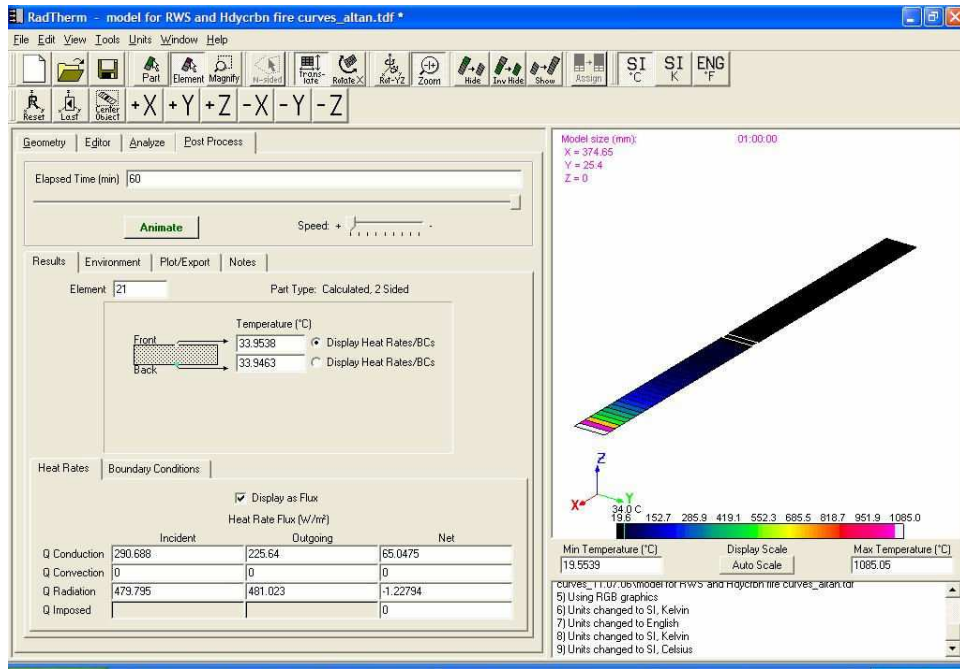


Figure 4.2 Heat Transfer Analysis Model

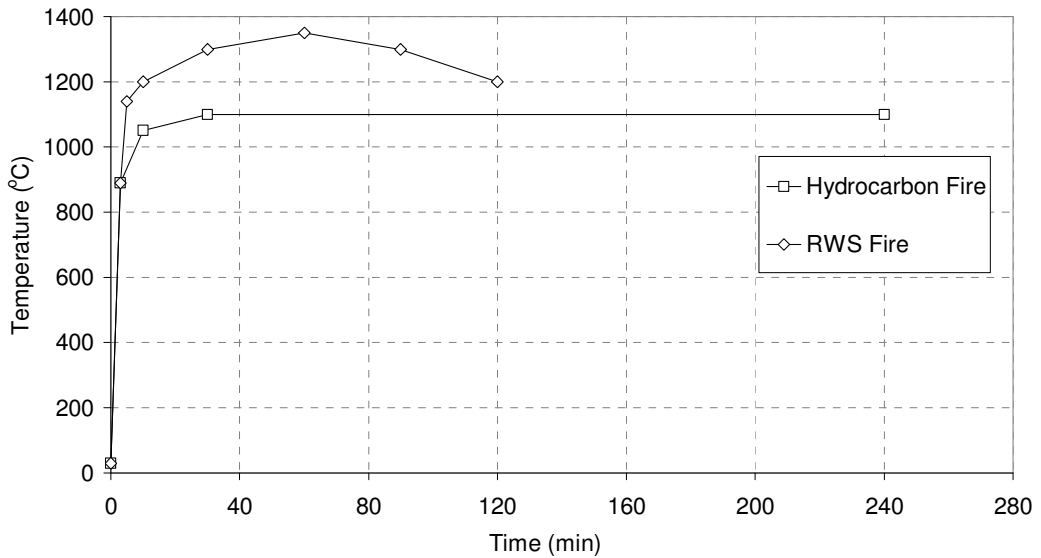


Figure 4.3 Induced Hydrocarbon and RWS Fire Curves

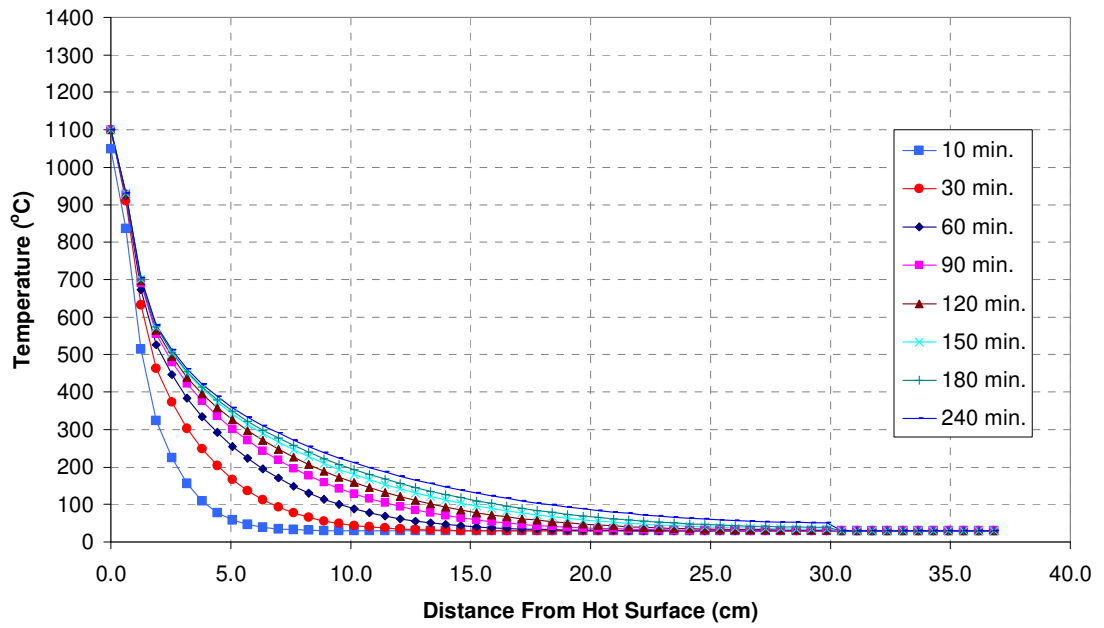
For the nonlinear heat transfer analysis, concrete segment is divided into fifty layers and thermal conductivity and specific heat values for each layer are assigned as the values for 30 °C initially. Then fire is applied to the inner face of the lining for a specific time. At the end of each time step, thermal conductivity and specific heat values of each layer is modified until they converge to a constant value.

Layer temperatures are determined at 10, 30, 60, 90, 120, 150, 180, and 240 minutes for hydrocarbon fire curve and layer temperatures are calculated at 10, 30, 60, 90, and 120 minute time stages for RWS fire curve. Temperature distribution inside concrete segment due to fire curves under consideration is shown in Figure 4.4.

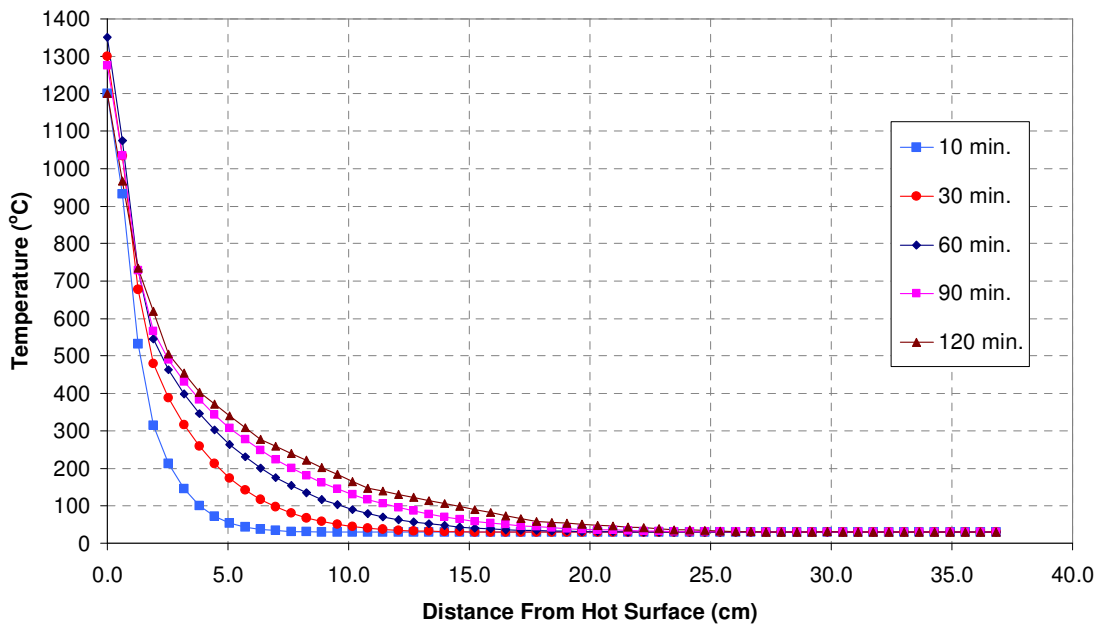
### **4.3 Computation of Primary, Equilibrating and Creep Strains**

Primary, equilibrating, creep and secondary strains are computed at different stages of fire. As the second step of the algorithm, the non-linear strain distribution computation including material nonlinearity, degradation and creep effects is performed using FIRECAP program.

Initial strains (primary strains) develop due to temperature penetration into concrete. A reinforced concrete section analysis considering material degradation including spalling is performed in this step to determine primary forces. Material strength of concrete and steel are reduced during fire [30].



(a)



(b)

Figure 4.4 Temperature Penetrations into Concrete Lining (a) Harmonized Hydrocarbon Fire for 4 Hour Rating, (b) Rijkswaterstaat Hydrocarbon Fire for 2 Hour Rating

Equilibrating strains are determined in second step of computation. The equilibrating strains are developed due to the fact that, cooler layers do not want to expand as much as hot layers induced by initial thermal strains. Therefore, cooler layers will restrain the expansion of hot layers and result in equilibrating strains at the cross-section of a lining. This effect is taken into consideration with a section analysis performed by FIRECAP. Creep strains are computed based on recommendations of ACI 216 [30].

#### **4.4 Structural Analysis and Computation of Secondary Strains**

Elastic field equations are fully applicable to solutions of tunnel problems. However, analytical closed form solutions to 3-D problems are sometimes difficult and time consuming to solve. In case of an axisymmetry or two dimensionality the forms and the solutions can be simplified relatively. An elasticity problem is two dimensional if field quantities such as stress and displacement are depend only on two coordinates, i.e.  $(x, y)$  as shown in Figure 4.5. If the body forces and tractions on the boundaries  $x$  and  $y$  are independent of  $z$  coordinate, then all the deformations can be expressed as Equation 4.3:

$$u = u(x, y), \quad v = v(x, y), \quad w = 0 \quad (4.3)$$

where,  $u$  and  $v$  are displacements in  $x$  and  $y$  coordinates respectively and  $w$  is the displacement in  $z$  direction. Consequently, the stresses develop in three principal axis depend only on strains in  $x$  and  $y$  directions, making it a plane strain problem [39, 40].

In tunnel design history, many tunnels were designed without use of computer programs. If there is no change in geometry for a certain length, engineers select to design tunnels in 2-D as a plane strain problem. As stated earlier, design is not governed by loads but by construction

requirements. A sophisticated 3-D analysis will not be feasible since geotechnical reports do not have a continuous investigation of soil conditions along the length of tunnel but only at selected stations. Under such uncertainty a two dimensional analysis is as good as a three dimensional analysis for a running tunnel with a constant section. Two dimensional ring analysis of a TBM section having 1.5 meters length is investigated in this step.

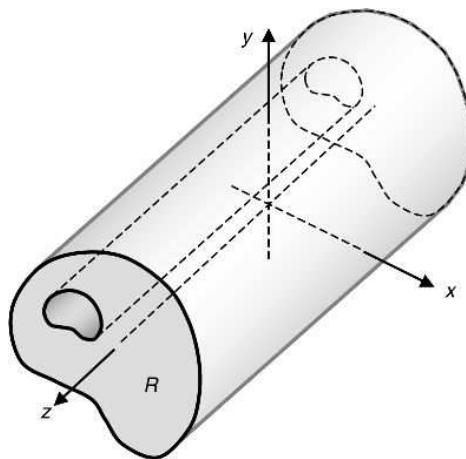


Figure 4.5 Long Cylindrical Body Representing Plane Strain Conditions [39]

Basically, there are four main parameters of the analytical models under consideration: subgrade reaction modulus,  $k_s$  ( $\text{kN/m}^3$ ), radius of the lining,  $R$  (m), thickness of the lining,  $t$  (m), and depth of the lining from the ground surface,  $h$  (m), as mentioned previously. As a combination of these parameters, thirty six models are formed. Investigated TBM tunnels together with related sectional and geometrical properties and loading conditions are presented in Table 4.1.

Table 4.1 Investigated Tunnel Sections

Tunnel Type	Inner Radius (m)	Lining Thickness (m)	H (m)	H <sub>w</sub> (m)	P <sub>v</sub> (kN/m)	P <sub>lt</sub> (kN/m)	P <sub>lb</sub> (kN/m)	P <sub>wsl</sub> (kN/m)
S3.30.010	2.85	0.30	15	11.5	350	240	310	145
S3.30.125	2.85	0.30	15	11.5	350	240	310	145
S3.30.240	2.85	0.30	15	11.5	350	240	310	145
S3.36.010	2.82	0.36	15	11.5	350	240	310	145
S3.36.125	2.82	0.36	15	11.5	350	240	310	145
S3.36.240	2.82	0.36	15	11.5	350	240	310	145
S4.30.010	3.85	0.30	15	10.5	350	240	310	145
S4.30.125	3.85	0.30	15	10.5	350	240	310	145
S4.30.240	3.85	0.30	15	10.5	350	240	310	145
S4.36.010	3.82	0.36	15	10.5	350	240	310	145
S4.36.125	3.82	0.36	15	10.5	350	240	310	145
S4.36.240	3.82	0.36	15	10.5	350	240	310	145
M3.30.010	2.85	0.30	45	52.5	360	230	305	555
M3.30.125	2.85	0.30	45	52.5	360	230	305	555
M3.30.240	2.85	0.30	45	52.5	360	230	305	555
M3.36.010	2.82	0.36	45	52.5	360	230	305	555
M3.36.125	2.82	0.36	45	52.5	360	230	305	555
M3.36.240	2.82	0.36	45	52.5	360	230	305	555
M4.30.010	3.85	0.30	45	51.5	360	230	305	555
M4.30.125	3.85	0.30	45	51.5	360	230	305	555
M4.30.240	3.85	0.30	45	51.5	360	230	305	555
M4.36.010	3.82	0.36	45	51.5	360	230	305	555
M4.36.125	3.82	0.36	45	51.5	360	230	305	555
M4.36.240	3.82	0.36	45	51.5	360	230	305	555
D3.30.010	2.85	0.30	75	106	395	205	315	1090
D3.30.125	2.85	0.30	75	106	395	205	315	1090
D3.30.240	2.85	0.30	75	106	395	205	315	1090
D3.36.010	2.82	0.36	75	106	395	205	315	1090
D3.36.125	2.82	0.36	75	106	395	205	315	1090
D3.36.240	2.82	0.36	75	106	395	205	315	1090
D4.30.010	3.85	0.30	75	105	395	205	315	1090
D4.30.125	3.85	0.30	75	105	395	205	315	1090
D4.30.240	3.85	0.30	75	105	395	205	315	1090
D4.36.010	3.82	0.36	75	105	395	205	315	1090
D4.36.125	3.82	0.36	75	105	395	205	315	1090
D4.36.240	3.82	0.36	75	105	395	205	315	1090

For the tunnel type abbreviation shown in the first column, the first letter indicates depth level: S for shallow region, M for medium region, and D for deep region. The first number indicates radius of ring: R=3.0 m and R=4.0 m. The second number indicates thickness of lining: t=0.30 m and t=0.36 m. The third number indicates the subgrade reaction modulus:  $k_s=10,000 \text{ kN/m}^3$ ,  $k_s=125,000 \text{ kN/m}^3$  and  $k_s=240,000 \text{ kN/m}^3$ .

The thicknesses of the lining, i.e. t=0.30 and t=0.36 m., are chosen as 8-10% of lining radius, R=3.0 and R=4.0 m., which is a practical application in industry. The selected subgrade reaction modulus values,  $k_s$ , are representative for soil-structure interaction for TBM tunnels. The range of tunnel depths from ground surfaces is typical and at these depths, tunnel lining will be subjected to axial forces that will develop 0.1 \*  $f_c'$  to 0.3 \*  $f_c'$  axial compressive strength capacity of concrete. Such variation in depth simulates shallow and deep tunnel situations.

Nonlinear time dependent structural analysis including material degradation and ground lining interaction is performed using LARSA 4D software. A typical loading scheme is shown in Figure 4.6.

The global model of ring includes the lining-ground interaction. The lining ring is modeled by beam elements and the ground is modeled by compression only spring elements as shown in Figure 4.7. The stiffness of the spring elements is based on the subgrade reaction modulus of the surrounding soil.

Secondary strains determined from global model develop due to lining structural response to equilibrating strains is the third step. In this structural response analysis at global level, section and material properties are based on heat induced material degradation. Geometric non-linearity is also included in the analysis.

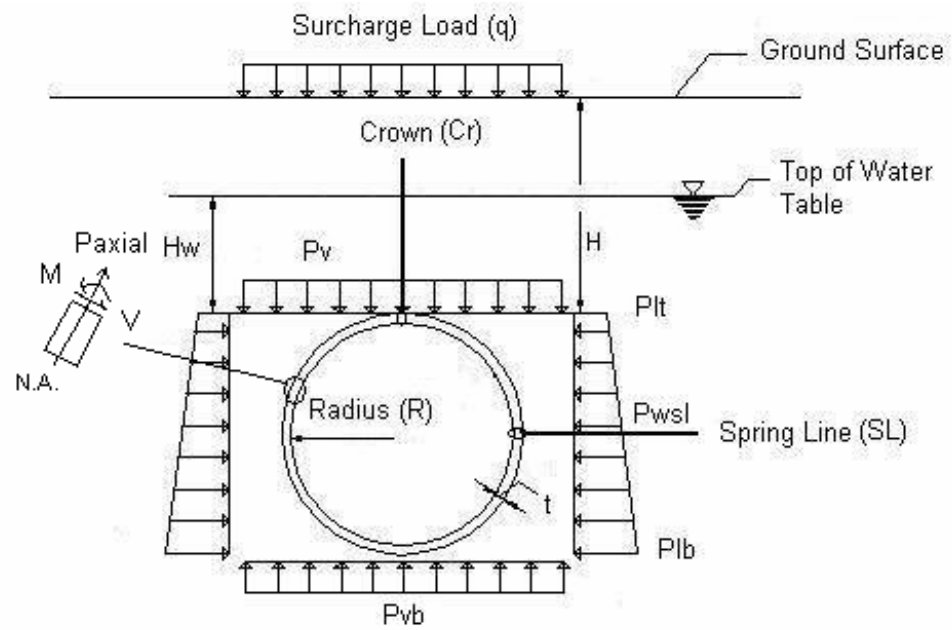


Figure 4.6 Typical Service Loads on a TBM Tunnel

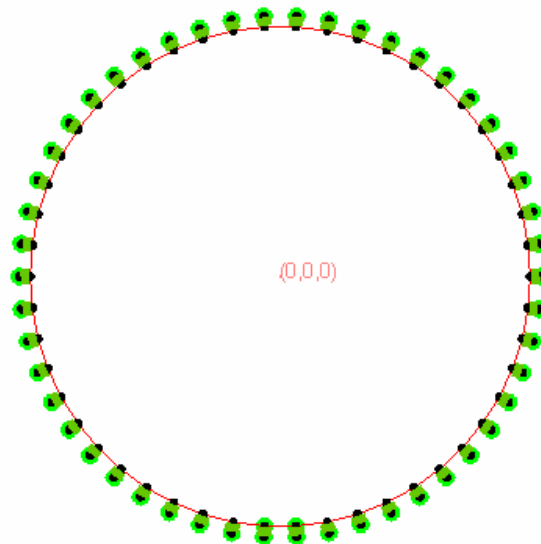


Figure 4.7 2D Beam-Spring Model of a TBM Tunnel Lining

A typical deformation pattern of the lining in the fire time steps of analysis is shown in Figure 4.8. For the representation purpose, only deformed shapes of S3.30.010 tunnel analyzed for hydrocarbon fire simulation are presented. The segment has a tendency to expand into soil. Segment joint locations become clearer at long duration fires.

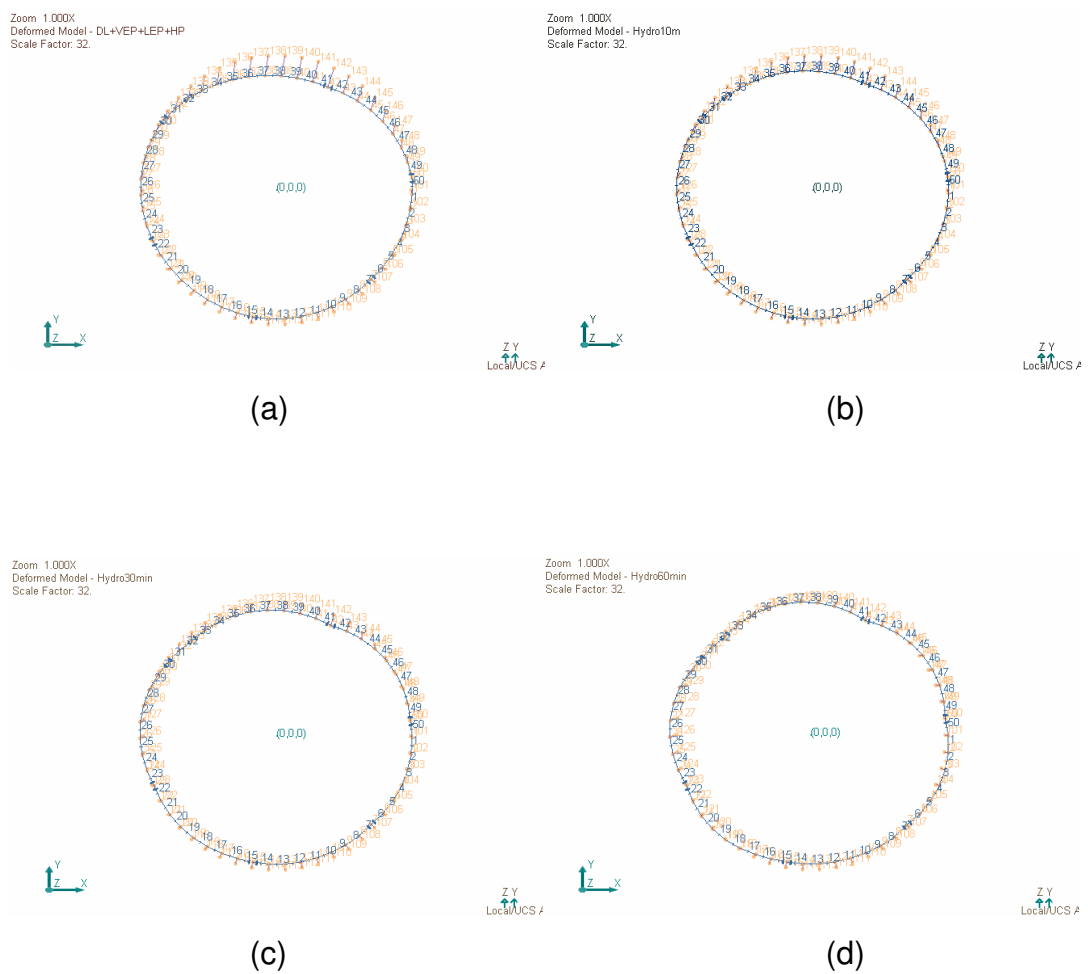
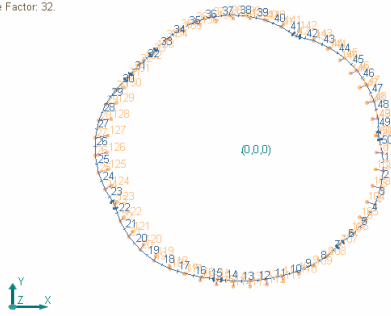


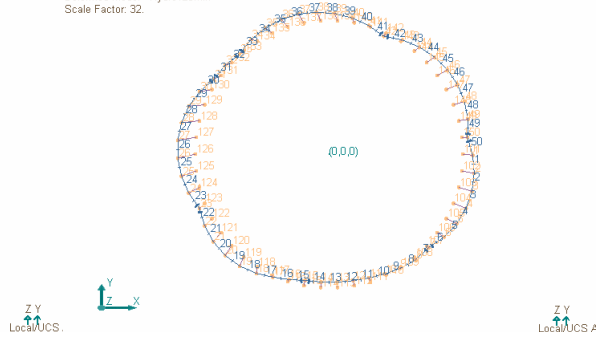
Figure 4.8 Deformed Shape of S3.30.010 (a) t = 0 min., (b) t = 10 min., (c) t = 30 min., (d) t = 60 min.,

Zoom 1.000X  
Deformed Model - Hydro00min  
Scale Factor: 32.



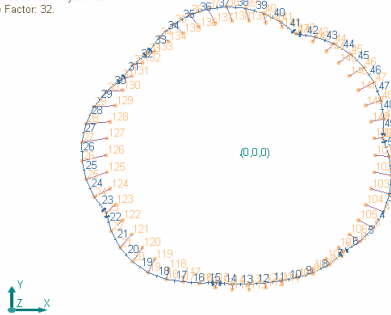
(e)

Zoom 1.000X  
Deformed Model - Hydro120min  
Scale Factor: 32.



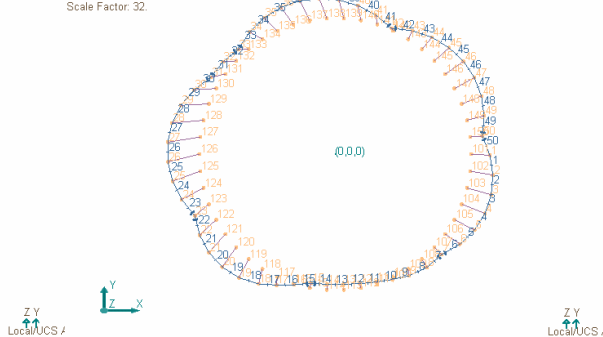
(f)

Zoom 1.000X  
Deformed Model - Hydro150min  
Scale Factor: 32.



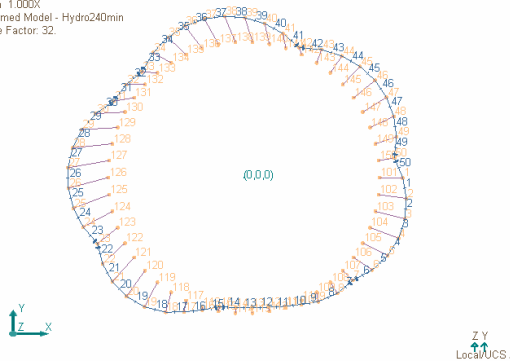
(g)

Zoom 1.000X  
Deformed Model - Hydro180min  
Scale Factor: 32.



(h)

Zoom 1.000X  
Deformed Model - Hydro240min  
Scale Factor: 32.



(i)

Figure 4.8 (Continued) Deformed Shape of S3.30.010 (e)  $t = 90$  min.,  
(f)  $t = 120$  min., (g)  $t = 150$  min., (h)  $t = 180$  min. (i)  $t = 240$  min.

## 4.5 Computation of Total Strain Distribution

In the fourth step, all primary, equilibrating, secondary and creep strains are added to evaluate the total strain distribution of the section. For this purpose, FIRECAP is utilized again. Total strain components and distribution are shown in Figure 4.9.

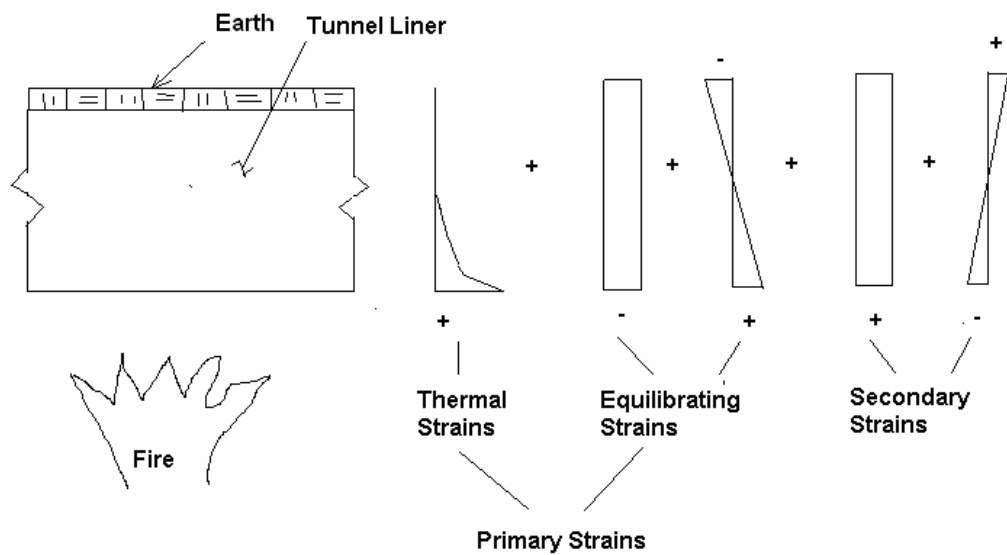


Figure 4.9 Total Strain Distribution [4]

## 4.6 Computation of Capacity and Demand

In fire safety evaluations, the following load combination is used:

$$1.0 \text{ DL} + 1.0 (\text{HL}+\text{PL}) + 1.0 (\text{FL}(t)) = R_u(t) < \phi_r R_{nr}(t) \quad (4.4)$$

where, DL is the dead load, HL is the hydrostatic load, PL is the earth pressure, FL(t) is the fire induced structural load at the investigated time of the fire,  $\phi_r$  is the resistance factor (= 1.0 for extreme events per ACI ( 2001)) and  $R_{nr}(t)$  is the reduced capacity due to material degradation at the investigated time of the fire.

Design load combinations develop stresses as much as 10%, 20% and 30% of  $fc'A_c$  at shallow, medium and deep depth tunnel sections respectively where  $fc'$  is the compressive strength of concrete including material factor and  $A_c$  is the cross-sectional concrete area of the section.

In general, axial compressive forces are more significant than bending terms in design of circular tunnel linings. The time-dependent axial load capacity can be taken as:

$$Pn(t) = 0.60 \int fc_{ti} A_{ti} dA \quad (4.5)$$

where,  $Pn(t)$  is the reduced axial load capacity,  $fc_{ti}$  is the reduced compressive strength of the concrete layer and  $A_{ti}$  is the reduced area of the corresponding layer at time t, a stage of fire. The axial load capacity defined in this study is taken about 10% less than the suggested axial load carrying capacity defined in ACI (2005) [36].

#### **4.7 Recommendations for Preliminary Structural Fire Safety Assessment of Circular Tunnel Linings**

Ground-tunnel lining interaction, service load safety and ratio of lining thickness to radius are investigated to assess the structural fire safety of the tunnel linings subjected to hydrocarbon and RWS fires. The sectional forces are evaluated along the ring. Only crown and spring-line results are reported here in this thesis.

Investigation of hydrocarbon fire cases indicates that spring-line axial forces are more critical compared to the crown axial forces. As the ratio of  $R/t$  increases, the range of factor of safety can widen up to 80% as shown in Figure 4.10 and 4.11.

Flexible rings, i.e. rings with high ratio of  $R/t$ , at soft soil conditions have a better fire performance compared to other cases. The particular reason for such a phenomenon can be explained by less resistance of soil against ring expansion induced by fire. In this case, the level of compressive axial force decreases by the amount of tension force developed during the fire which may result in an increase in factor of safety against failure. At stiff soil conditions whether the ring is flexible or not, the factor of safety does not change much.

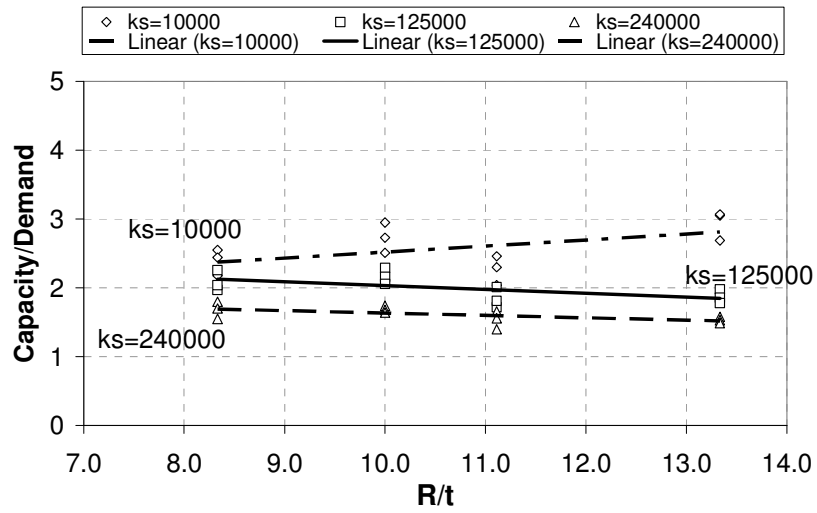


Figure 4.10 Hydrocarbon Fire R/t vs.  $P_{CAP}/P_{DEM}$  @ SL at 240<sup>th</sup> Minute

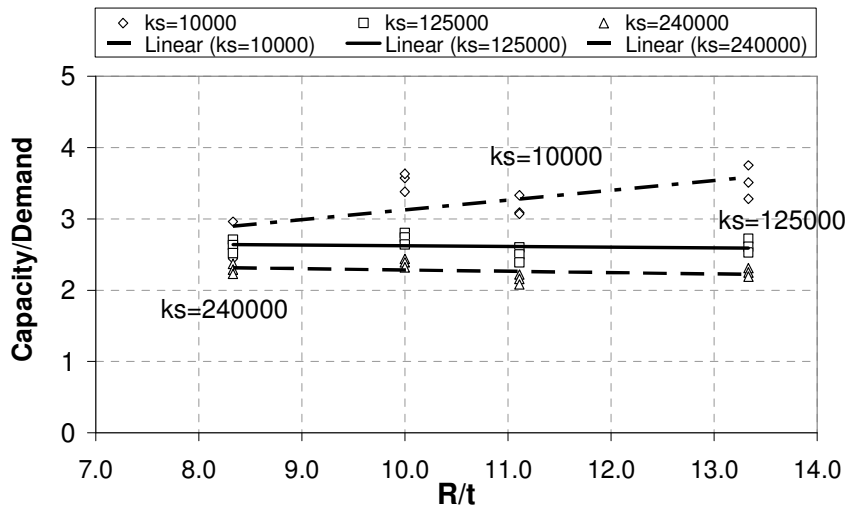


Figure 4.11 Hydrocarbon Fire R/t vs.  $P_{CAP}/P_{DEM}$  @ Cr at 240<sup>th</sup> Minute

In a RWS fire, there is a reduction in factor of safety against failure for flexible rings since the magnitude of expansion is not as much as that in a hydrocarbon fire, as shown in Figures 4.12 and 4.13. The range of factor of safety decreases by 50% on average as the ring segment gets flexible.

The minimum factor of safety against axial force failure at end of hydrocarbon fire is 1.4 with a pre-fire factor of safety of 3.37 for tunnel type M4.36.240. The maximum factor of safety at end of hydrocarbon fire is 3.75 with a pre-fire factor of safety of 7.85 for tunnel type S4.30.010. In any case, none of the investigated tunnels failed under compression.

The factor of safety at the end of a design fire event can be written in terms of pre-fire safety level as follows:

$$FS_{t\_end} = \alpha FS_{t_0} \quad (4.6)$$

where,  $FS_{t\_end}$  is the factor of safety at the end of the fire,  $\alpha$  is a lump-sum parameter defining effect of subgrade reaction modulus ( $k_s$ ) and ratio of  $R/t$ , and  $FS_{t_0}$  is the pre-fire factor of safety.

The  $\alpha$  term can be interpolated as percentage of initial factor of safety presented in Table 4.2. In this table, tunnel type start with S, M and D has initially loaded to 10%, 20% and 30% of their axial loading capacity ( $P_{CAP}$ ) as mentioned previously. Reduction in factor of safety against failure is significant at shallow depth TBM tunnels since there is much more reserve capacity in design. Temperature induced strains dominate the demand forces at the end of the fire. Therefore the demands are within the same range at the end of different investigated cases.

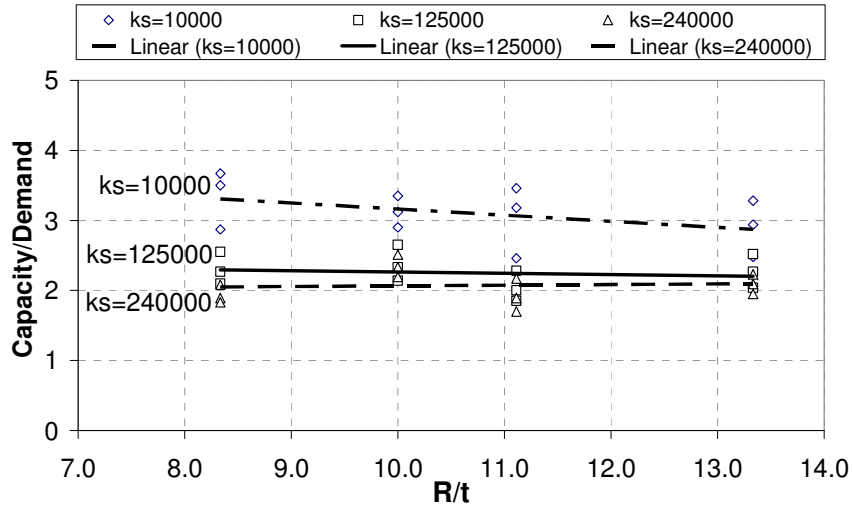


Figure 4.12 RWS Fire R/t vs.  $P_{CAP}/P_{DEM}$  @ SL at 240<sup>th</sup> Minute

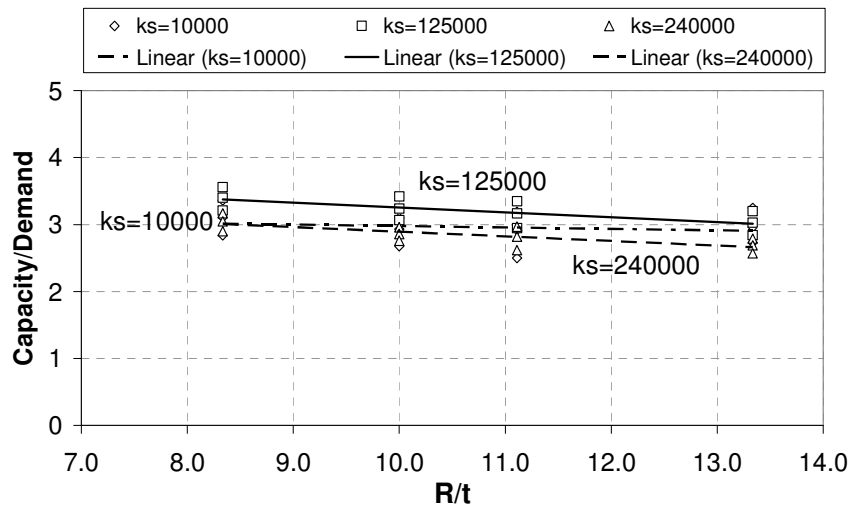


Figure 4.13 RWS Fire R/t vs.  $P_{CAP}/P_{DEM}$  @ SL at 240<sup>th</sup> Minute

Table 4.2 Axial Load Capacity-Demand ( $P_{CAP}$ - $P_{DEM}$ ) and  $\alpha$  Values

Tunnel Type	Pre-Fire Capacity-Demand			End of Fire Capacity-Demand			$\alpha$
	$P_{CAP}$ (kN)	$P_{DEM}$ (kN)	FS	$P_{CAP}$ (kN)	$P_{DEM}$ (kN)	FS	
S3.30.010	13256	1530	8.66	12070	4811	2.51	0.29
S3.30.125	13256	1556	8.52	12070	5260	2.29	0.27
S3.30.240	13256	1556	8.52	12070	6924	1.74	0.20
S3.36.010	13291	1545	8.61	12106	4952	2.44	0.28
S3.36.125	13291	1571	8.46	12106	5368	2.26	0.27
S3.36.240	13291	1571	8.46	12106	6719	1.80	0.21
S4.30.010	13256	2021	6.56	12070	4495	2.69	0.41
S4.30.125	13256	2066	6.42	12070	6111	1.98	0.31
S4.30.240	13256	2067	6.41	12070	7642	1.58	0.25
S4.36.010	13291	2036	6.53	12106	4921	2.46	0.38
S4.36.125	13291	2082	6.39	12106	6017	2.01	0.32
S4.36.240	13291	2083	6.38	12106	7278	1.66	0.26
M3.30.010	13256	2938	4.51	12070	4426	2.73	0.60
M3.30.125	13256	2955	4.49	12070	5598	2.16	0.48
M3.30.240	13256	2954	4.49	12070	7165	1.68	0.38
M3.36.010	13291	2966	4.48	12106	4966	2.44	0.54
M3.36.125	13291	2983	4.46	12106	6132	1.97	0.44
M3.36.240	13291	2983	4.46	12106	7811	1.55	0.35
M4.30.010	13256	3885	3.41	12070	3957	3.05	0.89
M4.30.125	13256	3915	3.39	12070	6482	1.86	0.55
M4.30.240	13256	3916	3.39	12070	7913	1.53	0.45
M4.36.010	13291	3914	3.40	12106	5255	2.30	0.68
M4.36.125	13291	3944	3.37	12106	7053	1.72	0.51
M4.36.240	13291	3945	3.37	12106	8633	1.40	0.42
D3.30.010	13256	4724	2.81	12070	4098	2.95	1.05
D3.30.125	13256	4737	2.80	12070	5860	2.06	0.74
D3.30.240	13256	4736	2.80	12070	7340	1.64	0.59
D3.36.010	13291	4770	2.79	12106	5549	2.18	0.78
D3.36.125	13291	4783	2.78	12106	5941	2.04	0.73
D3.36.240	13291	4782	2.78	12106	7140	1.70	0.61
D4.30.010	13256	6268	2.11	12070	3932	3.07	1.45
D4.30.125	13256	6285	2.11	12070	6787	1.78	0.84
D4.30.240	13256	6285	2.11	12070	8084	1.49	0.71
D4.36.010	13291	6315	2.10	12106	5930	2.04	0.97
D4.36.125	13291	6332	2.10	12106	6695	1.81	0.86
D4.36.240	13291	6332	2.10	12106	7764	1.56	0.74

The tunnel rings are dominantly designed for axial forces. The bending and shear forces typically do not govern the design. The factor of safety against bending increases as the ring gets more flexible. At stiff soil conditions, the factor of safety is higher compared to a ring at soft soil conditions. The ring can not expand in the stiff soil and the bending moments do not increase due to both of the fire scenarios as shown in Figures 4.14, 4.15, 4.16, and 4.17 respectively. In any case, none of the sections fail under bending. The shear terms are also evaluated and determined that there will be no shear failure at the segments.

The maximum crown sagging is observed at deep TBM tunnels around 1.5% of tunnel. However, during the fire, tunnel wants to expand outwards and the sagging at the crown is reversed in case of soft soil conditions. Crown of a tunnel at shallow depth is observed to move up about 0.8% of its radius from the design centerline. The same kind of upward movement referenced from design centerline of tunnel is observed to be 0.65% and 0.40% at medium and deep TBM tunnels respectively.

Even if the peak temperature at RWS fire is higher, the long duration hydrocarbon fire governs the structural fire performance. The peak temperature in hydrocarbon fire lasts for two hundred and ten minutes and the peak temperature at RWS fire lasts for forty minutes.

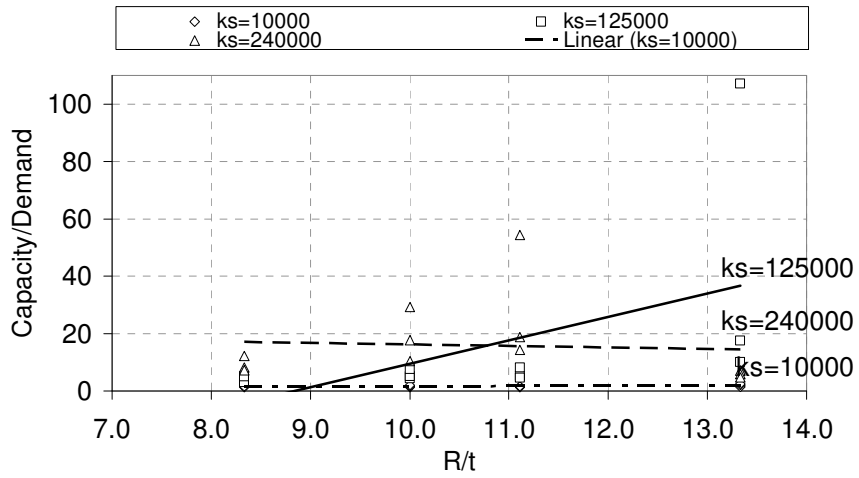


Figure 4.14 Hydrocarbon Fire  $R/t$  vs.  $M_{CAP}/M_{DEM}$  @ SL at 240<sup>th</sup> Minute

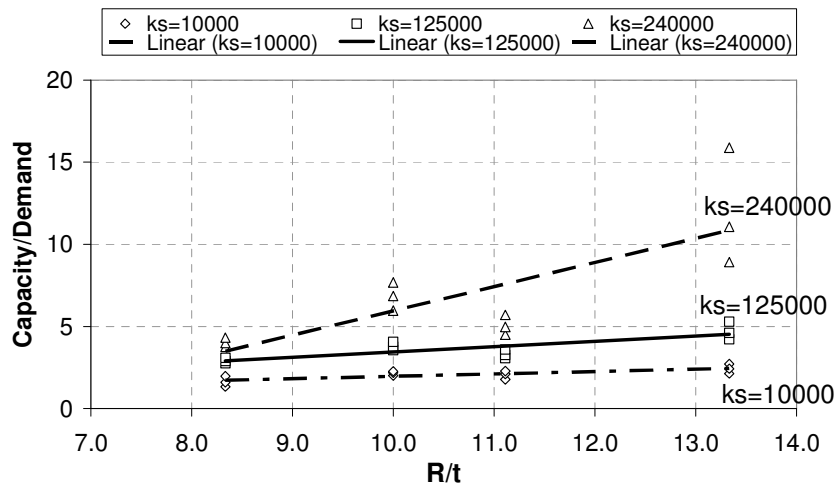


Figure 4.15 Hydrocarbon Fire  $R/t$  vs.  $M_{CAP}/M_{DEM}$  @ Cr at 240<sup>th</sup> Minute

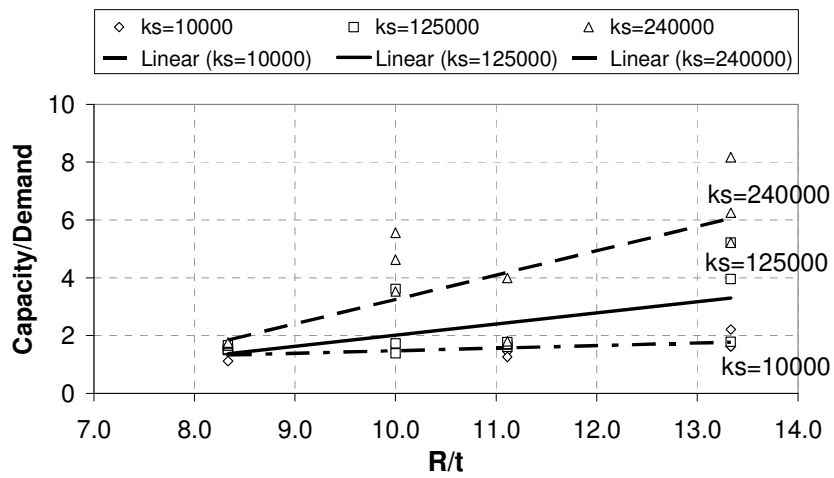


Figure 4.16 RWS Fire R/t vs.  $M_{CAP}/M_{DEM}$  @ SL at 120<sup>th</sup> Minute

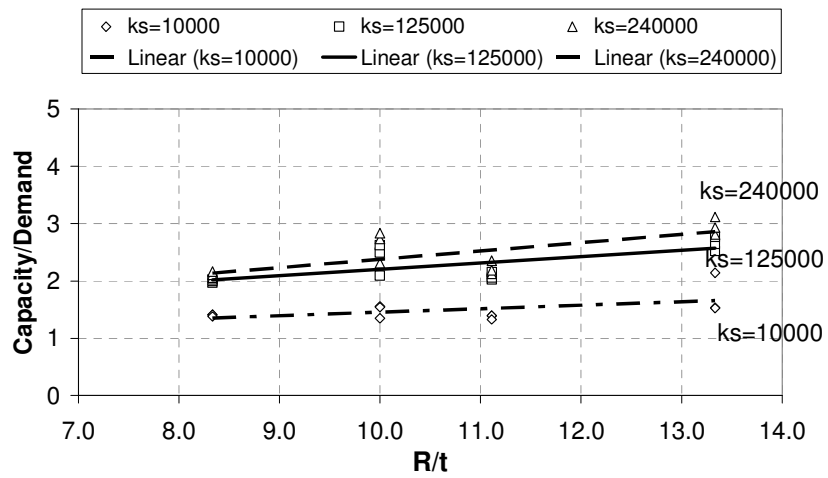


Figure 4.17 RWS Fire R/t vs.  $M_{CAP}/M_{DEM}$  @ Cr at 120<sup>th</sup> Minute

## CHAPTER 5

### RESULTS AND FINDINGS

In the present study, fire safety evaluation of standard circular tunnel linings is performed and consequent recommendations are developed. In nonlinear analysis, three main parameters are examined: tunnel radius ( $R$ ), subgrade reaction modulus ( $k_s$ ), and tunnel lining thickness ( $t$ ). These parameters are used to make the preliminary recommendations for a wider range of tunnels with different geometrical features and constructed in different soil profiles.

A series of hydrocarbon fire tests were conducted on precast TBM key segments at Middle East Technical University to investigate the material response. Experimental setup was designed and constructed by joint work of Civil Engineering Department and Mechanical Engineering Department of METU in 2007-2008.

The explosive spalling of concrete in the tests does not govern the spalling mechanism even if the segments are moisturized on purpose. The concrete gradually degrades after the first 15 to 20 minutes of fire. At early stages of fire, there is a minor explosive spalling, which only affects the surface concrete layer. Most of the concrete surface spalling happens at surfaces touching flames. The test results and analytical studies are in good agreement with prediction of damaged concrete section. Depth of concrete segment that needs to be repaired estimated in analytical studies is in conformance with test results as presented in Table 5.1.

Depth of concrete needs to be repaired is the summation of spalled concrete thickness and thickness of layers exposed to more than 380 °C. Typically these layers exposed to high temperature are observed to be colorized. Above 380 °C, the concrete will only have about 50% of its initial compressive strength after cooling.

In industry, the repair limit for concrete subjected to fire is set to  $0.5 * f_c'$  [30]. In any case, compressive strength of cores from fire tested segments was much higher than the repair limit. The rebars were not affected much. Those taken from fire tested segments had similar tensile properties compared to the rebars taken from the reference segment.

Table 5.1 Summary of Depth of Concrete Needs to be Repaired

Method Used	Total Depth of Concrete Needs to be Repaired	
	1 Hour Fire	4 Hour Fire
Test	~4 cm	~11 cm
Analytical	~5 cm	~10 cm

Key segment hydrocarbon fire test results validated the material degradation properties used in the analyses as explained in Chapter 4. The segments were tested in a very undesirable condition at an unloaded state with flame touching its surface and with high moisture content close to its absorption capacity.

After the fire tests, no surface crack was observed on the segments but just minor surface spalling. However, internal cracking at mid height region was

observed on the cores taken from the fire tested segments. This effect was predicted by FIRECAP program strain distribution for an unloaded segment.

At high temperatures, concrete can develop 0.011 compressive crushing strain that will result in spalling [10, 30]. Externally applied design loads under service conditions can develop an average of 0.001 compressive strain, which is only 9% of the ultimate strain capacity. If the tests are repeated with the external loads, depth of spalling will increase around 2 mm on average and average spalling will increase to 22 mm.

Investigation of hydrocarbon fire cases, which are the most critical scenario for a tunnel fire, indicates that spring-line axial forces are more critical compared to the crown axial forces. As the ratio of  $R/t$  increases, the range of factor of safety can widen up to 80%.

Flexible rings, i.e. rings with high ratio of  $R/t$ , at soft soil conditions have a better fire performance compared to other cases. This type of behavior is mainly due to relatively softer resistance of soil, as opposed to the stiffer cases, against ring expansion induced by fire. In this case, the level of compressive axial force decreases by the amount of tension force developed during the fire which may result in an increase in factor of safety against failure. At stiff soil conditions whether the ring is flexible or not, the factor of safety does not change much.

## CHAPTER 6

### CONCLUSION

#### 6.1 Conclusion

Structural fire safety of standard circular tunnel liners is investigated analytically and experimentally. Conclusions of this study can be summarized as follows:

- The analytical studies developed in the previous research are in good agreement with the test results.
- Hydrocarbon fire typically governs fire curve for the fire endurance of the tunnel linings compared to RWS fire curve.
- In soft soil condition, demand does not increase significantly due to expansion of TBM lining compared to a stiff soil case.
- As the TBM tunnel gets flexible, the range of factor of safety widens from soft soil condition to stiff soil condition for the hydrocarbon fire.
- Initial level of design loads increase spalling slightly since the temperature induced strains are much higher than initial strains induced by design loads. Therefore the tests do not need to be performed under load. Also design loads can prevent inner cooler layer cracking that will result in a better fire performance.
- The initial crown sagging is either neutralized or crown moves upward during the fire. Therefore, the moment terms or shear terms are not that significant compared to axial forces induced by fire.

- Minor repairs shall be targeted after tunnel fires instead of using fire proofing materials. In literature, fire proofing materials are reported to have major durability and maintenance problems.
- The analytical results presented in this research can be used for assessment of structural fire safety of tunnels.

## **6.2 Recommendations for Future Work**

- Fire test results of prefabricated reinforced concrete TBM key segment are in good agreement with the analytical calculations. Based on those, preliminary design recommendation developed in Chapter 4 can be used for fire safety evaluation of a tunnel liner instead of further tests.
- Two different fire curves are considered in this study. Tunnel fires can last longer (like 7-9 hours) than the design curves in the calculations. For such cases, different design fire curves are needed and consequently further research and test on specific basis shall be performed.
- More research is needed on selection of concrete mix design resistant to fire.

## REFERENCES

- [1] Bickel J. O., Kuesel T. R., King E. H., Tunnel Engineering Hand Book, Second Edition, 1, 86, 203, 205-207, 209, 1997.
- [2] “75. Yıl Selatin Tunnel, İzmir-Aydın Highway / Belevi District” from Kutlutaş-Dillingham Joint Venture Achieve, 2000.
- [3] Transit Cooperative Research Program and National Cooperative Highway Research Program, TCRP Report 86 / NCHRP Report 525, “Making Transportation Tunnels Safe and Secure”, Transportation Research Board, Vol.12, 52, 2006.
- [4] Caner A., Zlatanic S., Muntaf N., “Structural Fire Performance of Concrete and Shotcrete Tunnel Liners”, ASCE Journal of Structural Engineering, Vol.131, 1920-1925, 2005.
- [5] Thelandersson S., “Mechanical Behavior of Heated Concrete under Torsional Loading at Transient High Temperature Conditions”, Lund Institute of Technology, Bulletin No. 46, Lund, 1974.
- [6] “Modern Tunnel Boring Machine”  
<http://www.karaelmas.edu.tr/linkler/kisisel/nuriakcin/tefotos/TBM3.jpg>,  
Last accessed 30.03.2008.
- [7] “Shield Tunneling Methods, Principle of Excavation”  
<http://www.daiho.co.jp/english/rdt/dk.htm>, Last Accessed 07.04.2008.

- [8] "TBM Cutting Head" and "Rapid Transition TBM Tunnel" from Gama-Gürüş Joint Venture Achieve, 1995.
- [9] "Selective TBM Machines for Railway Tunnels around the World" <http://www.lovat.com>, Last accessed 26.10.2007.
- [10] Anderberg Y., "The Effects of Constitutive Models on the Prediction of Concrete Mechanical Behaviour and on the Design of Concrete Structures Exposed to Fire", Proceedings of the Workshop, Fire Design of Concrete Structures: What Now? What Next?, 37-47, December 2004.
- [11] Anderberg Y., Thelandersson S., "Stress and Deformation Characteristics of Concrete at High Temperatures", Lund Institute of Technology, Bulletin No. 54, Lund, 1976.
- [12] Schneider U., "Zur Kinetik Festigkeitsmindernder Reaktionen in Normalbetonen bei Temperaturen bis 1000 °C", (Loss of Strength due to Kinetic Reactions of Normal Concretes up to 1000 °C), PhD Thesis Submitted to Technical University Braunschweig, Germany, 1973.
- [13] Anderberg Y., "Fire-exposed Hyperstatic Concrete Structures: An Experimental and Theoretical Study", Lund Institute of Technology, Bulletin 55, Lund, 1976.
- [14] Cheng F.P., Kodur V.K.R., Wang T.C., "Stress-Strain Curves for High Strength Concrete at Elevated Temperatures", ASCE Journal of Materials in Civil Engineering, Vol.16, 84-90, 2004.

- [15] Guerrini G. L., Gambarova P. G., Rosati G., "Microstructure of High-Strength Concrete Subjected to High Temperature", Proceedings of the Workshop, Fire Design of Concrete Structures: What Now? What Next?, 89-94, December 2004.
- [16] Cattaneo S., Rosati G., Guerrini G.L., "Hybrid Polypropylene-Dteeş Fiber Reinforced Concrete at High Temperatures", Proc. Of RILEM Symposium "Advances in Concrete through Science and Engineering", Chicago U.S.A., 10, March 22-24, 2004.
- [17] Khoury, G. A., "Passive Protection against Fire", Tunnels and Tunneling International, 40-42, November 2002.
- [18] Tatnall, P. C., "Shotcrete in Fires: Effects of Fibers on Explosive Spalling", American Shotcrete Association, Farmington Hills, Michigan, 10-12, 2002.
- [19] Msaad Y., Bonnet G., "Analyses of Heated Concrete Spalling due to Restrained Thermal Dilation: Application to the 'Chunnel' Fire", ASCE Journal of Engineering Mechanics, Vol.132, No.10, October 2006.
- [20] Pichler C., Lackner R., Mang H. A., "Safety Assessment of Concrete Tunnel Linings under Fire Load", ASCE Journal of Structural Engineering , Vol.132, No.6, 961-969, June 2006.
- [21] Tajima H., Kishida M., Kanda T., Morita T., "Study on the Deformation and Load Bearing Capacity of TBM Shield Tunnel Lining in Fire", Underground Space Use: Analysis of the Past and Lessons for the Future, Vol.2, 793-799, 2005.

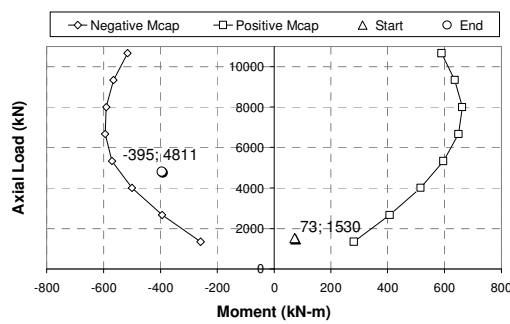
- [22] Richards D. P., Hudson M. A., Whitaker M., "A Risk Based Methodology for Optimum Tunnel Configuration", *Underground Space Use: Analysis of the Past and Lessons for the Future*, Vol.1, 71-76, 2005.
- [23] Bamonte P., Cangiano S., Felicetti R., Gambarova P. G., Billi R., Busnelli F., Quaglia M., "Thermo-Mechanical Characterization of Concrete Mixes Suitable for the Rehabilitation of Fire-Damaged Tunnel Linings", *Proceedings of the Fourth International Workshop SIF '06, Aveiro*, 545-559, 2006.
- [24] Kutzinig, L., "Fire Resistance of High Performance Concrete with Fiber Cocktails", *LACER*, No. 4, 185-192, 1999.
- [25] Pichler, C., Lackner, R. and Mang, H.A., "Safety Assessment of Concrete Tunnel Linings under Fire Load", *Journal of Structural Engineering*, 132 (6), 961-969, 2006.
- [26] Martinola, G., Bauml, M. F. and Walliser, A., "Numerical Modeling of the Long-Term Behavior of Passive Fire Protection Mortars Applied on Concrete Tunnels", *Journal of Materials in Civil Engineering*, 19(6), 484-491, 2007.
- [27] ATC-33, "NEHRP Commentary on the Guidelines for the Seismic Rehabilitation of Buildings (FEMA Publication 274)", *Building Seismic Safety Council*, Washington D.C., USA, 427, 1997.
- [28] Kodur, V.K.R., and Sultan, M.A., "Effect of Temperature on Thermal Properties of High Strength Concrete", *Journal of Materials in Civil Engineering*, 15 (2), 101-107, 2003.

- [29] Flynn, D. R., "Response of High Performance Concrete to Fire Conditions: Review of Thermal Property Data and Measurement Techniques", NIST GCR 99-767, U.S. Department of Commerce Building and Fire Research Laboratory National Institute of Standards and Technology, Gaithersburg, Maryland, 1999.
- [30] American Concrete Institute (ACI), "Fire Endurance of Concrete Elements", ACI 2003 Manual of Concrete Practice, ACI 216R-89, Farmington Hills, Michigan, 2001.
- [31] Both C. Wolinsk G. M. and Breunese A.J., "Spalling of Concrete Tunnel Linings in Fire (Re)Claiming the Underground Space", Sauver, Swets & Zeitlinger, Lisse, 227-231, 2003.
- [32] "The Memorial Tunnel Fire Ventilation Test Program" <http://www.fhwa.dot.gov/bridge/tunnel/tunres2.htm>, Last accessed 17.04.2008.
- [33] Iranian Petroleum Standards (IPS), "Engineering Standard for Temperature Instruments Original Edition", IPS-E-IN-120, 28, May 1993.
- [34] PIARC Committee on Road Tunnels (C5), Smoke Control in Road Tunnels, 1999.
- [35] American Concrete Institute (ACI), "Guide for Obtaining Cores and Interpreting Compressive Strength Results", ACI 214.4R-03, Farmington Hills, Michigan, 16, 2003.
- [36] American Concrete Institute (ACI), "Building Code Requirements for Structural Concrete" ACI 318, Farmington Hills, Michigan, 2005.

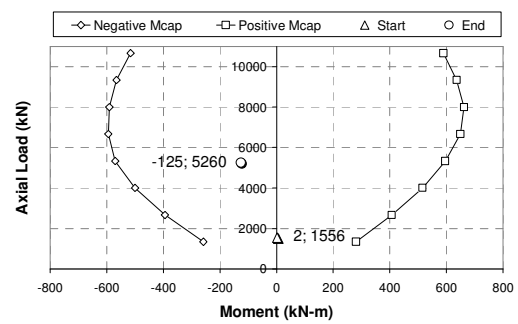
- [37] Akman M. S., “Betonarme Yapılarda Yangın Hasarı ve Yangın Sonunda Taşıyıcılığın Belirlenmesi”, Sika Teknik Bülten / Makaleler, 141, İstanbul, 2007.
- [38] “K’ (Chromel–Alumel) Type Thermocouples”, [http://www.watch-hill.co.uk/bayonet\\_tc.htm](http://www.watch-hill.co.uk/bayonet_tc.htm), Last accessed 02.06.2008.
- [39] Sadd M. H., Elasticity Theory, Applications, and Numerics, Elsevier Academic Press, 123-124, 2005.
- [40] Barber J. R., Elasticity, Second Edition, Kluwer Academic Press, 33, 2002.

## APPENDIX A

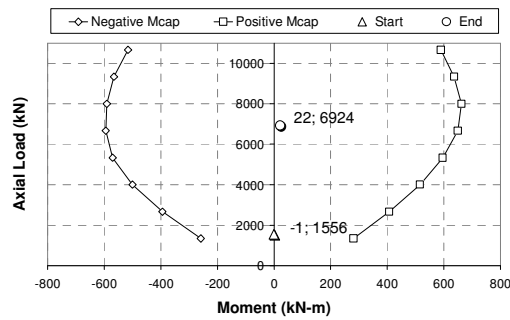
### INTERACTION DIAGRAMS AT THE END OF HYDROCARBON FIRE FOR SPRING LINE AND CROWN



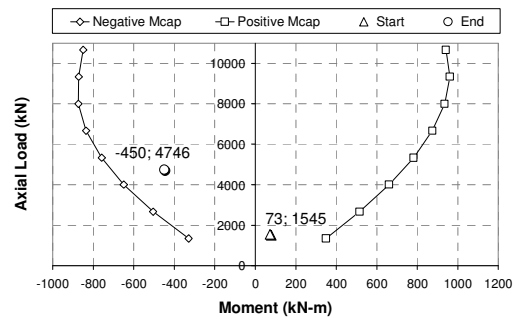
(a)



(b)

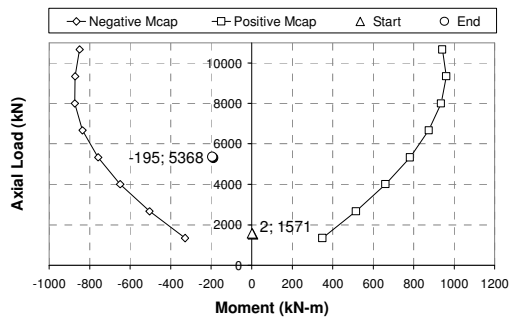


(c)

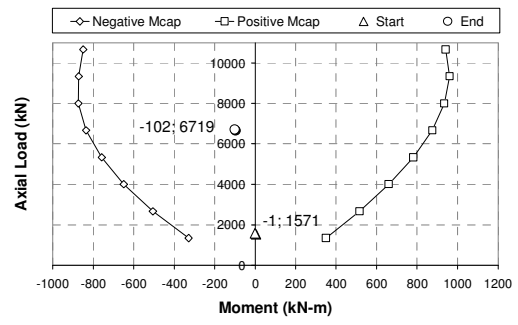


(d)

Figure A.1 M-P @ SL: (a) S3.30.010, (b) S3.30.125, (c) S3.30.240,  
(d) S3.36.010

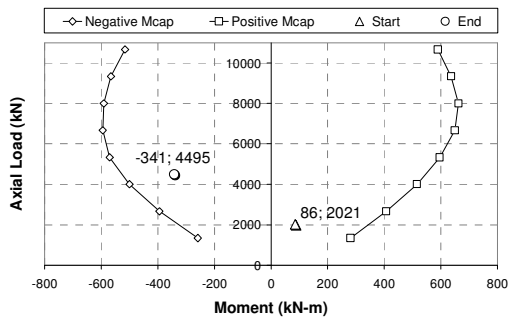


(e)

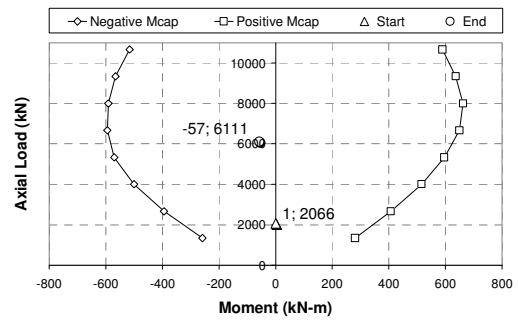


(f)

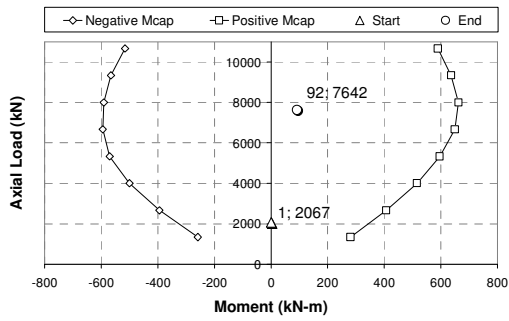
Figure A.1 (Continued) M-P @ SL: (e) S3.36.125, (f) S3.36.240



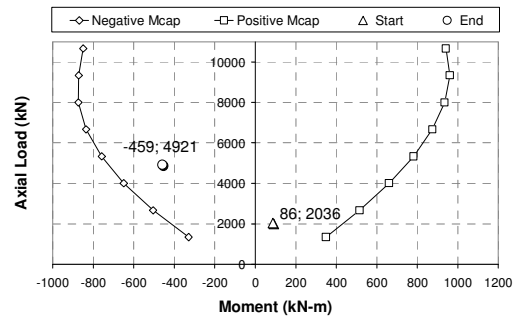
(a)



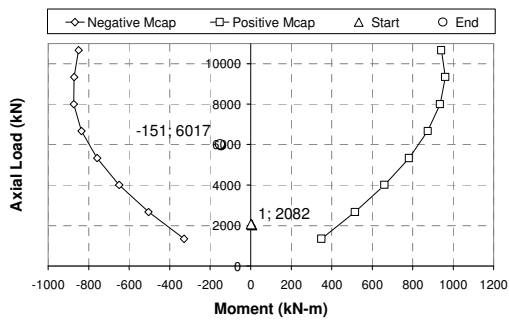
(b)



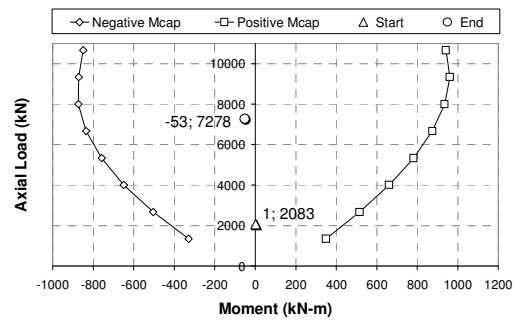
(c)



(d)

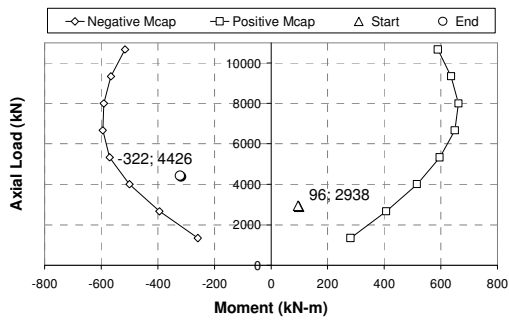


(e)

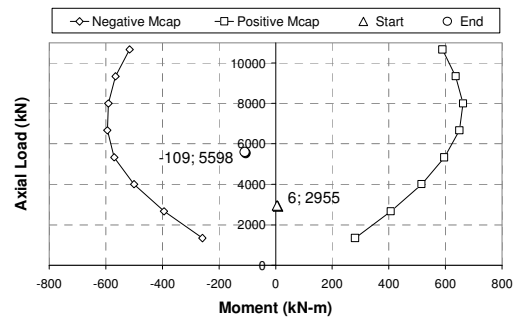


(f)

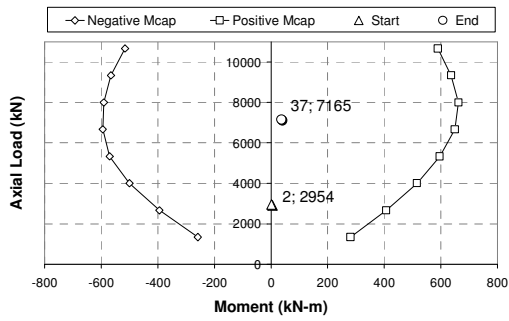
Figure A.2 M-P @ SL: (a) S4.30.010, (b) S4.30.125, (c) S4.30.240, (d) S4.36.010, (e) S4.36.125, (f) S4.36.240



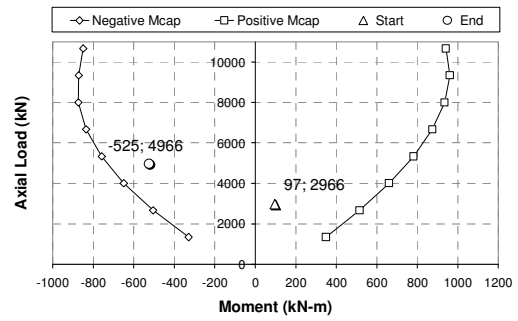
(a)



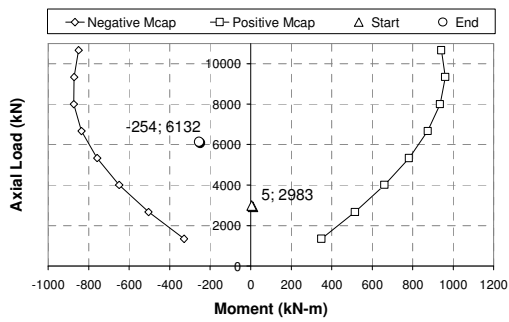
(b)



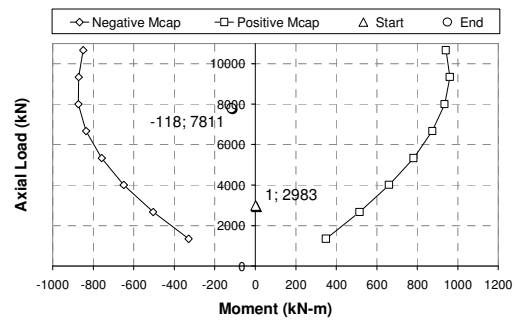
(c)



(d)

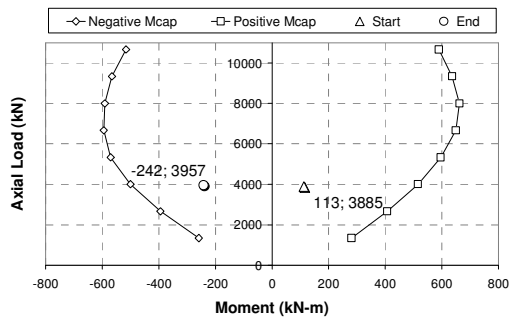


(e)

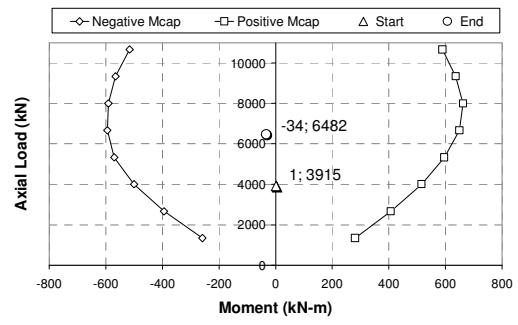


(f)

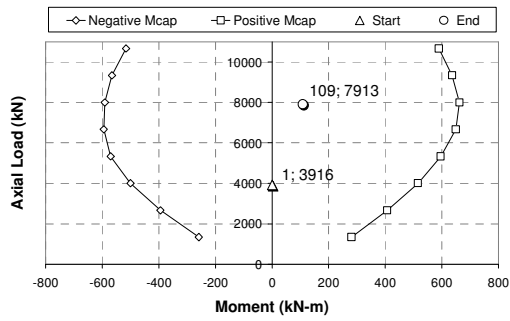
Figure A.3 M-P @ SL: (a) M3.30.010, (b) M3.30.125, (c) M3.30.240, (d) M3.36.010, (e) M3.36.125, (f) M3.36.240



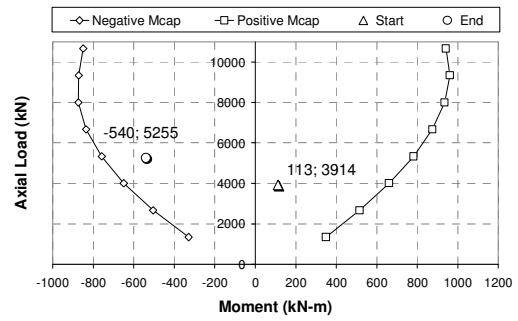
(a)



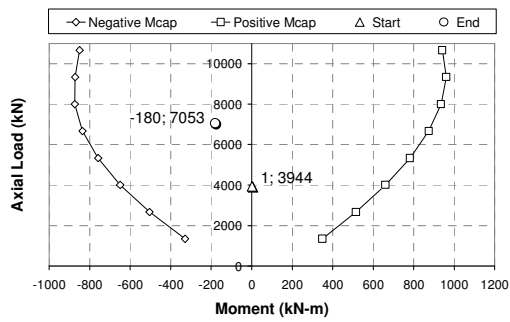
(b)



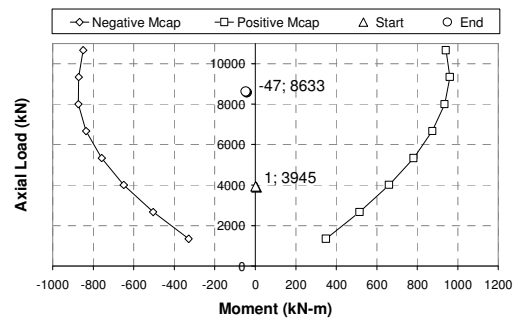
(c)



(d)

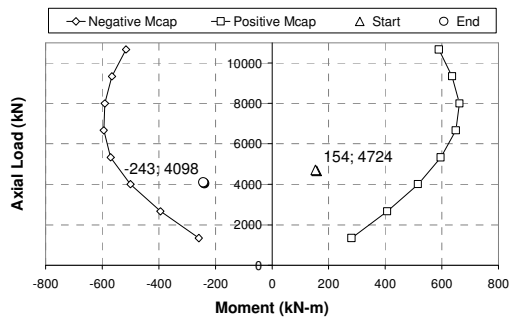


(e)

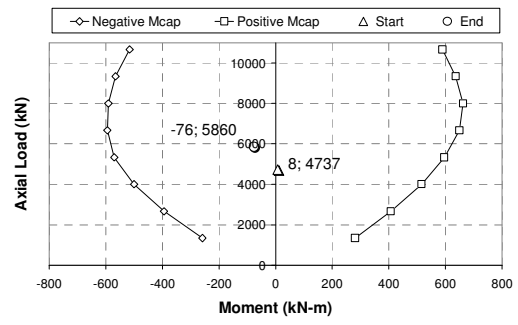


(f)

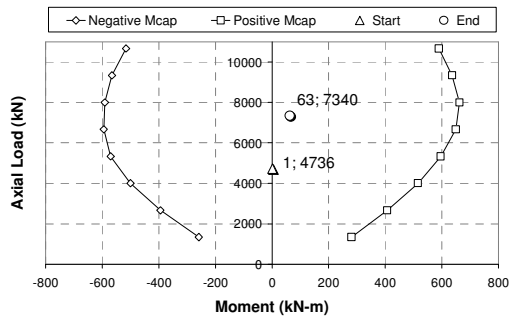
Figure A.4 M-P @ SL: (a) M4.30.010, (b) M4.30.125, (c) M4.30.240, (d) M4.36.010, (e) M4.36.125, (f) M4.36.240



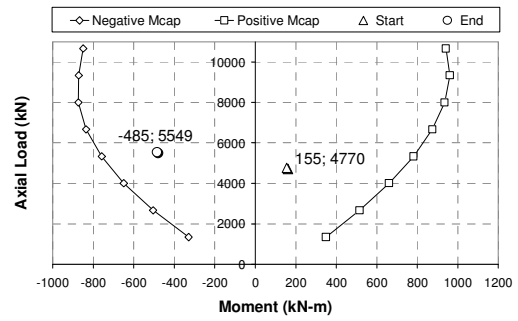
(a)



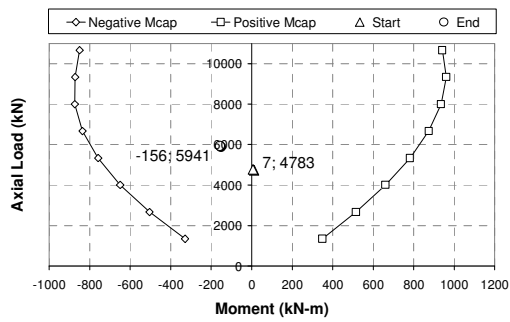
(b)



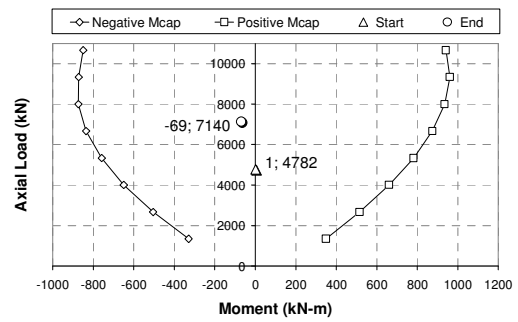
(c)



(d)

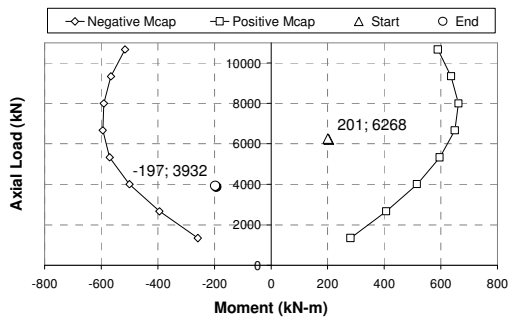


(e)

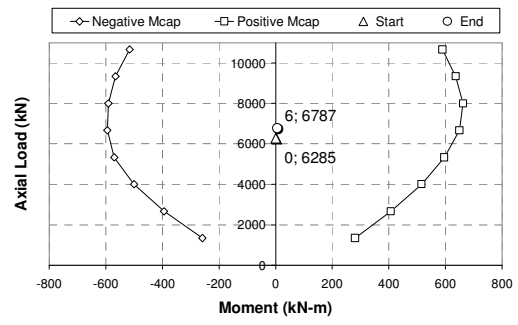


(f)

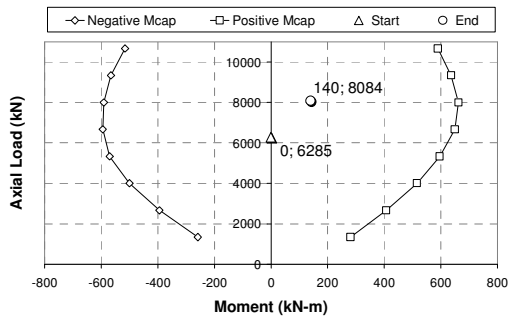
Figure A.5 M-P @ SL: (a) D3.30.010, (b) D3.30.125, (c) D3.30.240, (d) D3.36.010, (e) D3.36.125, (f) D3.36.240



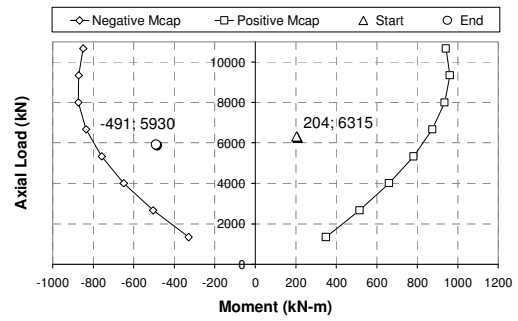
(a)



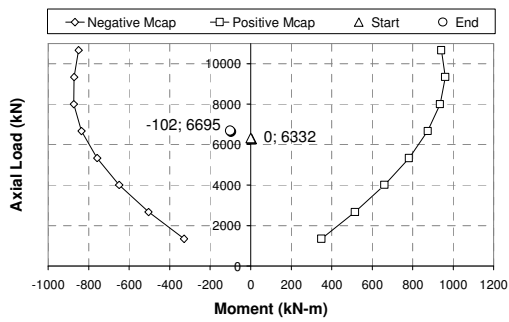
(b)



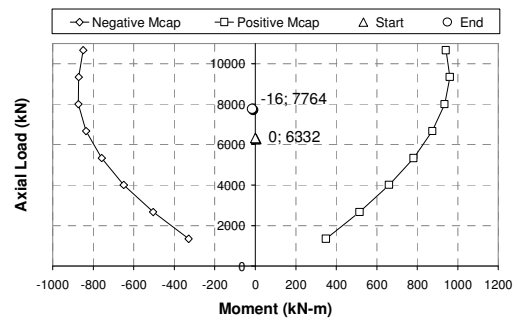
(c)



(d)

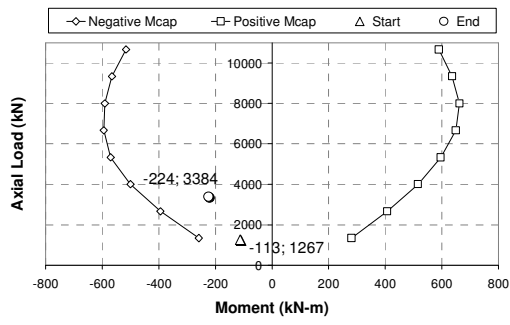


(e)

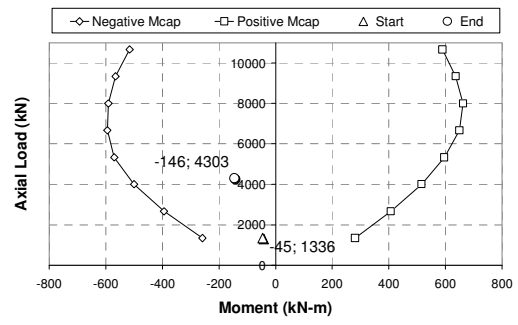


(f)

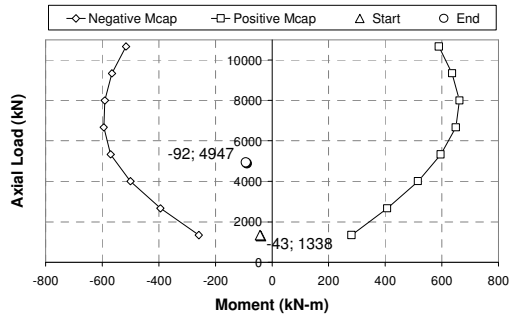
Figure A.6 M-P @ SL: (a) D4.30.010, (b) D4.30.125, (c) D4.30.240, (d) D4.36.010, (e) D4.36.125, (f) D4.36.240



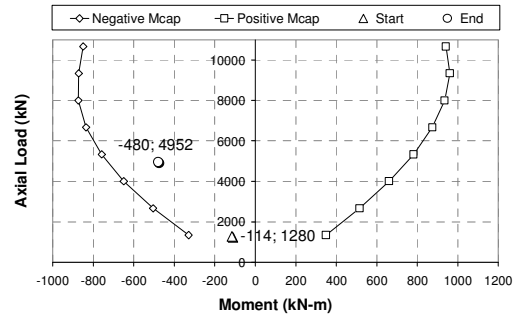
(a)



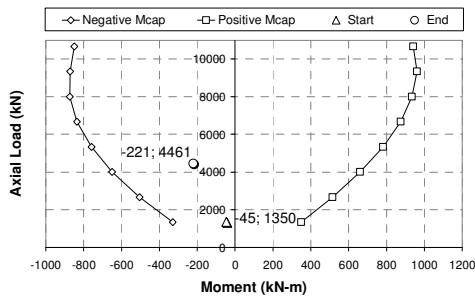
(b)



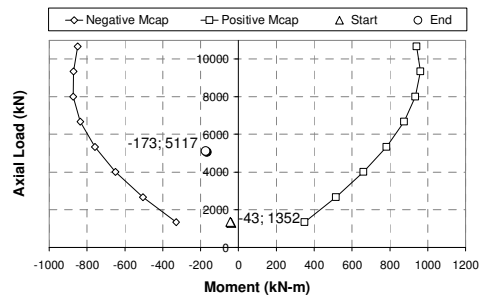
(c)



(d)

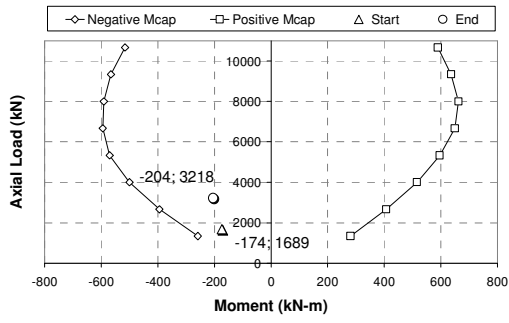


(e)

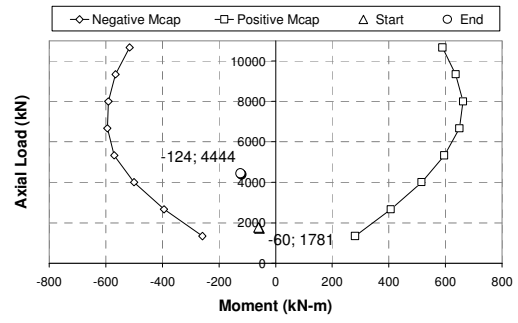


(f)

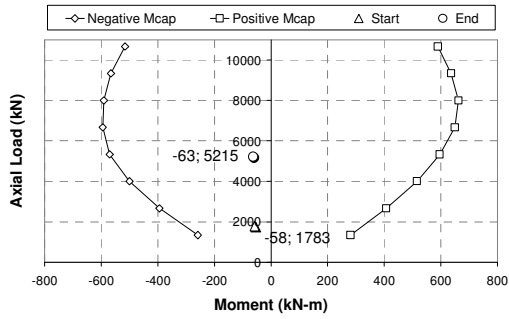
Figure A.7 M-P @ Cr: (a) S3.30.010, (b) S3.30.125, (c) S3.30.240, (d) S3.36.010, (e) S3.36.125, (f) S3.36.240



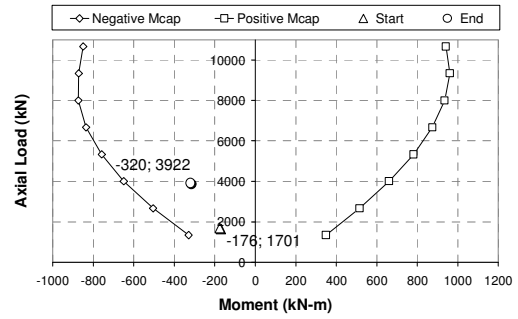
(a)



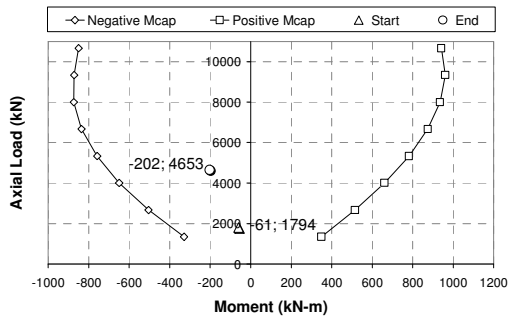
(b)



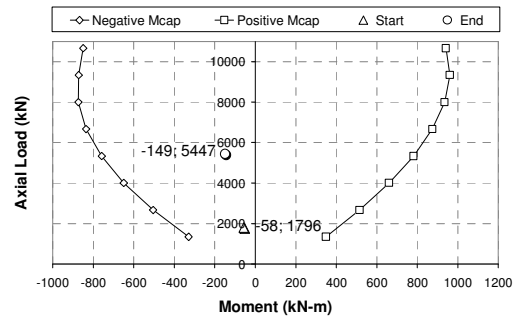
(c)



(d)

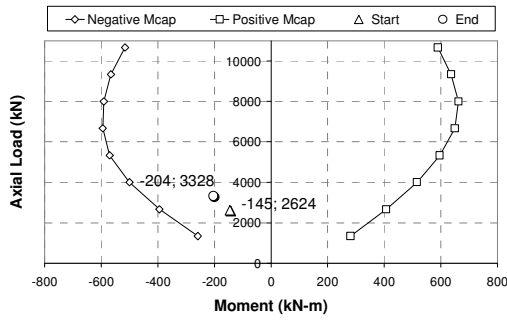


(e)

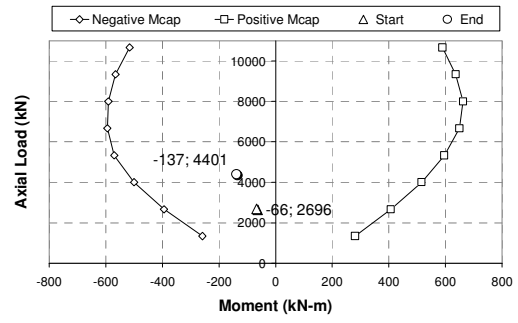


(f)

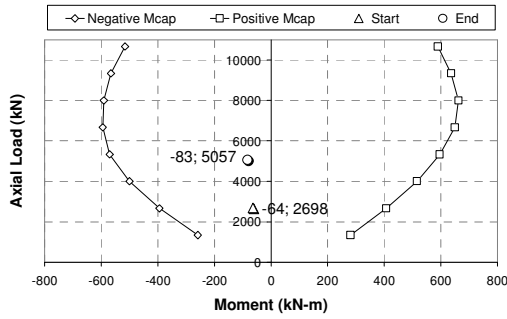
Figure A.8 M-P @ Cr: (a) S4.30.010, (b) S4.30.125, (c) S4.30.240, (d) S4.36.010, (e) S4.36.125, (f) S4.36.240



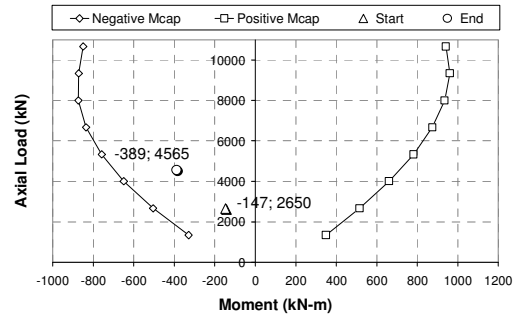
(a)



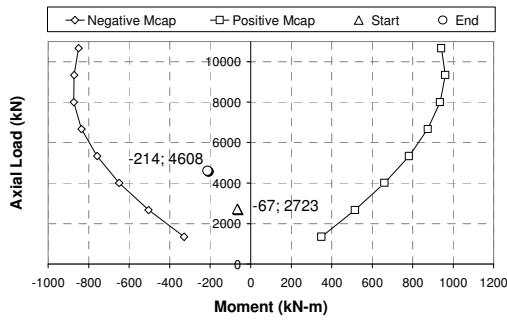
(b)



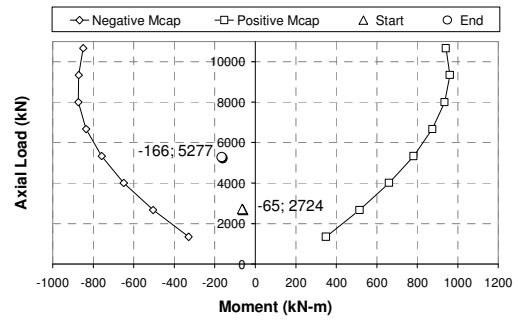
(c)



(d)

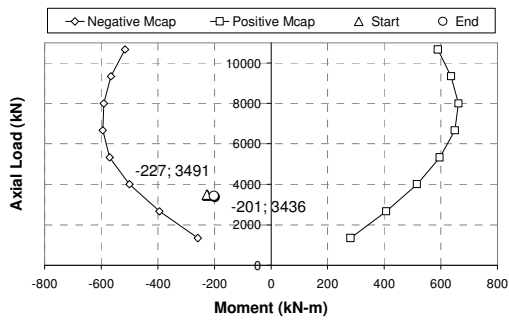


(e)

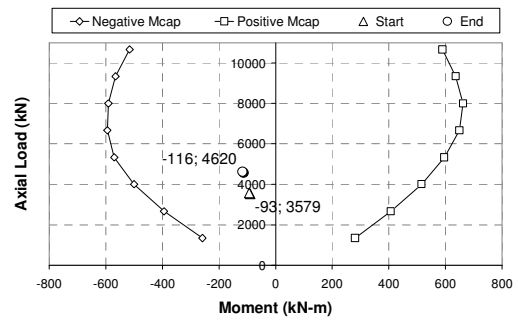


(f)

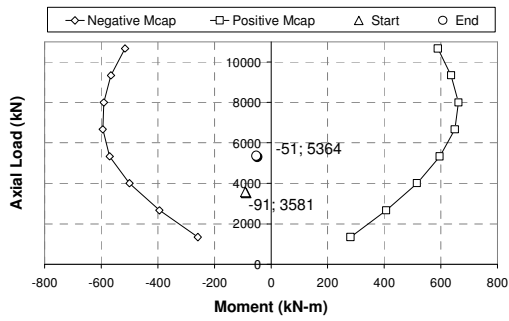
Figure A.9 M-P @ Cr: (a) M3.30.010, (b) M3.30.125, (c) M3.30.240, (d) M3.36.010, (e) M3.36.125, (f) M3.36.240



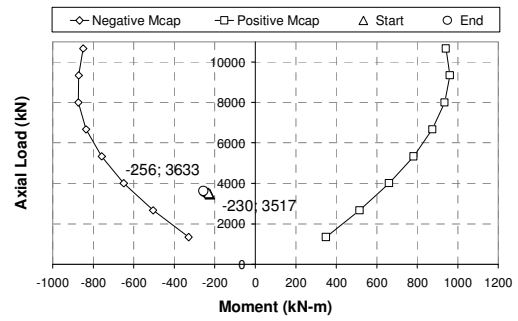
(a)



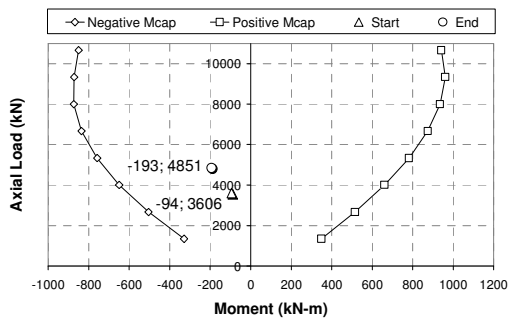
(b)



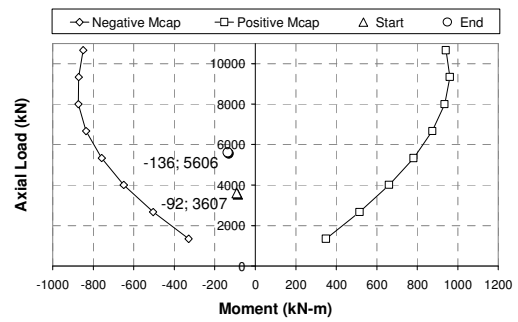
(c)



(d)

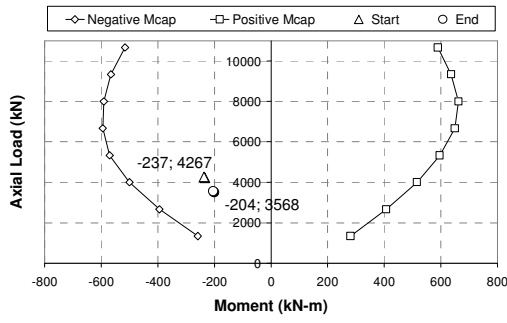


(e)

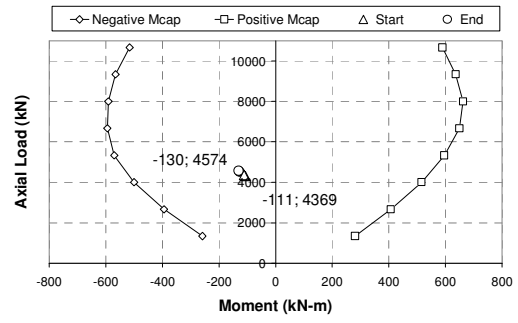


(f)

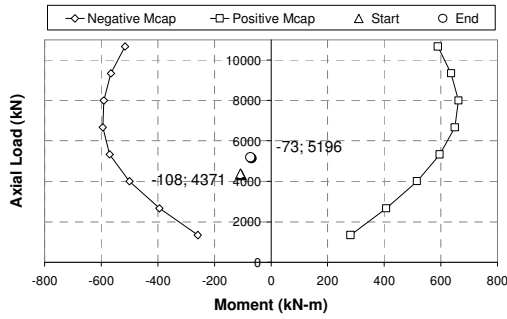
Figure A.10 M-P @ Cr: (a) M4.30.010, (b) M4.30.125, (c) M4.30.240, (d) M4.36.010, (e) M4.36.125, (f) M4.36.240



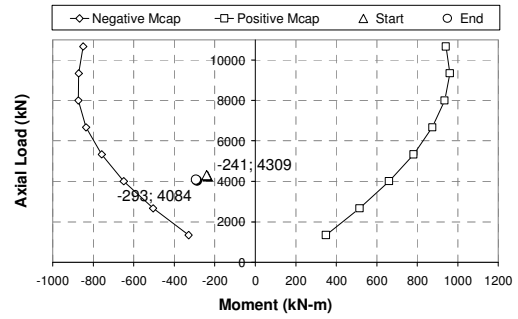
(a)



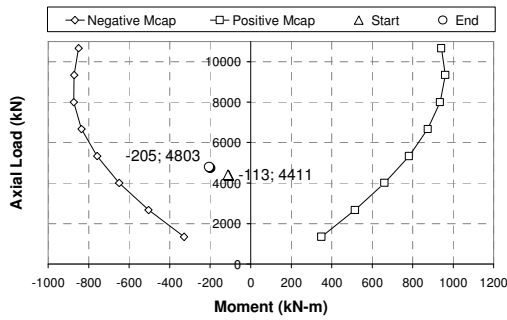
(b)



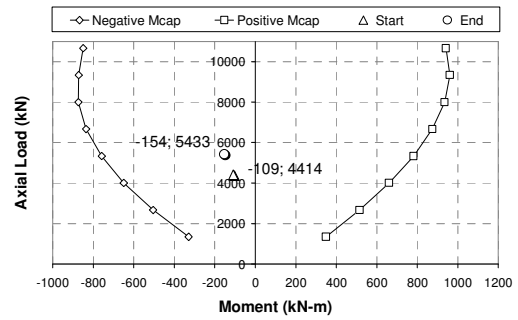
(c)



(d)

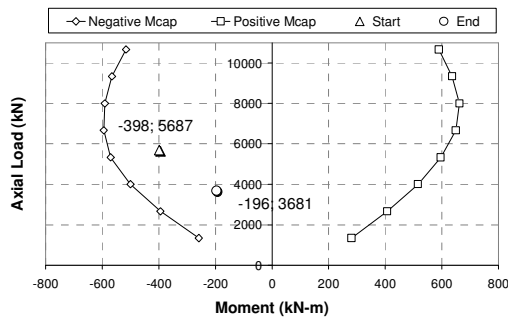


(e)

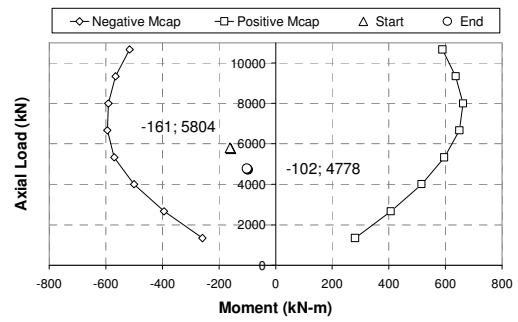


(f)

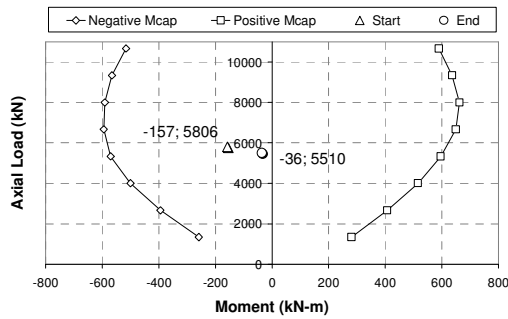
Figure A.11 M-P @ Cr: (a) D3.30.010, (b) D3.30.125, (c) D3.30.240, (d) D3.36.010, (e) D3.36.125, (f) D3.36.240



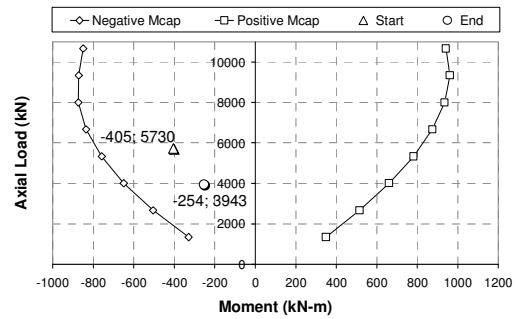
(a)



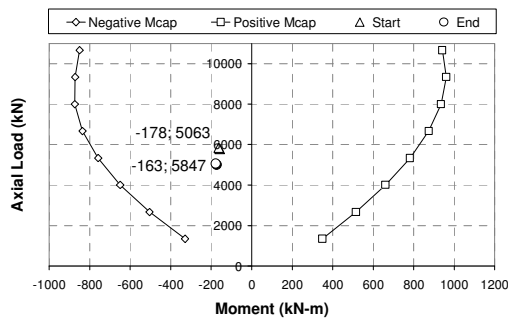
(b)



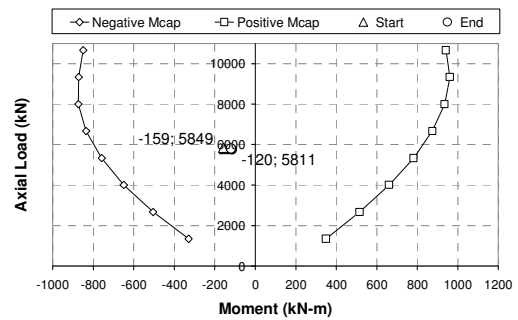
(c)



(d)



(e)

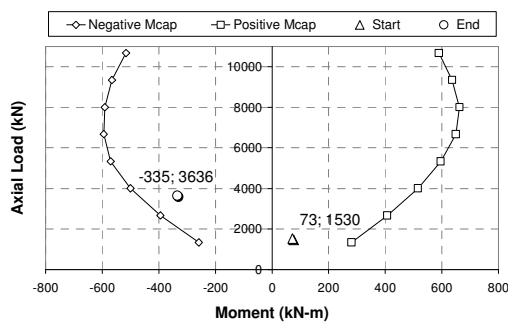


(f)

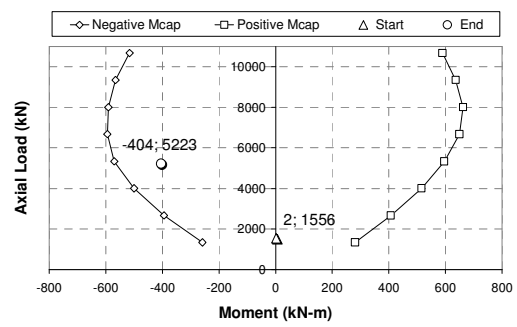
Figure A.12 M-P @ Cr: (a) D4.30.010, (b) D4.30.125, (c) D4.30.240, (d) D4.36.010, (e) D4.36.125, (f) D4.36.240

## APPENDIX B

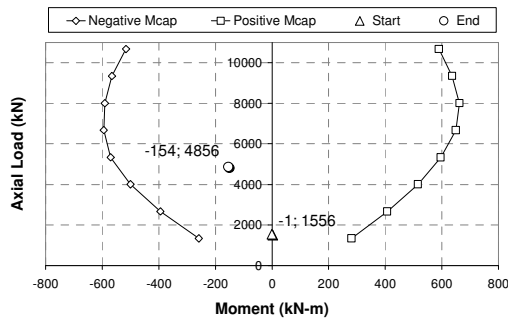
### INTERACTION DIAGRAMS AT THE END OF RWS FIRE FOR SPRING LINE AND CROWN



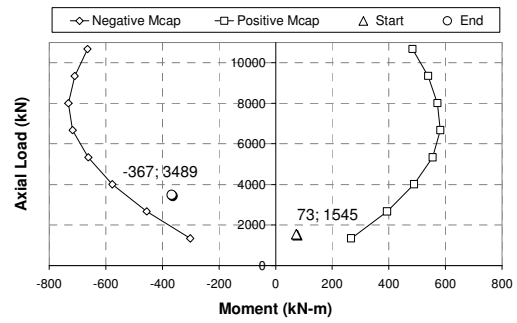
(a)



(b)

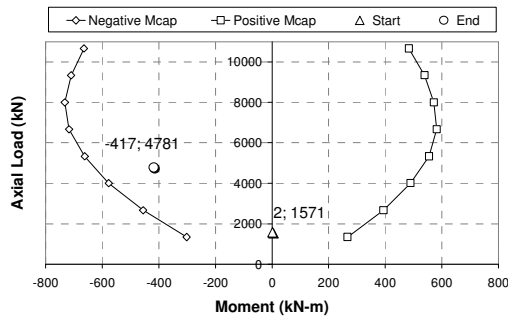


(c)

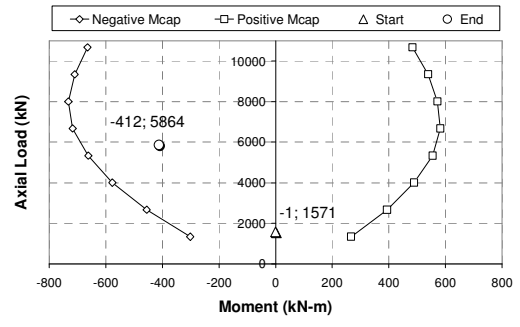


(d)

Figure B.1 M-P @ SL: (a) S3.30.010, (b) S3.30.125, (c) S3.30.240,  
(d) S3.36.010

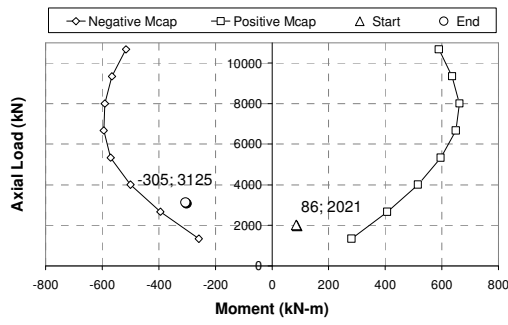


(e)

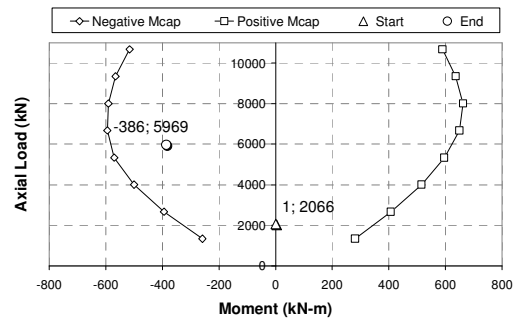


(f)

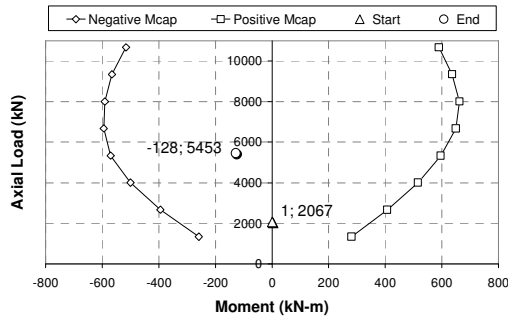
Figure B.1 (Continued) M-P @ SL: (e) S3.36.125, (f) S3.36.240



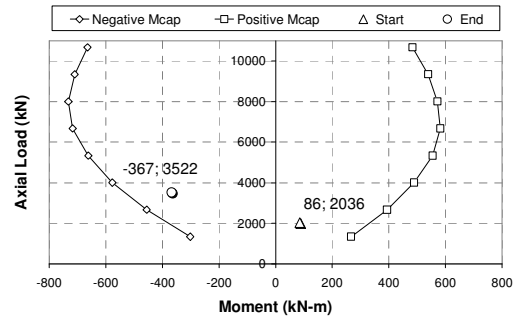
(a)



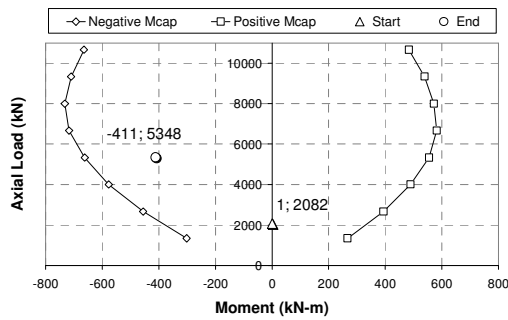
(b)



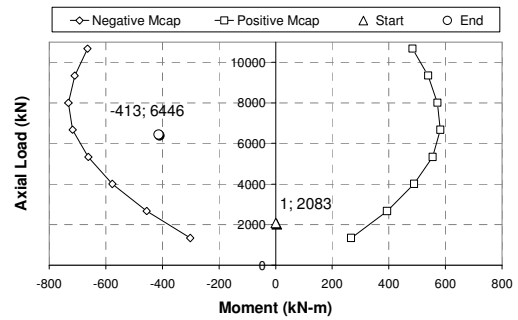
(c)



(d)

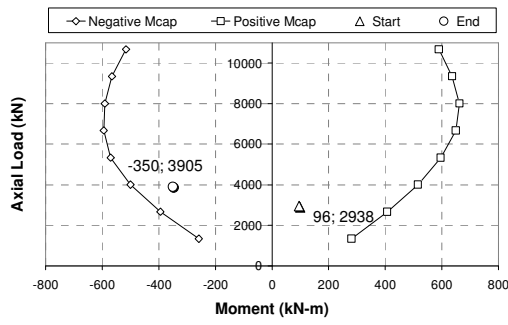


(e)

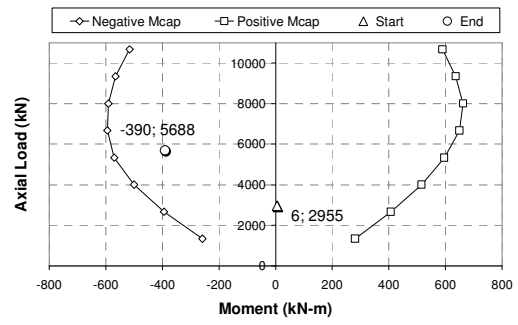


(f)

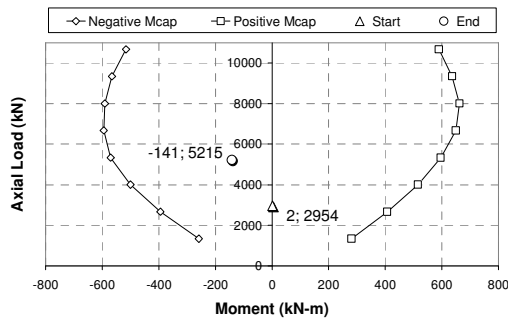
Figure B.2 M-P @ SL: (a) S4.30.010, (b) S4.30.125, (c) S4.30.240, (d) S4.36.010, (e) S4.36.125, (f) S4.36.240



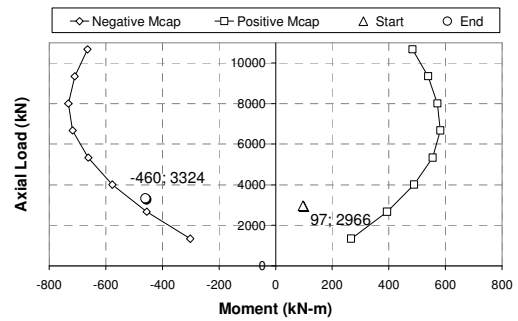
(a)



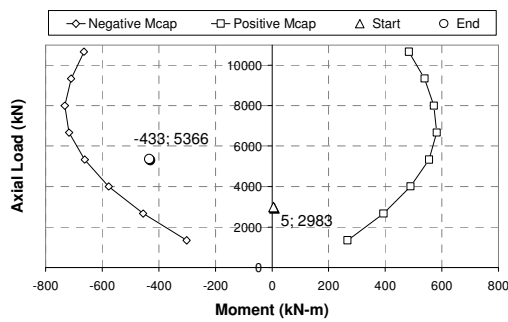
(b)



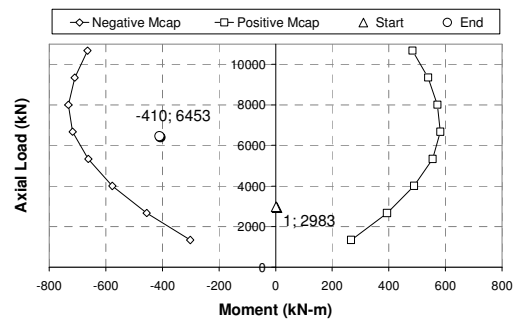
(c)



(d)

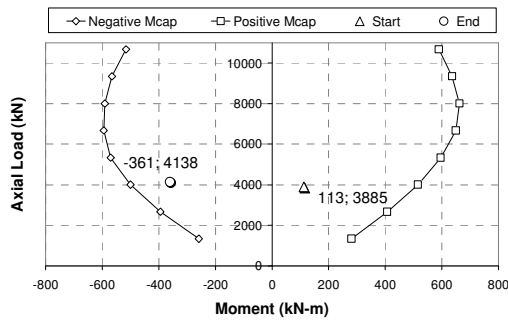


(e)

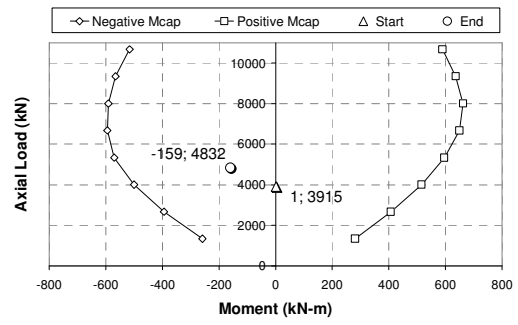


(f)

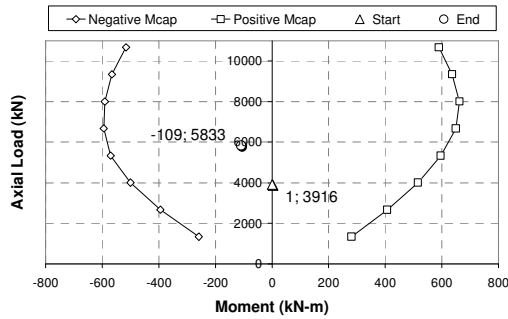
Figure B.3 M-P @ SL: (a) M3.30.010, (b) M3.30.125, (c) M3.30.240, (d) M3.36.010, (e) M3.36.125, (f) M3.36.240



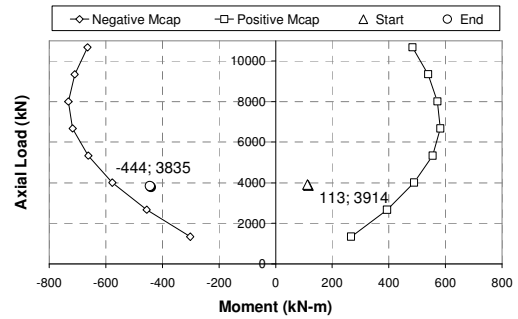
(a)



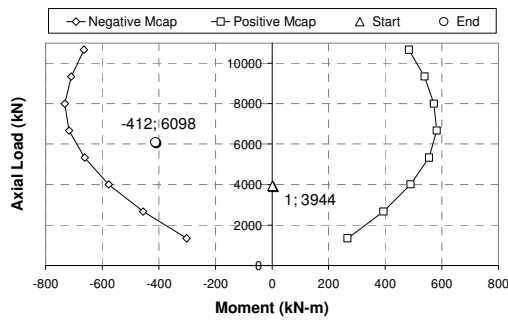
(b)



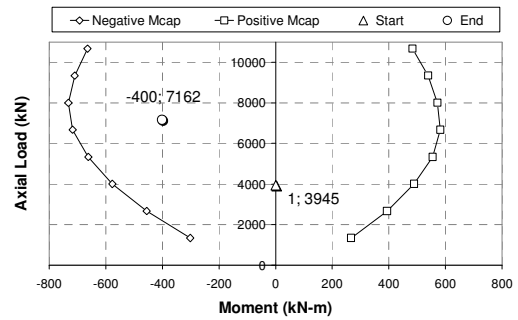
(c)



(d)

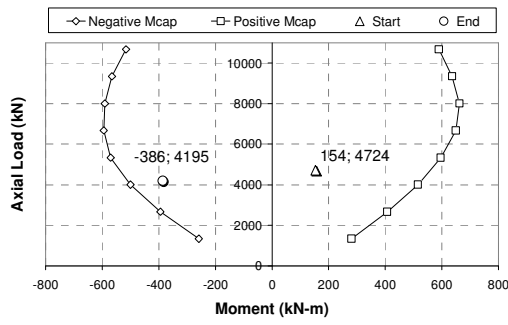


(e)

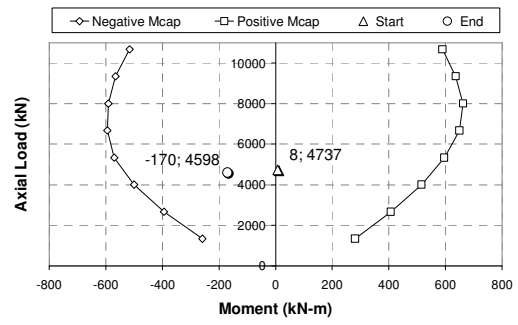


(f)

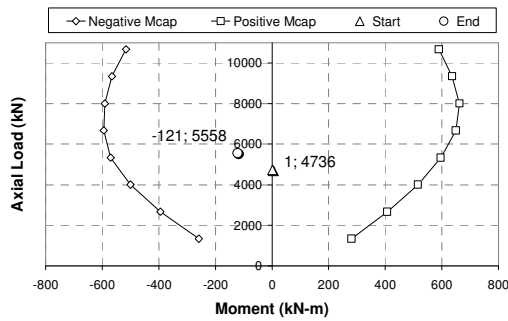
Figure B.4 M-P @ SL: (a) M4.30.010, (b) M4.30.125, (c) M4.30.240, (d) M4.36.010, (e) M4.36.125, (f) M4.36.240



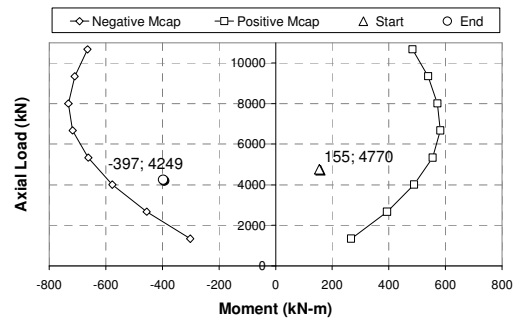
(a)



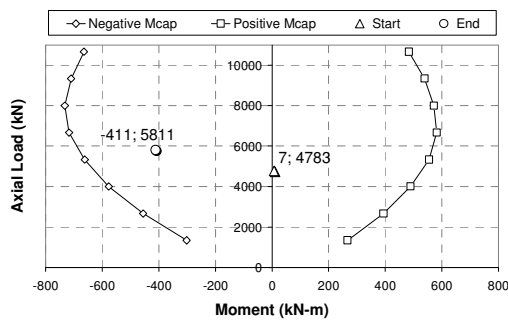
(b)



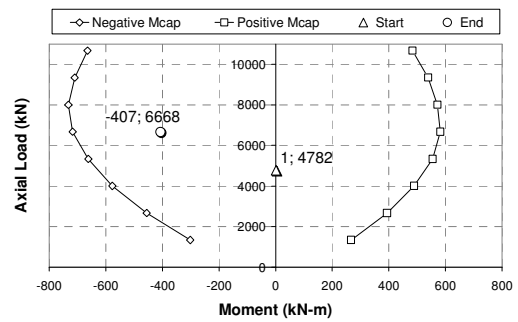
(c)



(d)

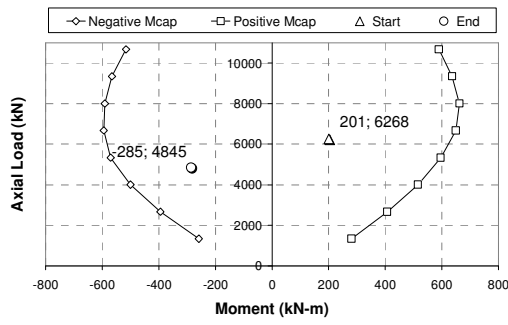


(e)

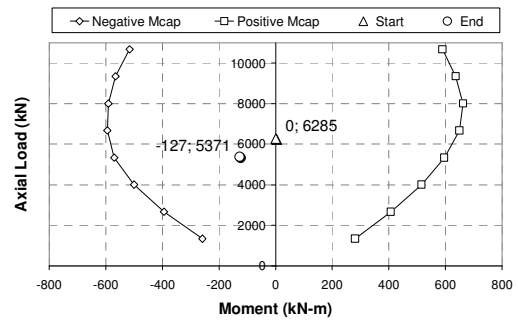


(f)

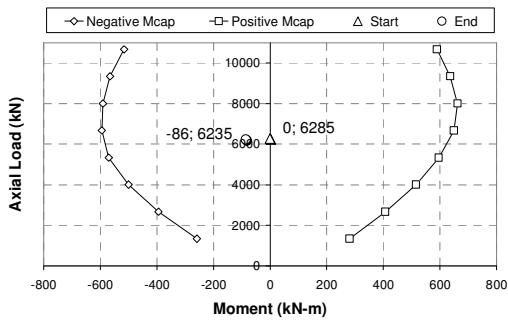
Figure B.5 M-P @ SL: (a) D3.30.010, (b) D3.30.125, (c) D3.30.240, (d) D3.36.010, (e) D3.36.125, (f) D3.36.240



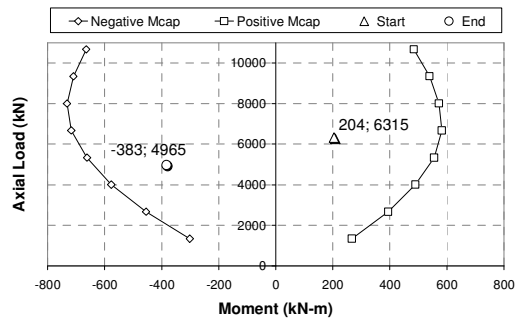
(a)



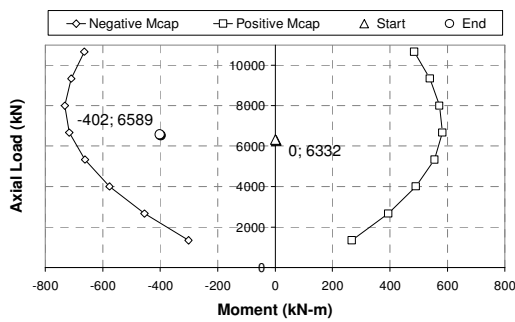
(b)



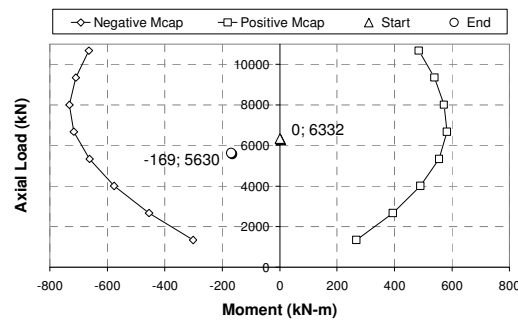
(c)



(d)

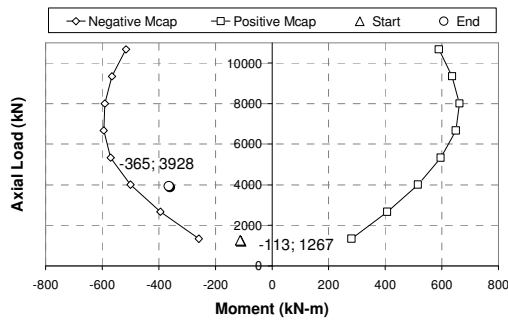


(e)

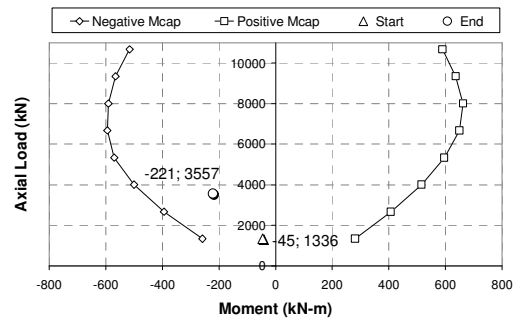


(f)

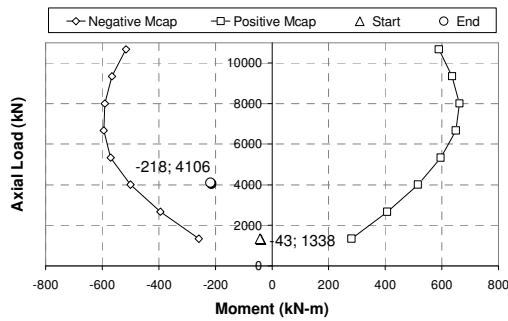
Figure B.6 M-P @ SL: (a) D4.30.010, (b) D4.30.125, (c) D4.30.240, (d) D4.36.010, (e) D4.36.125, (f) D4.36.240



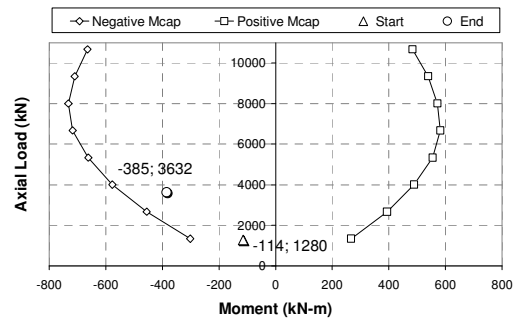
(a)



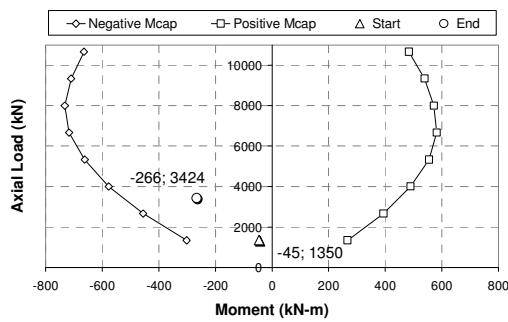
(b)



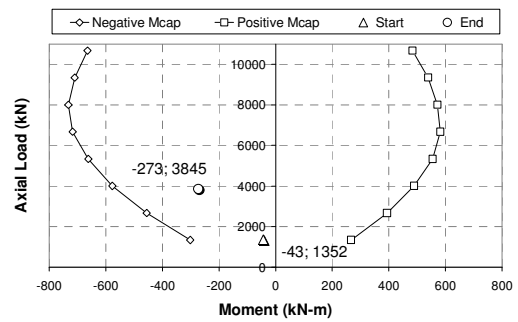
(c)



(d)

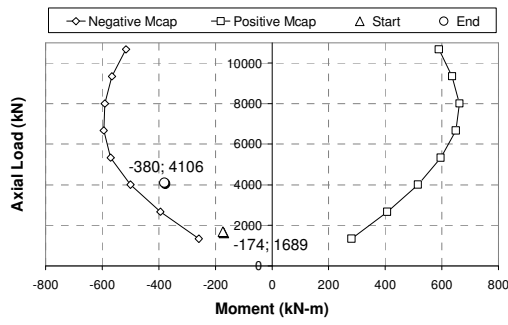


(e)

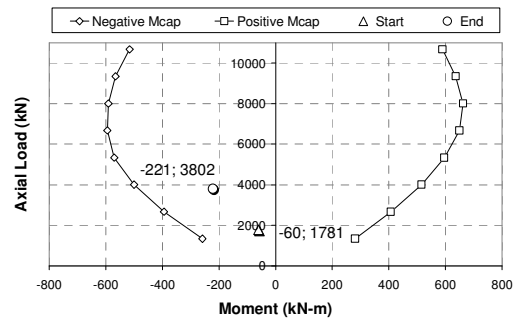


(f)

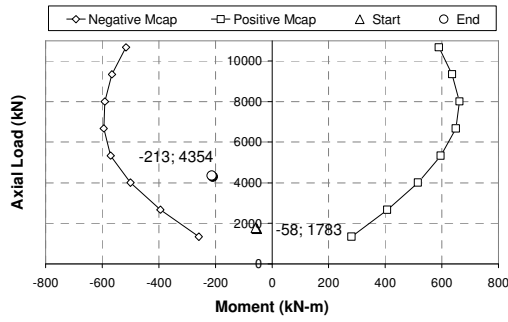
Figure B.7 M-P @ Cr: (a) S3.30.010, (b) S3.30.125, (c) S3.30.240, (d) S3.36.010, (e) S3.36.125, (f) S3.36.240



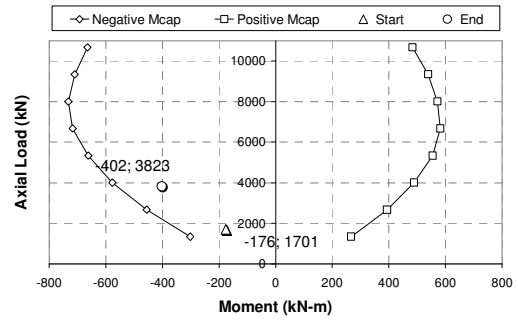
(a)



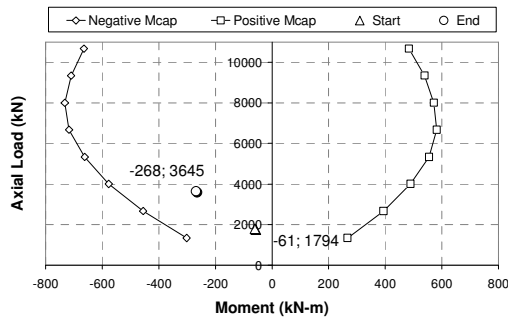
(b)



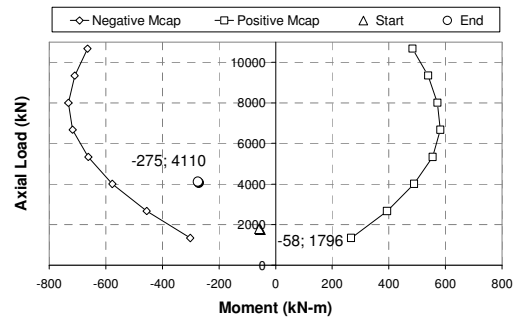
(c)



(d)

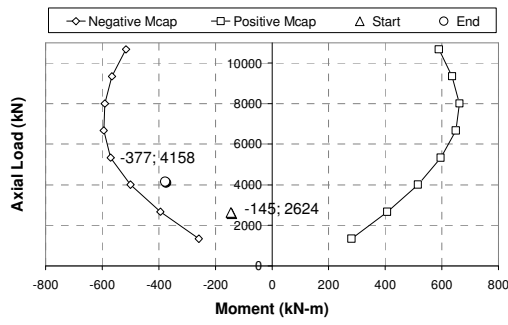


(e)

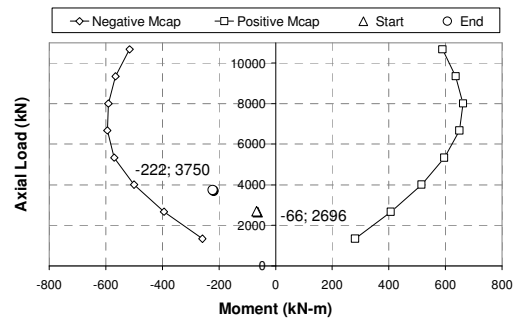


(f)

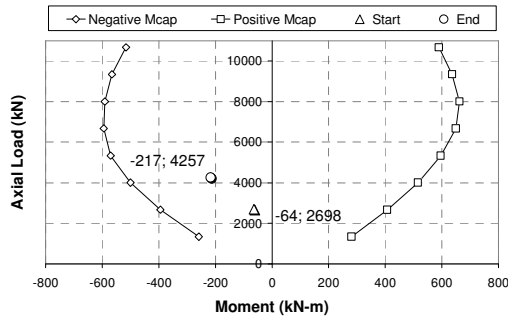
Figure B.8 M-P @ Cr: (a) S4.30.010, (b) S4.30.125, (c) S4.30.240, (d) S4.36.010, (e) S4.36.125, (f) S4.36.240



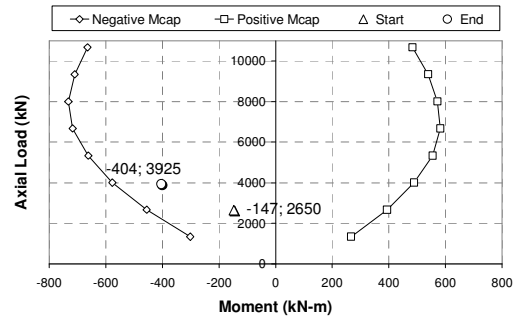
(a)



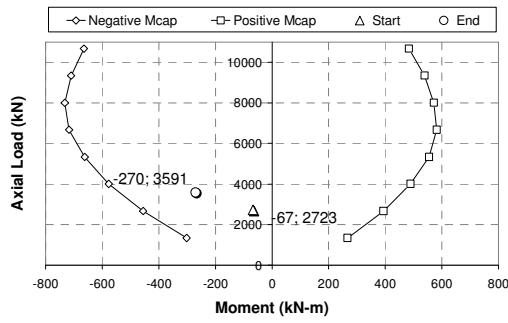
(b)



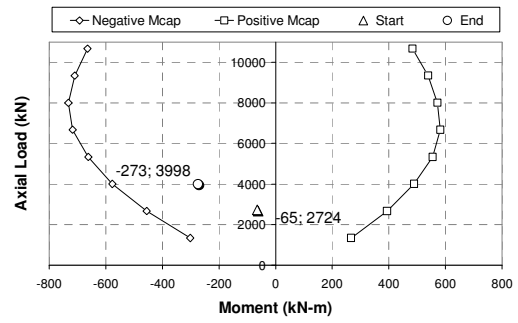
(c)



(d)

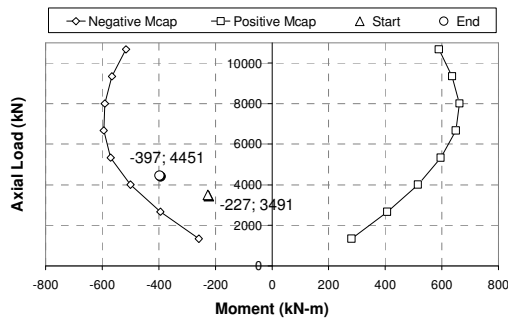


(e)

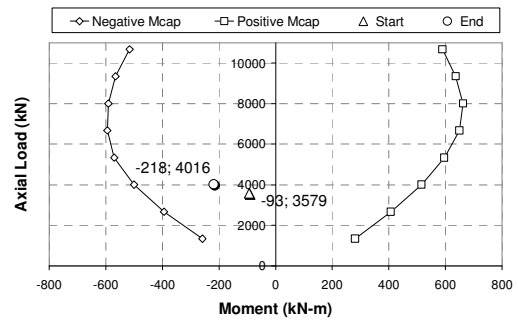


(f)

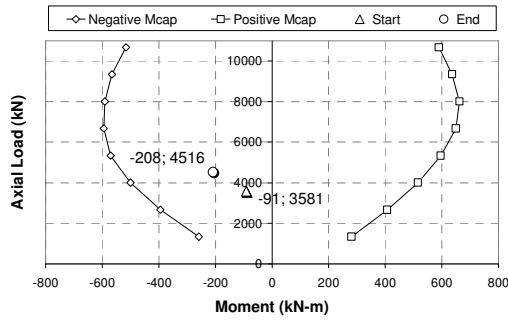
Figure B.9 M-P @ Cr: (a) M3.30.010, (b) M3.30.125, (c) M3.30.240, (d) M3.36.010, (e) M3.36.125, (f) M3.36.240



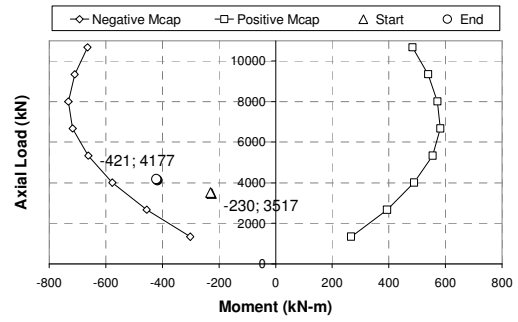
(a)



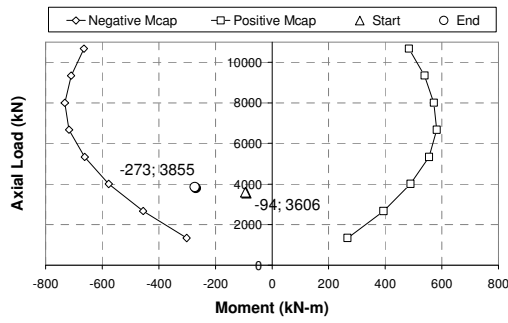
(b)



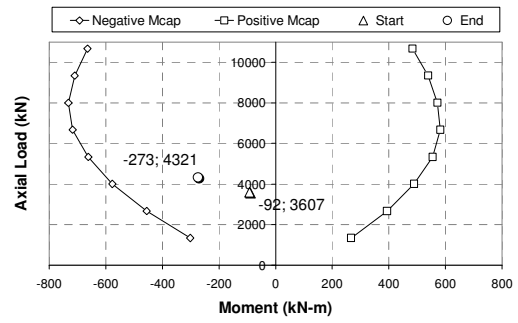
(c)



(d)

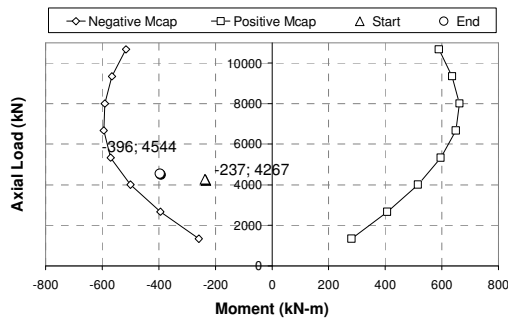


(e)

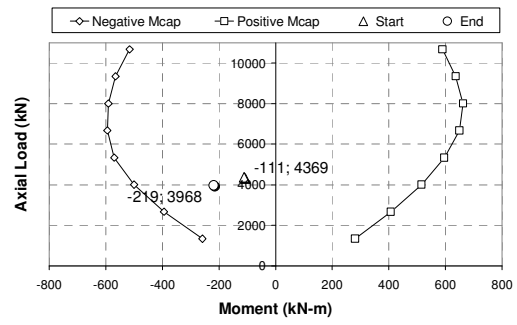


(f)

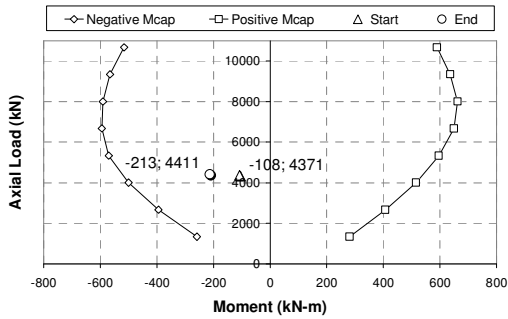
Figure B.10 M-P @ Cr: (a) M4.30.010, (b) M4.30.125, (c) M4.30.240, (d) M4.36.010, (e) M4.36.125, (f) M4.36.240



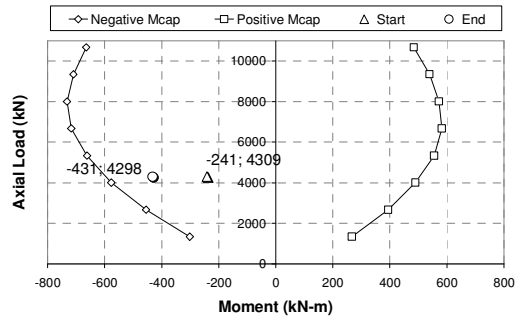
(a)



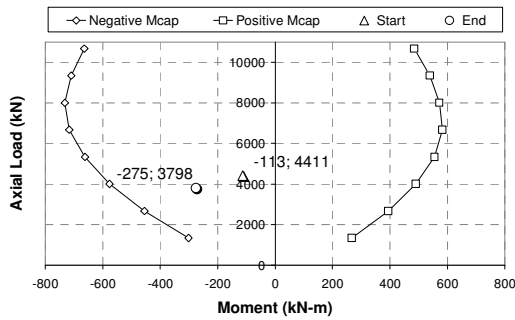
(b)



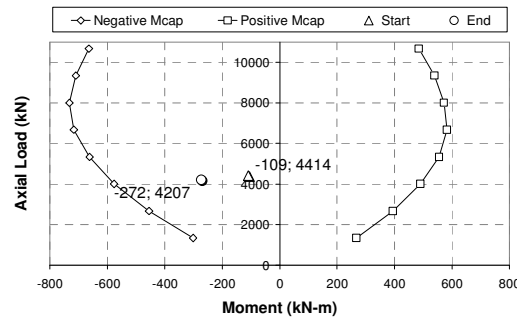
(c)



(d)

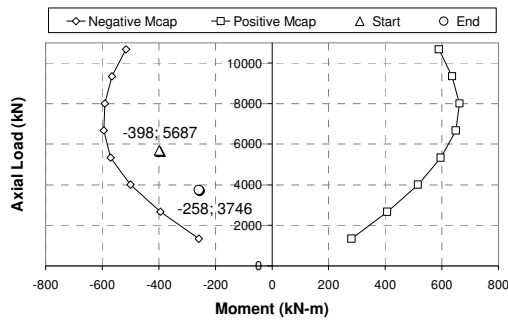


(e)

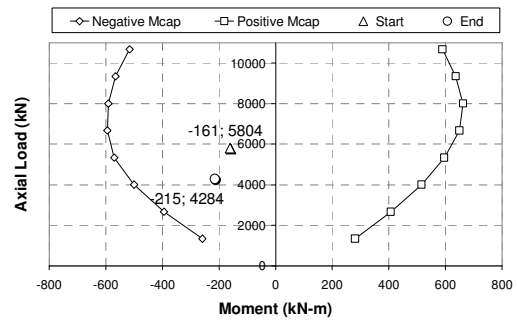


(f)

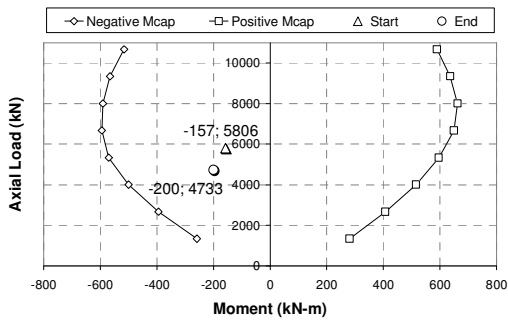
Figure B.11 M-P @ Cr: (a) D3.30.010, (b) D3.30.125, (c) D3.30.240, (d) D3.36.010, (e) D3.36.125, (f) D3.36.240



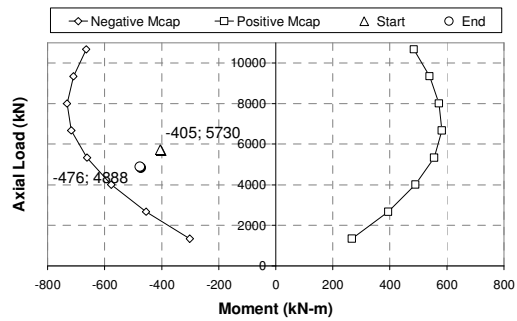
(a)



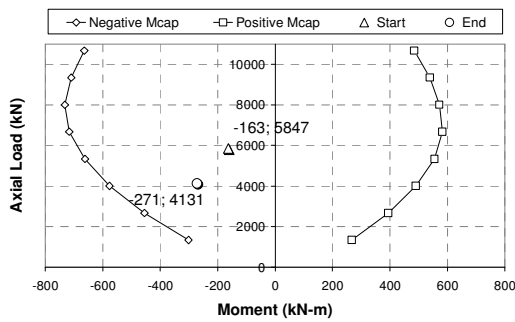
(b)



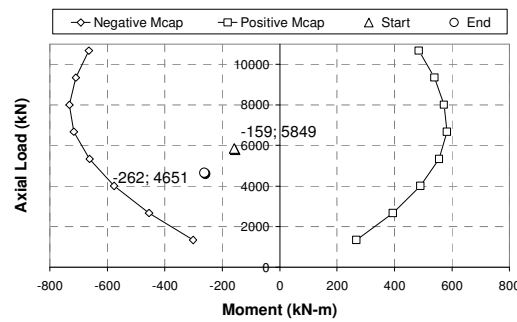
(c)



(d)



(e)

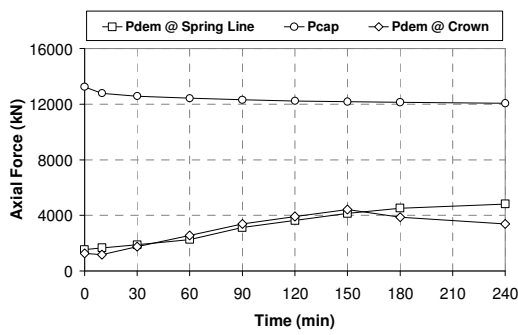


(f)

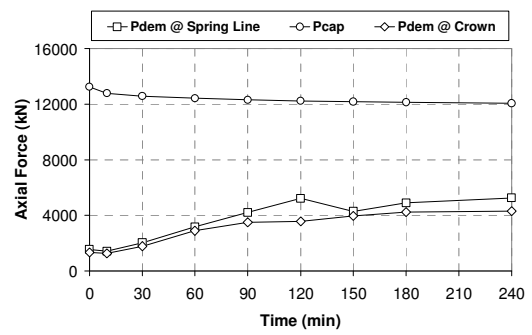
Figure B.12 M-P @ Cr: (a) D4.30.010, (b) D4.30.125, (c) D4.30.240, (d) D4.36.010, (e) D4.36.125, (f) D4.36.240

## APPENDIX C

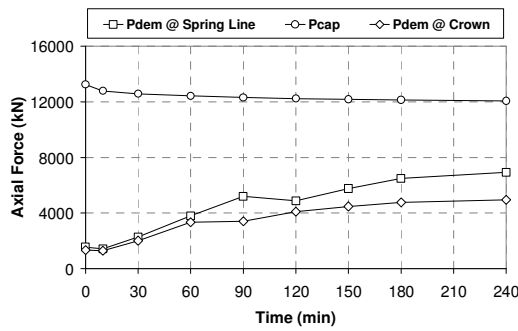
### AXIAL LOAD DEMAND AND CAPACITY DURING HYDROCARBON FIRE FOR SPRING LINE AND CROWN



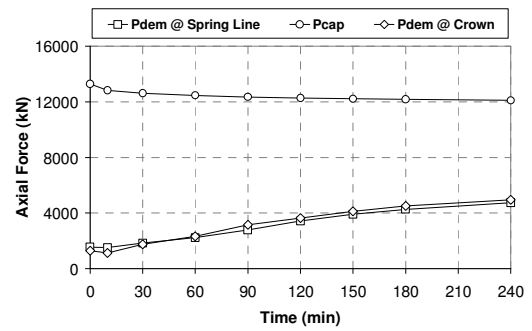
(a)



(b)

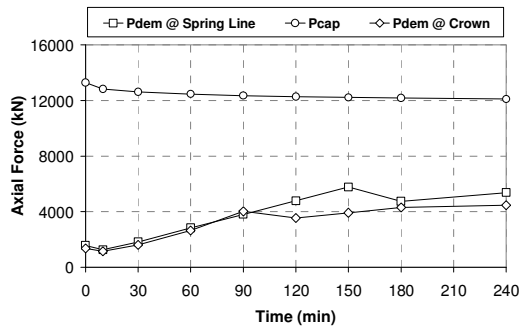


(c)

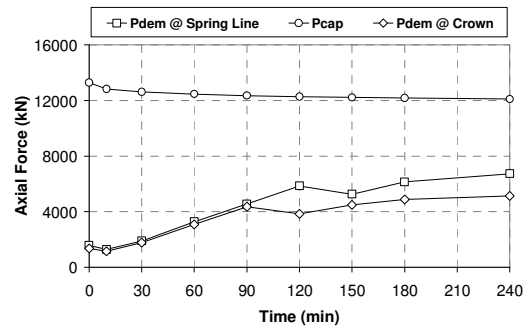


(d)

Figure C.1  $P_{CAP}-P_{DEM}$ : (a) S3.30.010, (b) S3.30.125, (c) S3.30.240,  
(d) S3.36.010

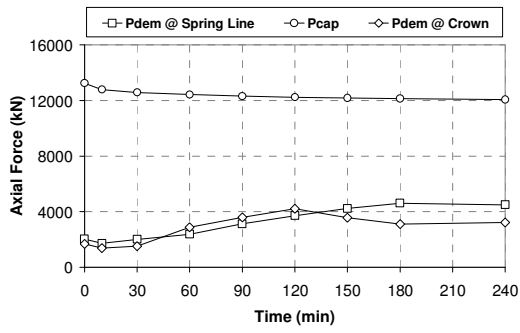


(e)

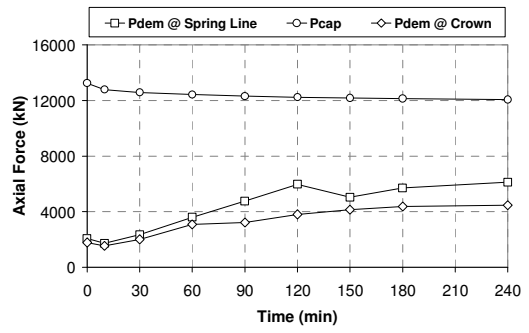


(f)

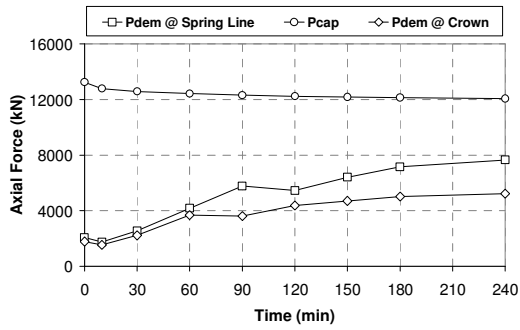
Figure C.1 (Continued)  $P_{CAP}$ - $P_{DEM}$ : (e) S3.36.125, (f) S3.36.240



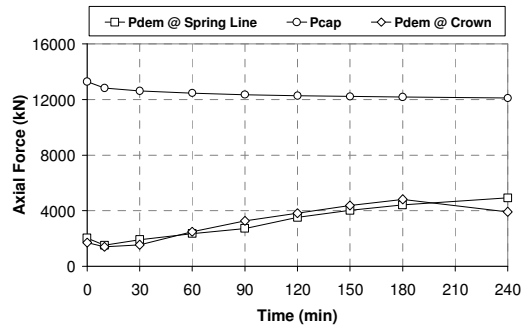
(a)



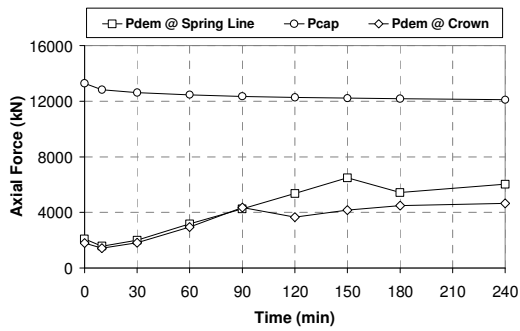
(b)



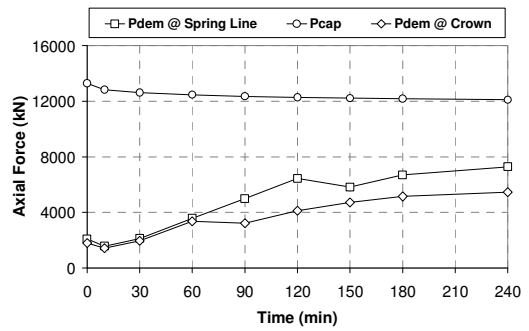
(c)



(d)

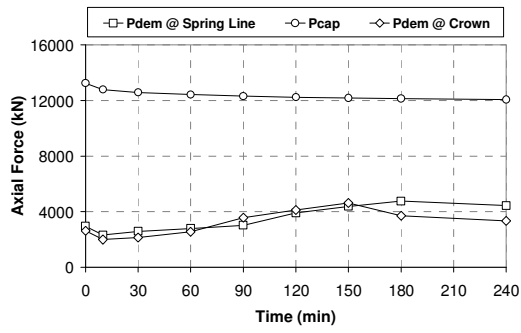


(e)

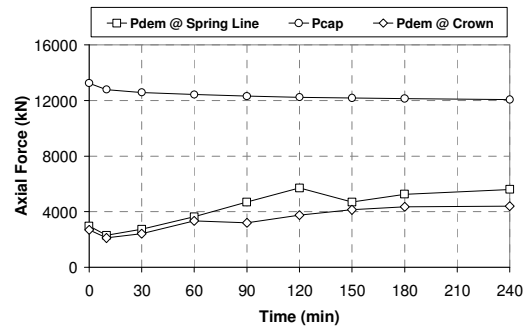


(f)

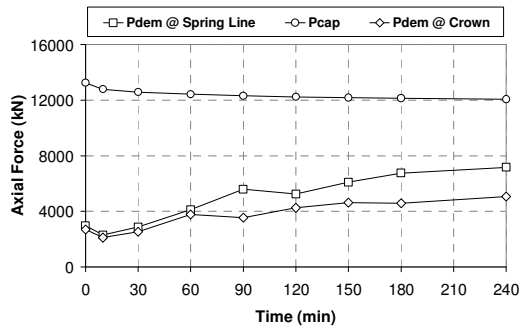
Figure C.2  $P_{CAP}$ - $P_{DEM}$ : (a) S4.30.010, (b) S4.30.125, (c) S4.30.240,  
 (d) S4.36.010, (e) S4.36.125, (f) S4.36.240



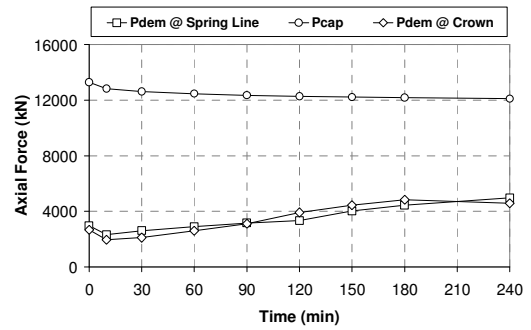
(a)



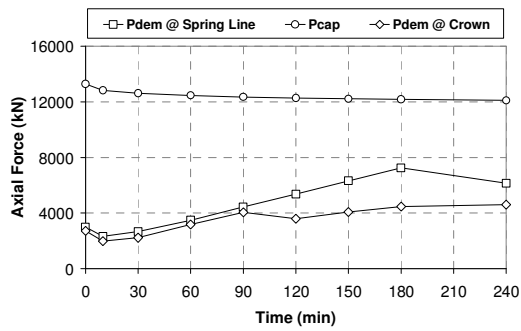
(b)



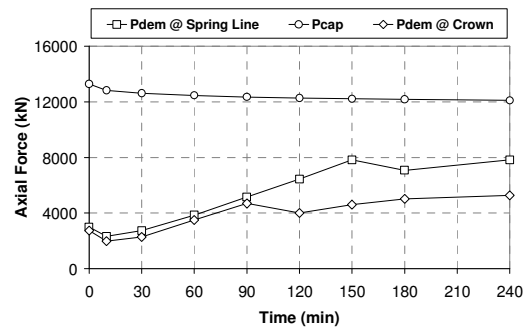
(c)



(d)

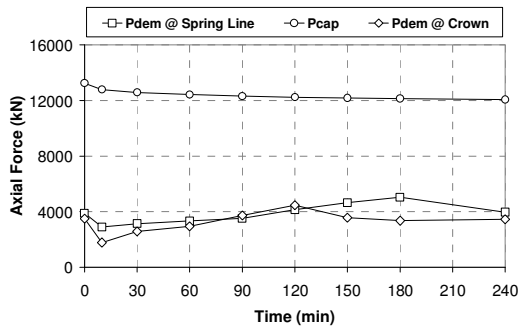


(e)

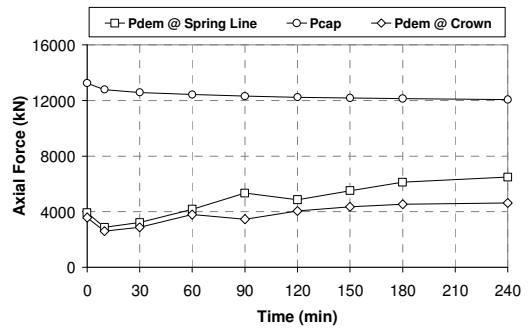


(f)

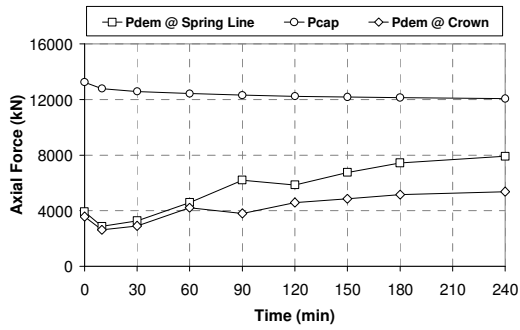
Figure C.3  $P_{CAP}$ - $P_{DEM}$ : (a) M3.30.010, (b) M3.30.125, (c) M3.30.240, (d) M3.36.010, (e) M3.36.125, (f) M3.36.240



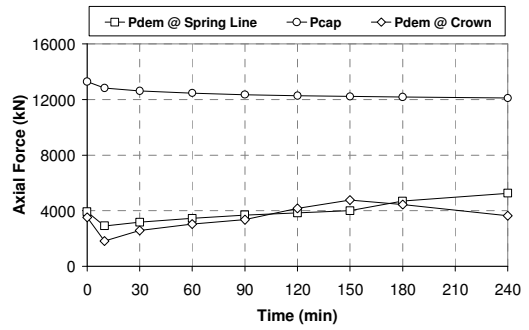
(a)



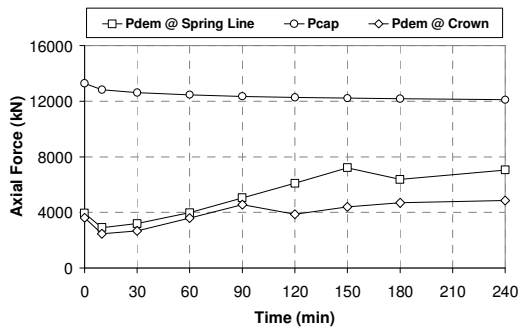
(b)



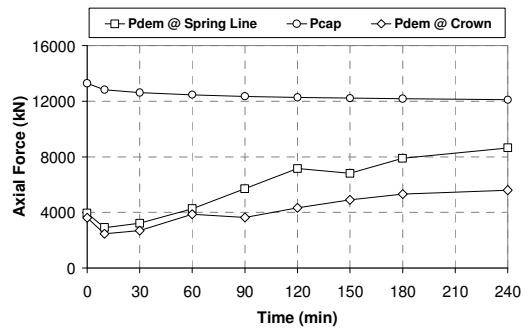
(c)



(d)

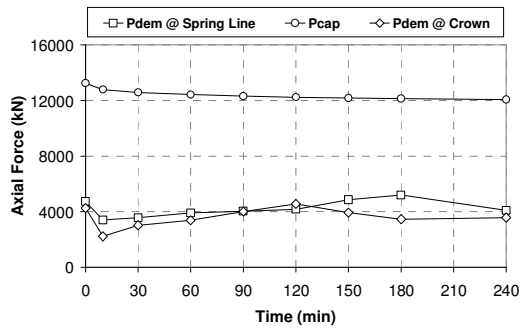


(e)

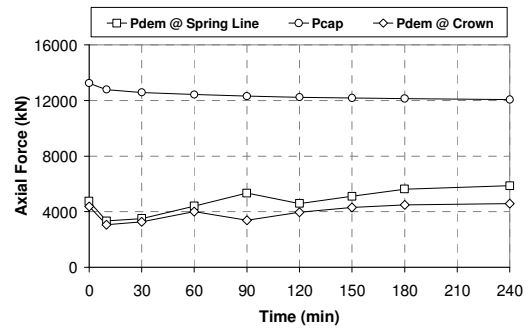


(f)

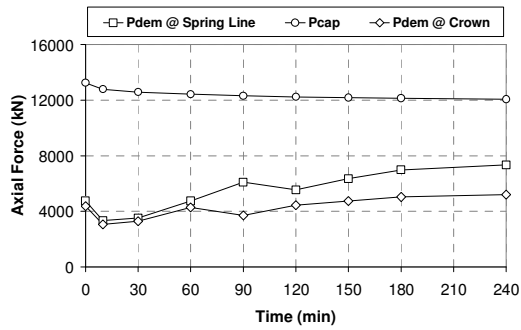
Figure C.4  $P_{CAP}$ - $P_{DEM}$ : (a) M4.30.010, (b) M4.30.125, (c) M4.30.240, (d) M4.36.010, (e) M4.36.125, (f) M4.36.240



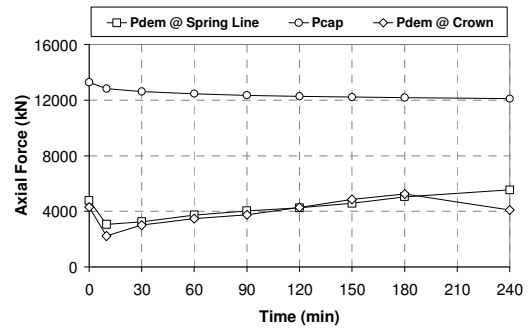
(a)



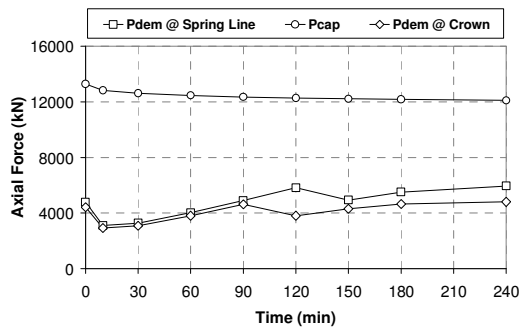
(b)



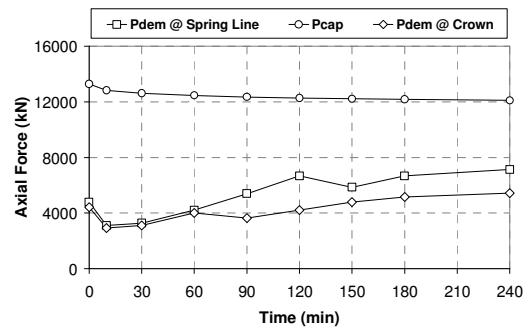
(c)



(d)

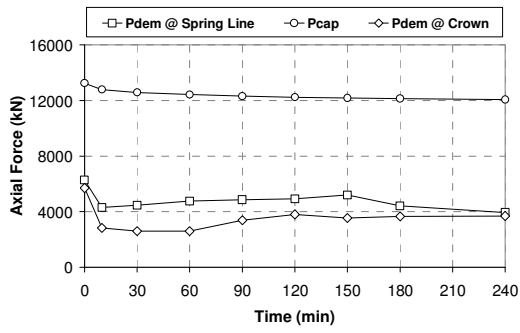


(e)

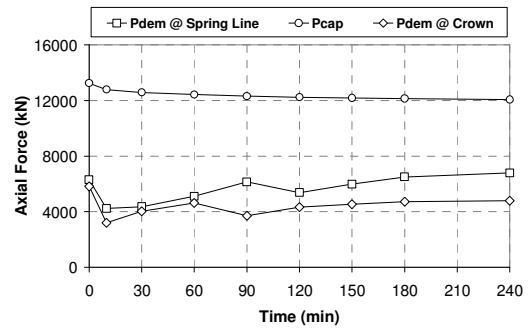


(f)

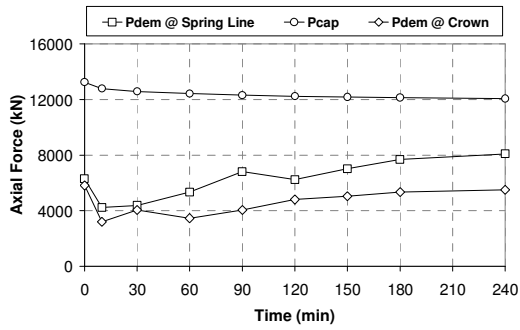
Figure C.5  $P_{CAP}-P_{DEM}$ : (a) D3.30.010, (b) D3.30.125, (c) D3.30.240,  
(d) D3.36.010, (e) D3.36.125, (f) D3.36.240



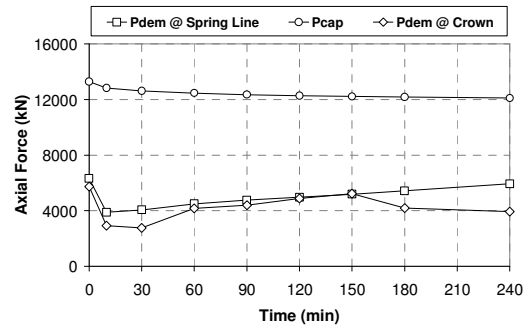
(a)



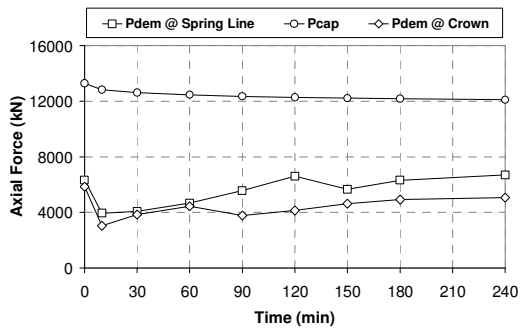
(b)



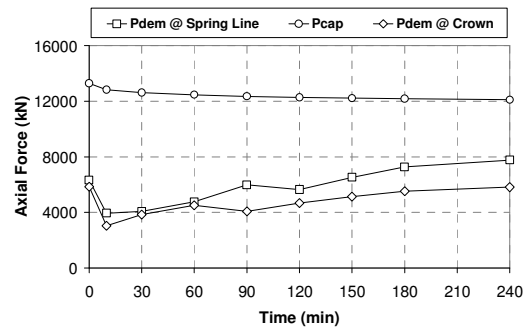
(c)



(d)



(e)

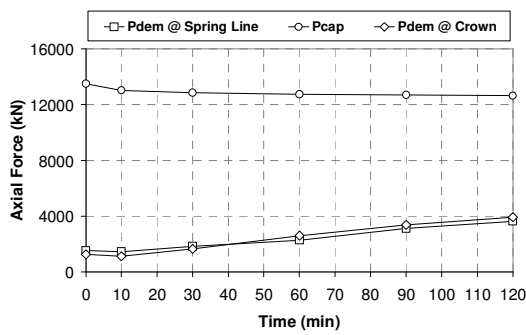


(f)

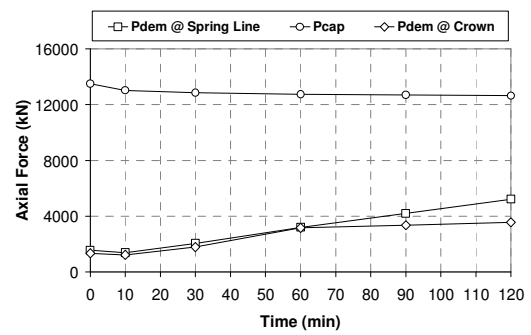
Figure C.6  $P_{CAP}$ - $P_{DEM}$ : (a) D4.30.010, (b) D4.30.125, (c) D4.30.240, (d) D4.36.010, (e) D4.36.125, (f) D4.36.240

## APPENDIX D

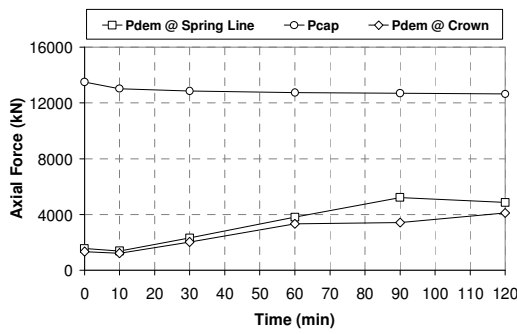
### AXIAL LOAD DEMAND AND CAPACITY DURING RWS FIRE FOR SPRING LINE AND CROWN



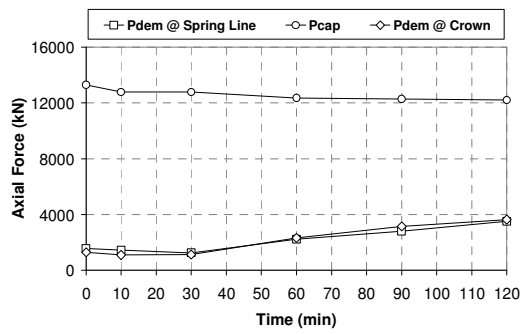
(a)



(b)

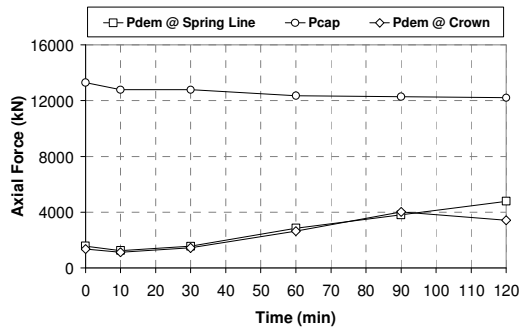


(c)

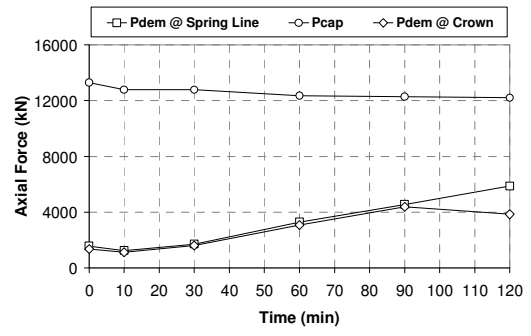


(d)

Figure D.1  $P_{CAP}-P_{DEM}$ : (a) S3.30.010, (b) S3.30.125, (c) S3.30.240,  
(d) S3.36.010

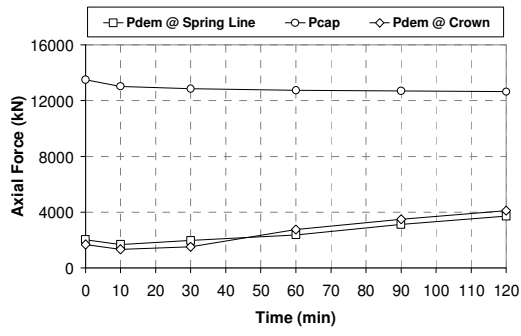


(e)

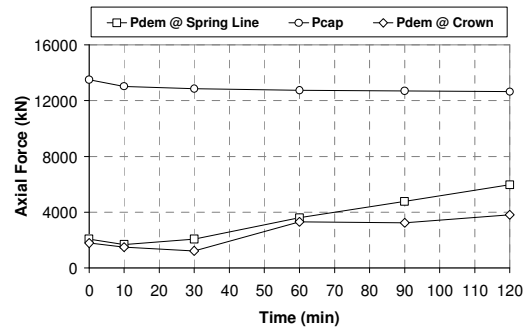


(f)

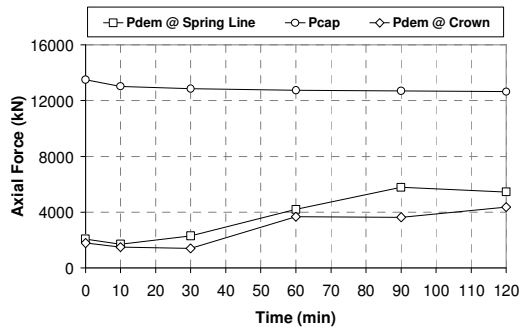
Figure D.1 (Continued)  $P_{CAP}$ - $P_{DEM}$ : (e) S3.36.125, (f) S3.36.240



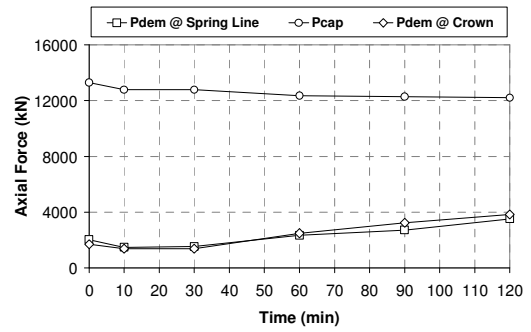
(a)



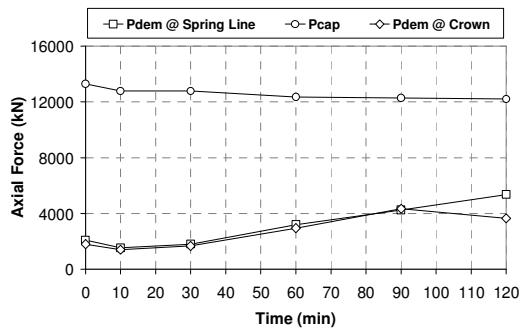
(b)



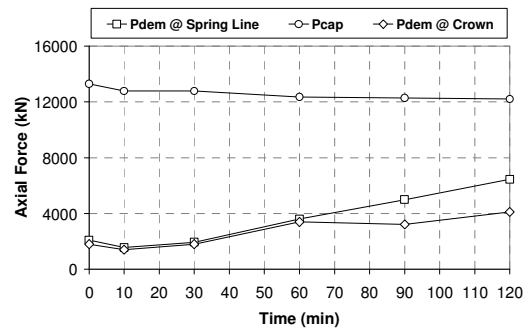
(c)



(d)

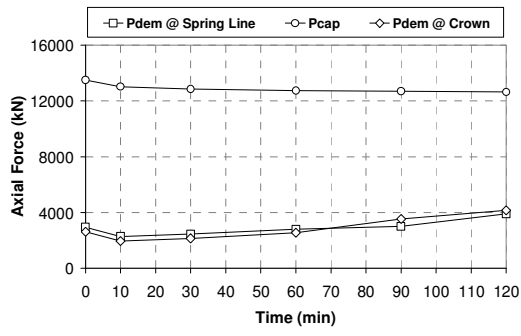


(e)

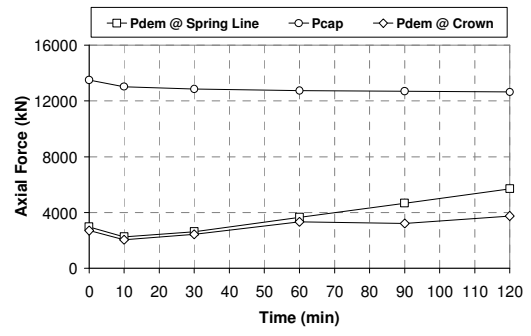


(f)

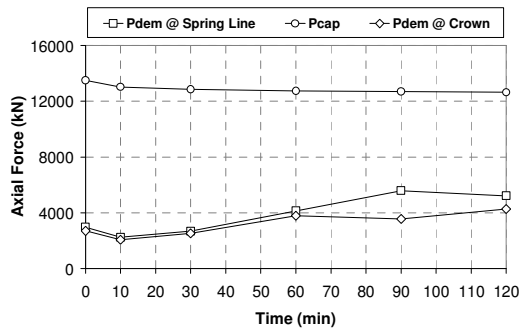
Figure D.2  $P_{CAP}-P_{DEM}$ : (a) S4.30.010, (b) S4.30.125, (c) S4.30.240,  
 (d) S4.36.010, (e) S4.36.125, (f) S4.36.240



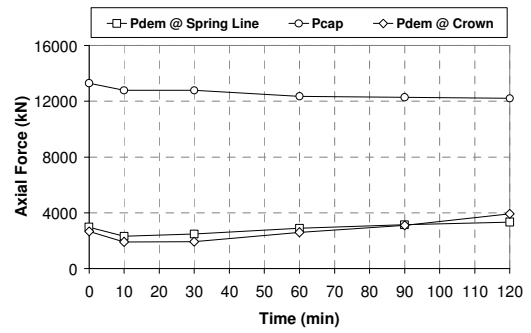
(a)



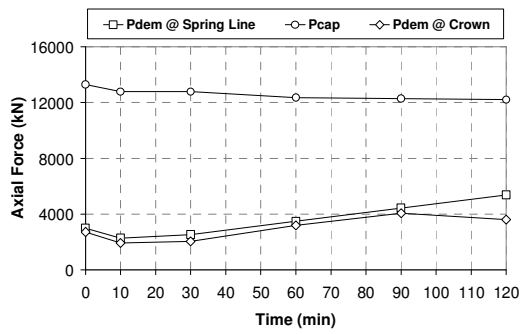
(b)



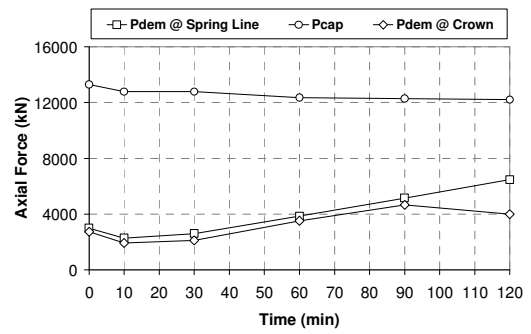
(c)



(d)

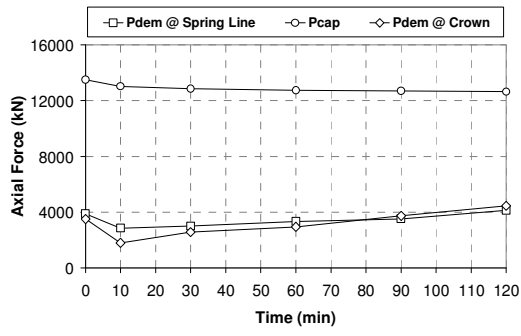


(e)

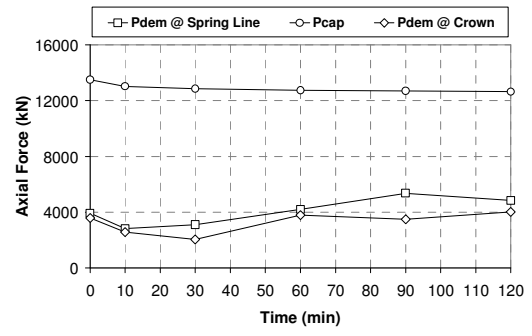


(f)

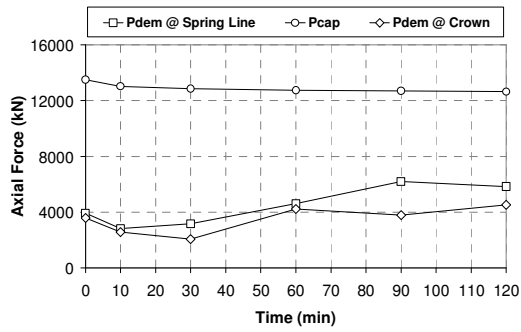
Figure D.3  $P_{CAP}-P_{DEM}$ : (a) M3.30.010, (b) M3.30.125, (c) M3.30.240,  
 (d) M3.36.010, (e) M3.36.125, (f) M3.36.240



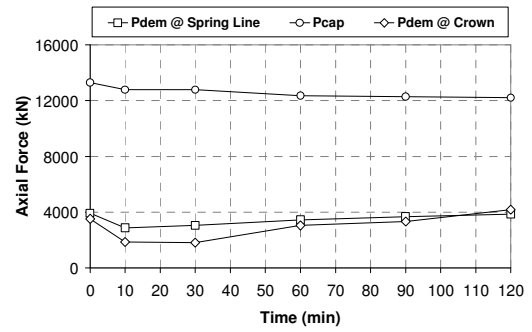
(a)



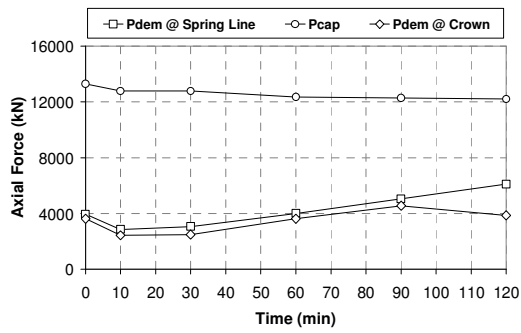
(b)



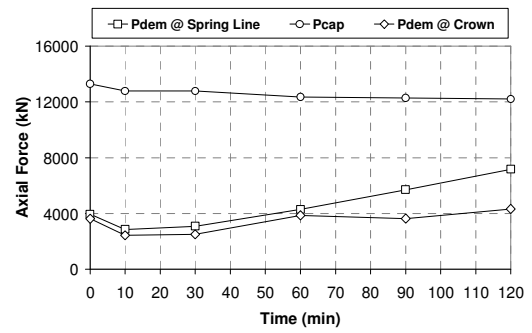
(c)



(d)

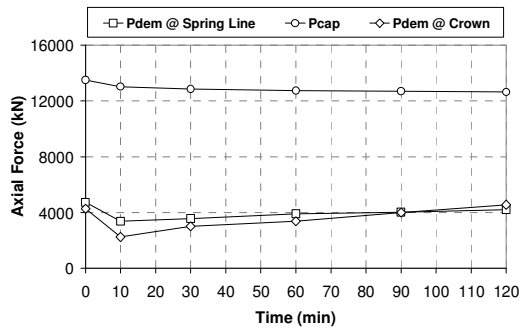


(e)

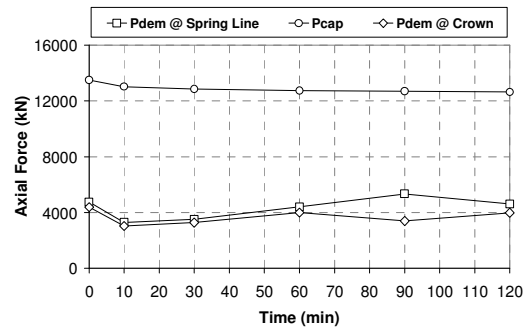


(f)

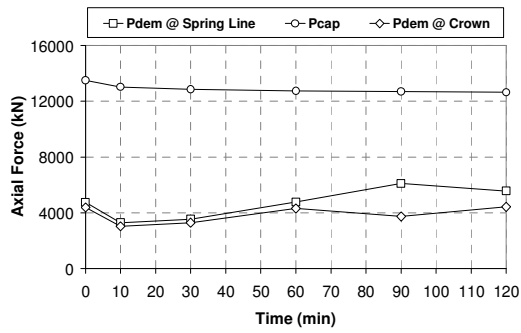
Figure D.4  $P_{CAP}-P_{DEM}$ : (a) M4.30.010, (b) M4.30.125, (c) M4.30.240, (d) M4.36.010, (e) M4.36.125, (f) M4.36.240



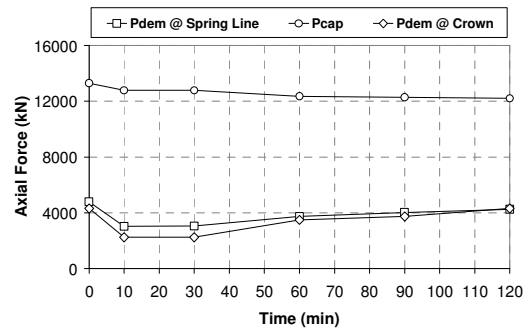
(a)



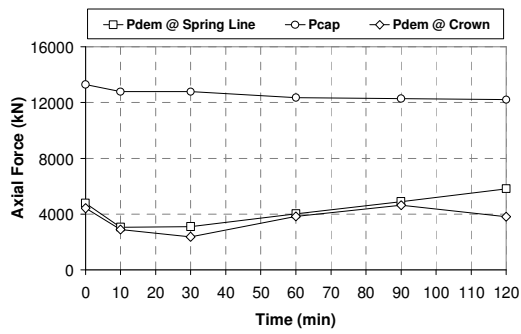
(b)



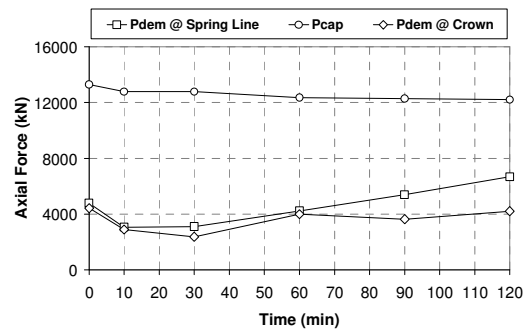
(c)



(d)

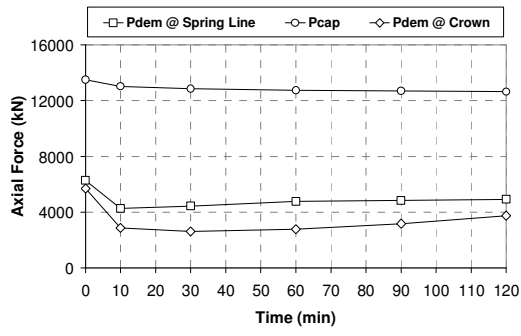


(e)

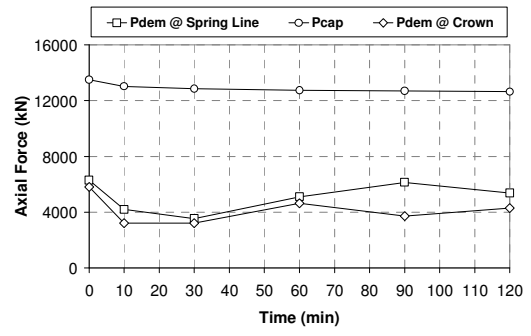


(f)

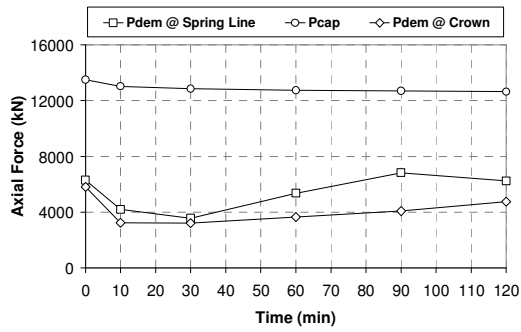
Figure D.5  $P_{CAP}$ - $P_{DEM}$ : (a) D3.30.010, (b) D3.30.125, (c) D3.30.240,  
 (d) D3.36.010, (e) D3.36.125, (f) D3.36.240



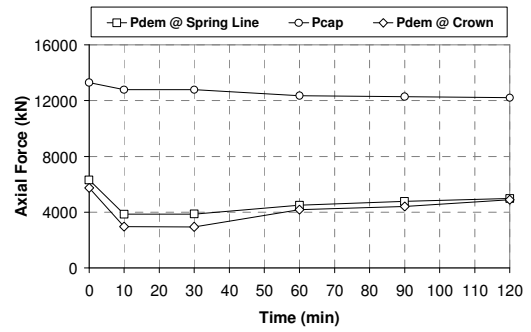
(a)



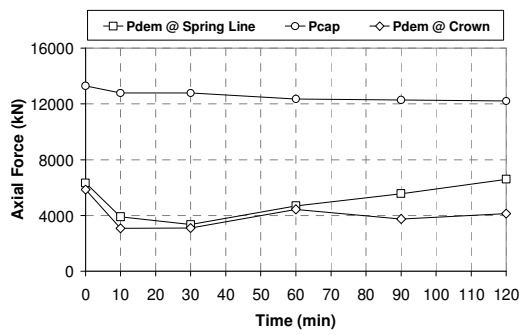
(b)



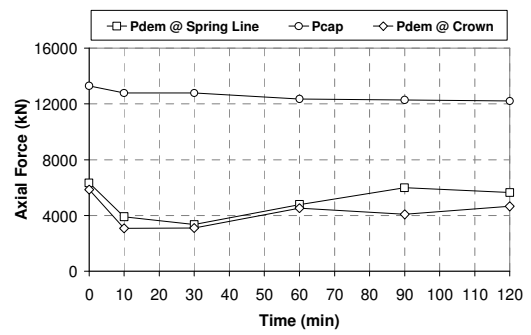
(c)



(d)



(e)

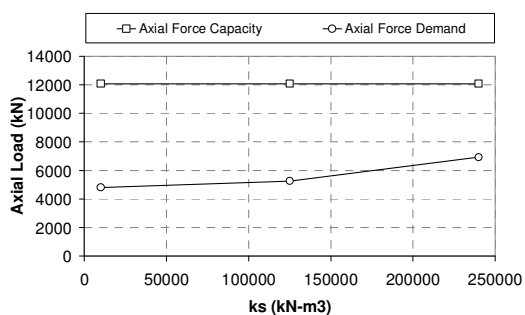


(f)

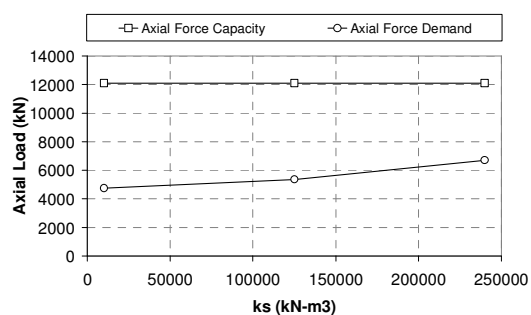
Figure D.6  $P_{CAP}$ - $P_{DEM}$ : (a) D4.30.010, (b) D4.30.125, (c) D4.30.240,  
 (d) D4.36.010, (e) D4.36.125, (f) D4.36.240

## APPENDIX E

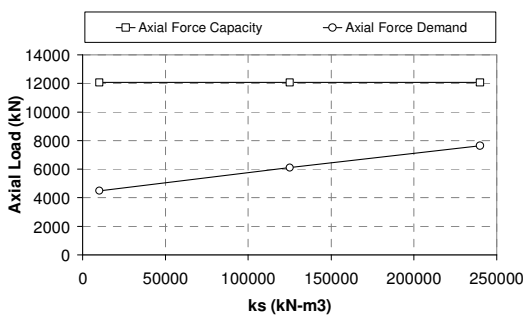
### AXIAL LOAD DEMAND AND CAPACITY VERSUS SUBGRADE REACTION MODULUS DURING HYDROCARBON FIRE FOR SPRING LINE



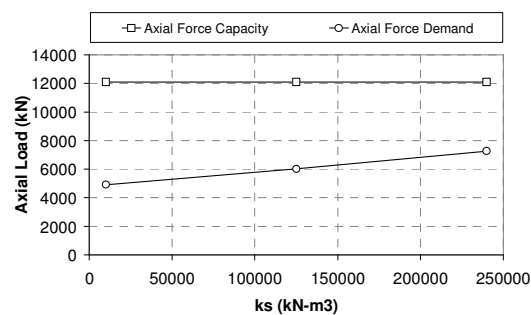
(a)



(b)

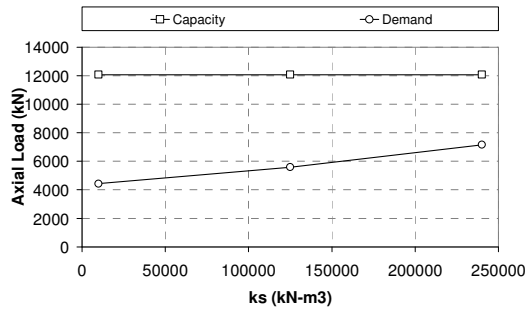


(c)

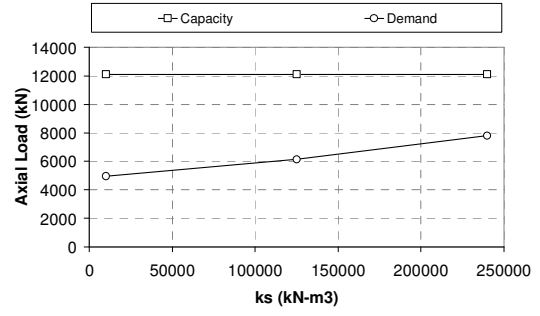


(d)

Figure E.1 P- $k_s$ : (a) S3.30, (b) S3.36, (c) S4.30,  
(d) S4.36

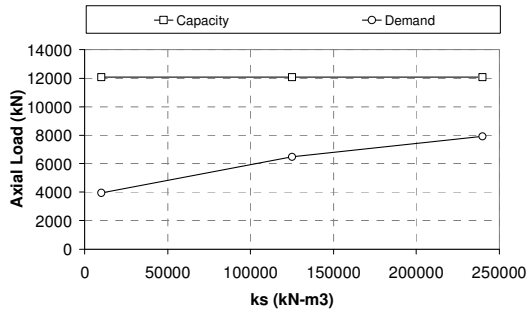


(e)

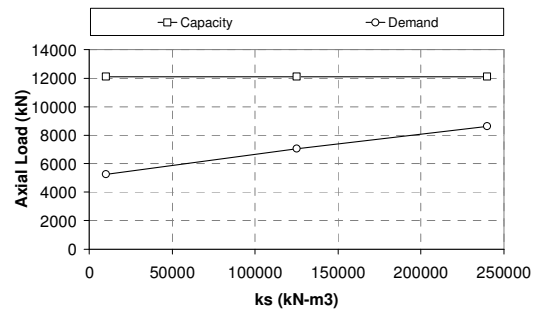


(f)

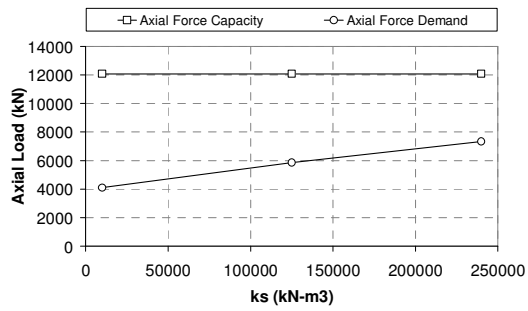
Figure E.1 (Continued) P-k<sub>s</sub>: (e) M3.30, (f) M3.36



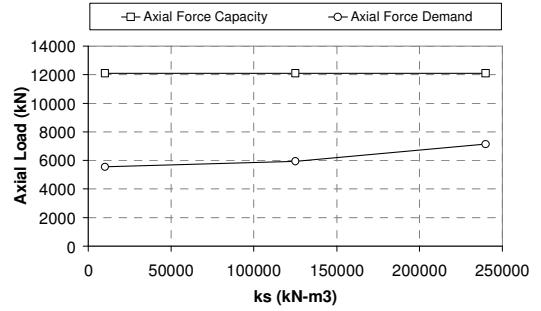
(a)



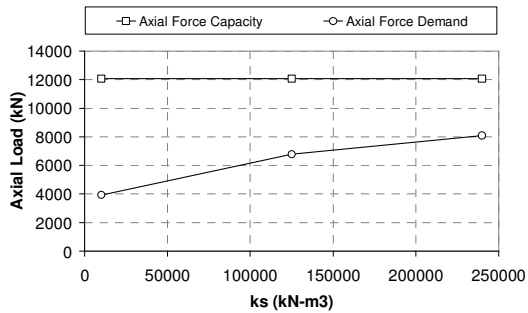
(b)



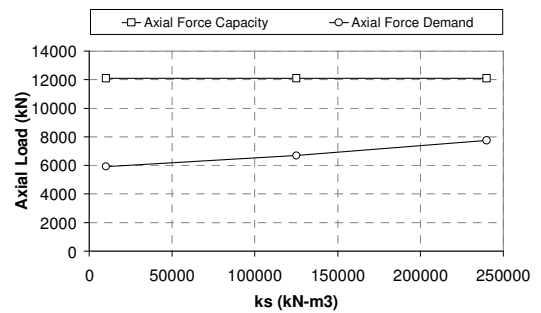
(c)



(d)



(e)

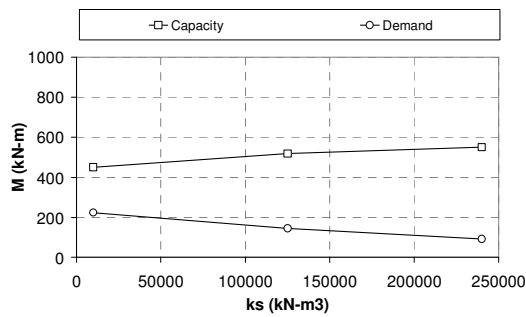


(f)

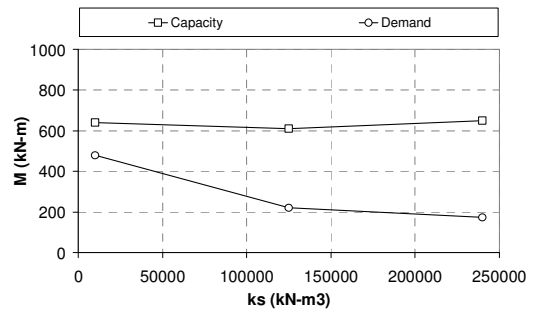
Figure E.2 P- $k_s$ : (a) M4.30, (b) M4.36, (c) D3.30, (d) D3.36, (e) D4.30, (f) D4.36

## APPENDIX F

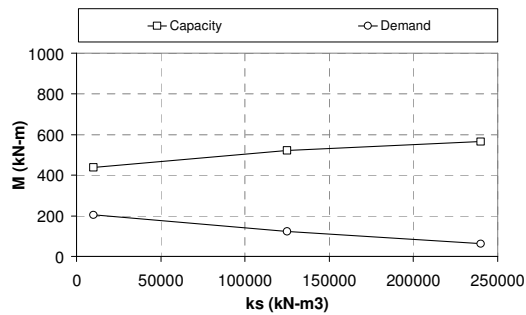
### BENDING MOMENT VERSUS SUBGRADE REACTION MODULUS AT THE END OF HYDROCARBON FIRE FOR CROWN



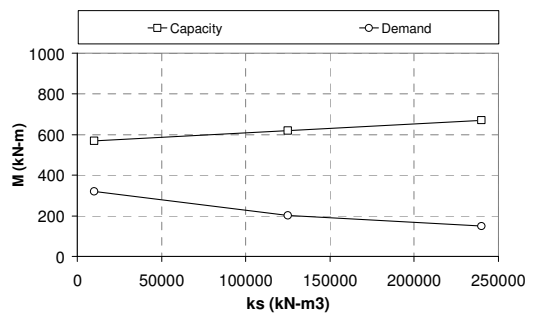
(a)



(b)

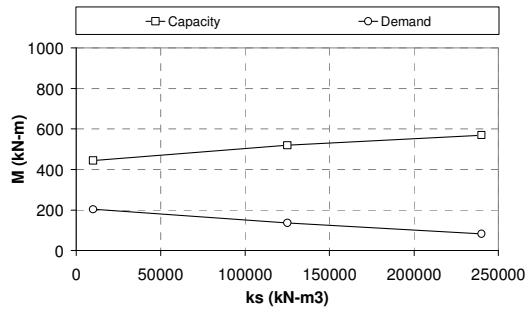


(c)

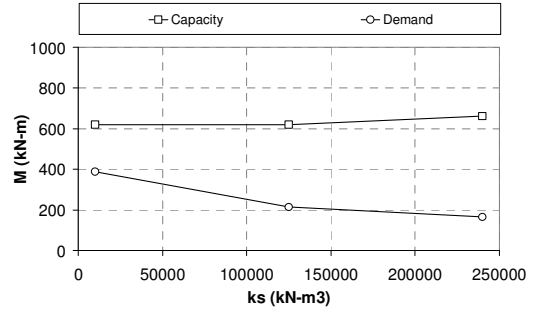


(d)

Figure F.1 M- $k_s$  : (a) S3.30, (b) S3.36, (c) S4.30,  
(d) S4.36

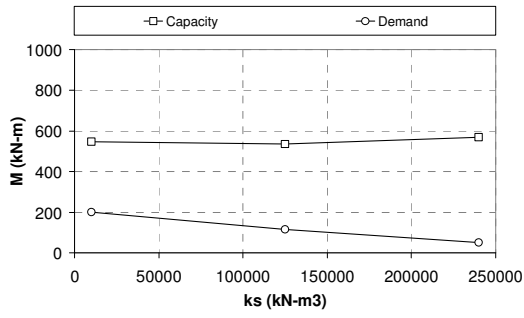


(e)

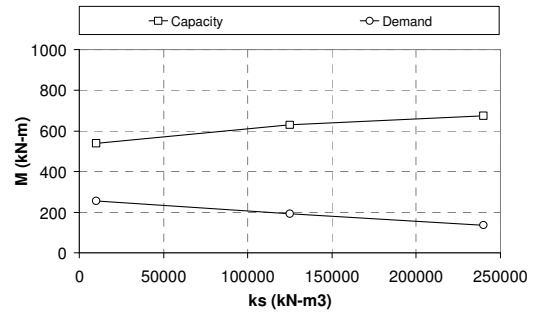


(f)

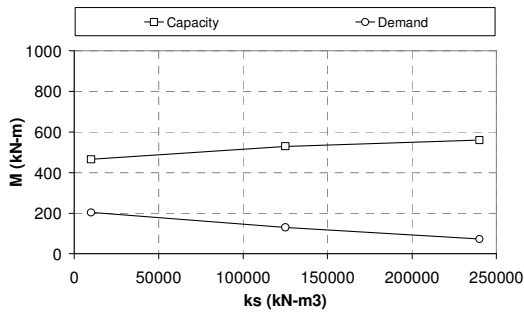
Figure F.1 (Continued) M-k<sub>s</sub> : (e) M3.30, (f) M3.36



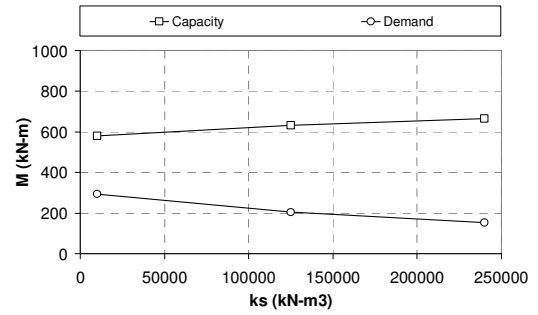
(a)



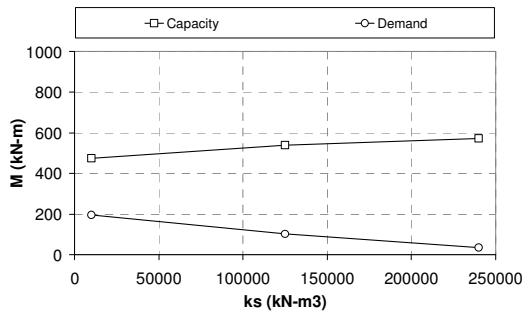
(b)



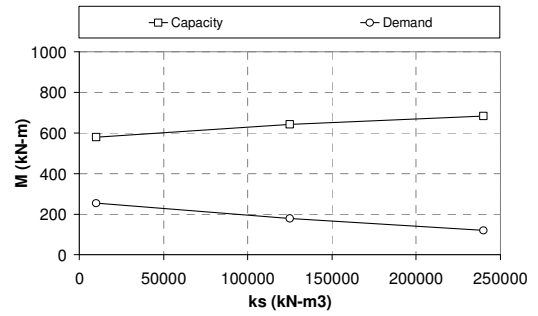
(c)



(d)



(e)

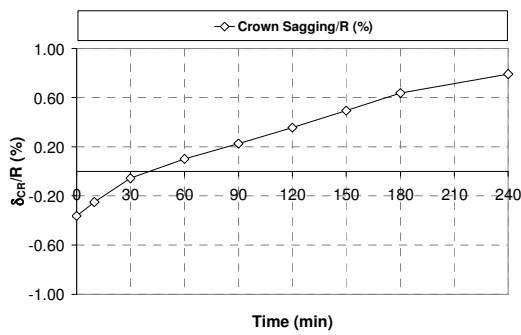


(f)

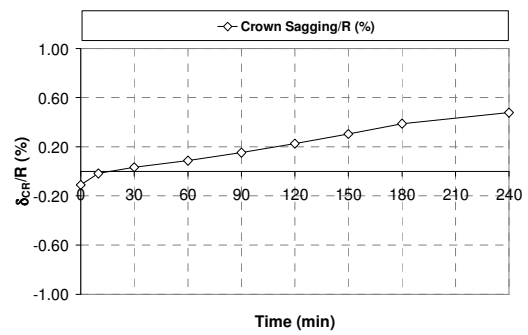
Figure F.2 M- $k_s$  : (a) M4.30, (b) M4.36, (c) D3.30, (d) D3.36, (e) D4.30, (f) D4.36

## APPENDIX G

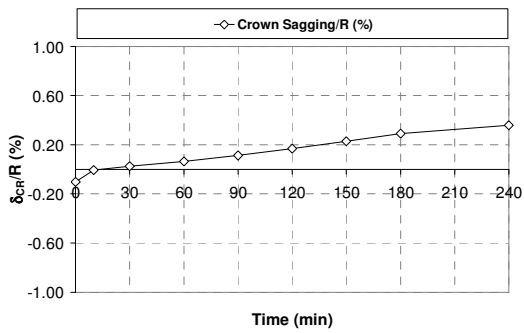
### RATIO OF CROWN DEFLECTION TO TUNNEL RADIUS DURING HYDROCARBON FIRE



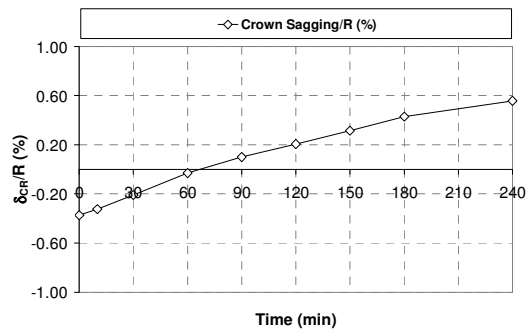
(a)



(b)

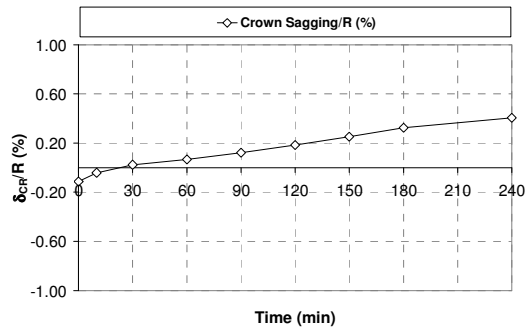


(c)

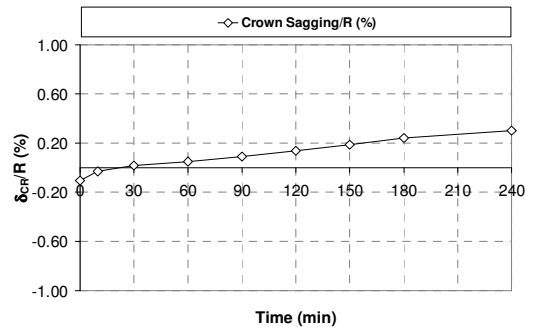


(d)

Figure G.1  $\delta_{CR}/R$ -t: (a) S3.30.010, (b) S3.30.125, (c) S3.30.240,  
(d) S3.36.010

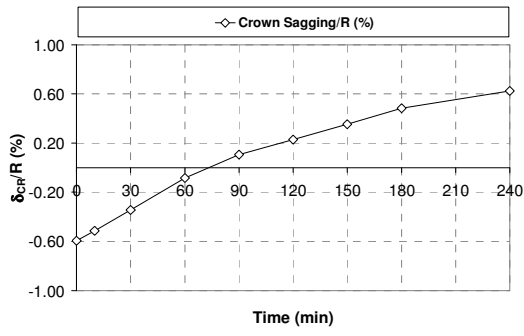


(e)

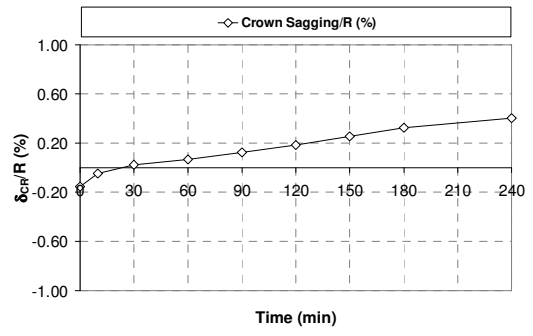


(f)

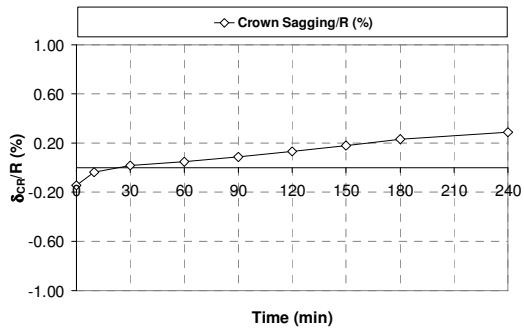
Figure G.1 (Continued)  $\delta_{CR}/R$ -t: (e) S3.36.125, (f) S3.36.240



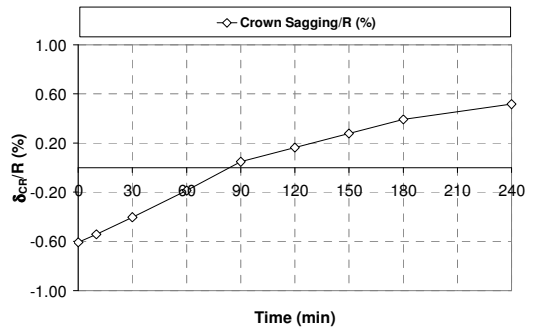
(a)



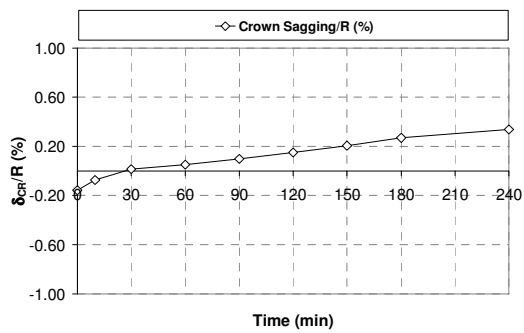
(b)



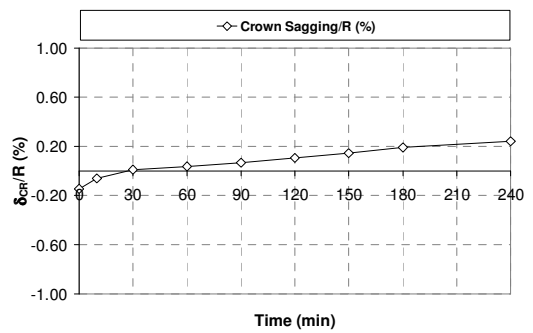
(c)



(d)

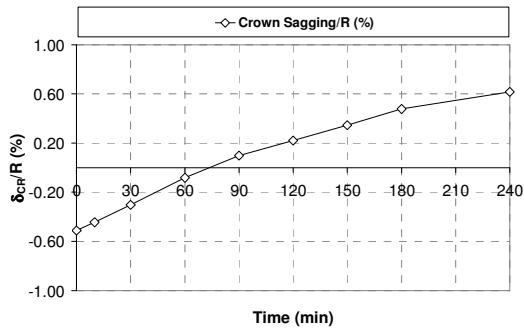


(e)

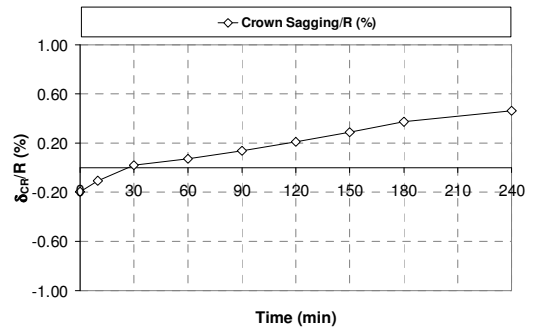


(f)

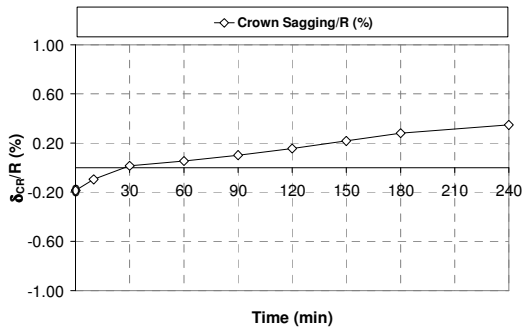
Figure G.2  $\delta_{CR}/R$ -t: (a) S4.30.010, (b) S4.30.125, (c) S4.30.240,  
 (d) S4.36.010, (e) S4.36.125, (f) S4.36.240



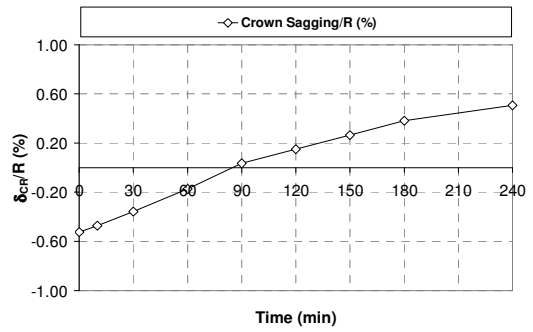
(a)



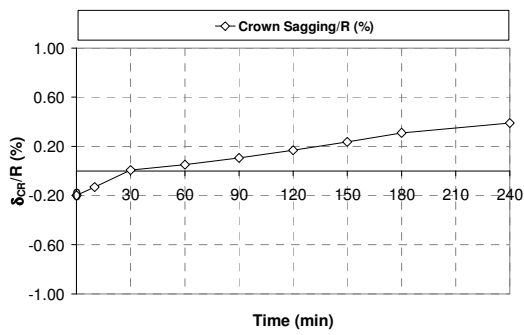
(b)



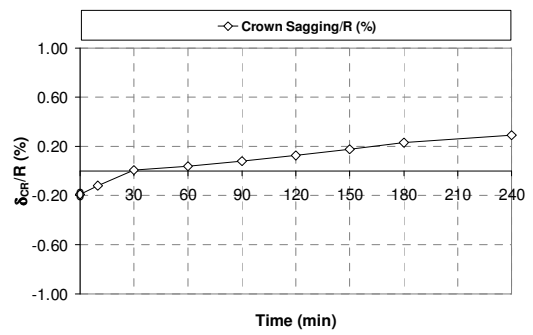
(c)



(d)

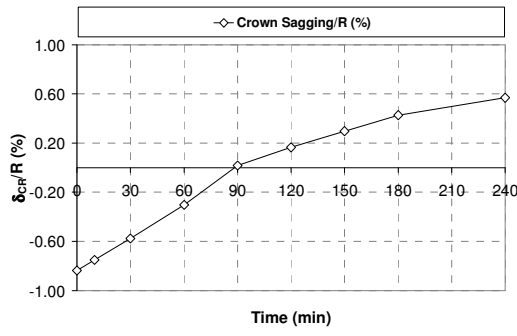


(e)

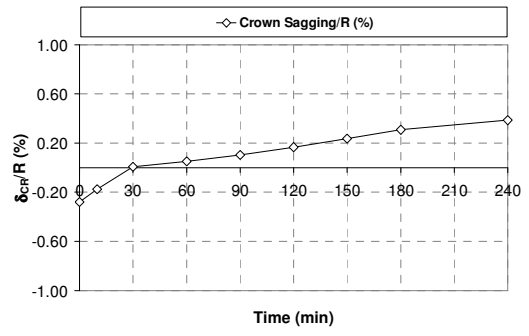


(f)

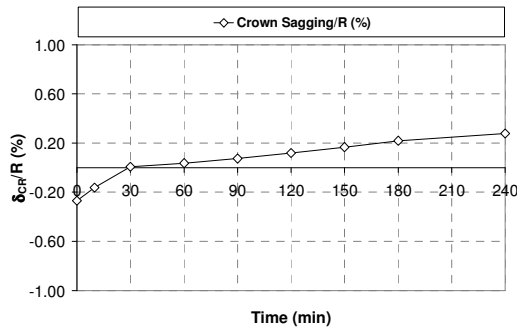
Figure G.3  $\delta_{CR}/R$ -t: (a) M3.30.010, (b) M3.30.125, (c) M3.30.240,  
(d) M3.36.010, (e) M3.36.125, (f) M3.36.240



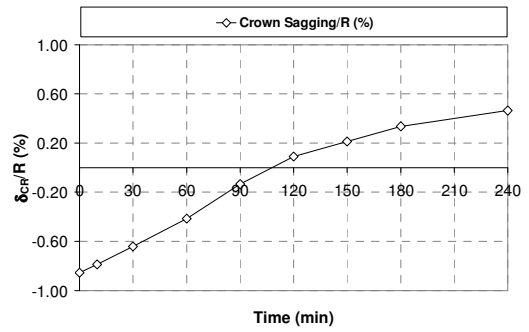
(a)



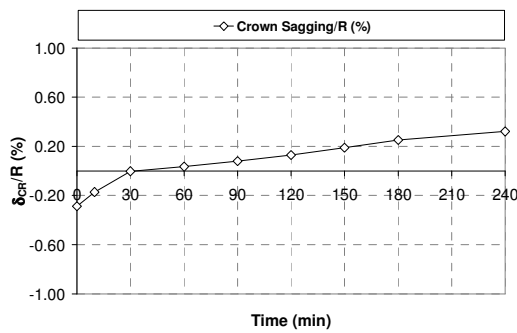
(b)



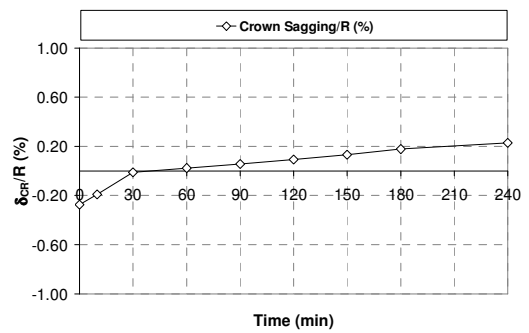
(c)



(d)

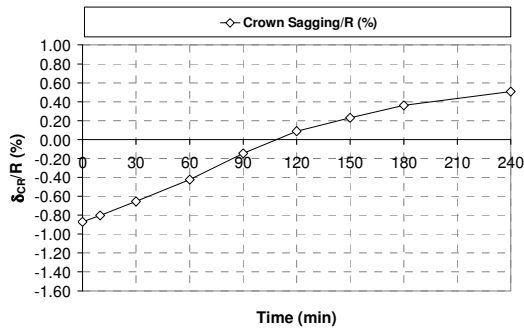


(e)

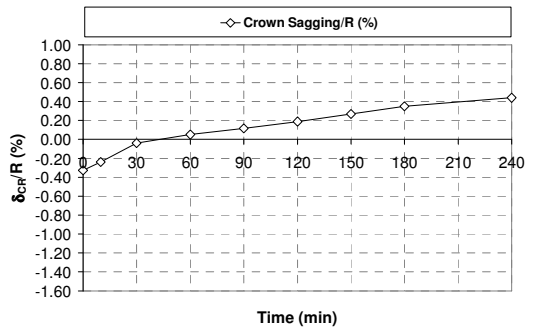


(f)

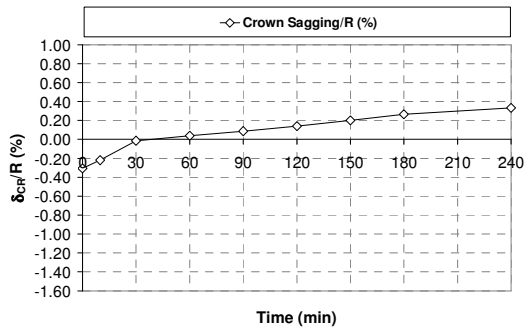
Figure G.4  $\delta_{CR}/R$ -t: (a) M4.30.010, (b) M4.30.125, (c) M4.30.240, (d) M4.36.010, (e) M4.36.125, (f) M4.36.240



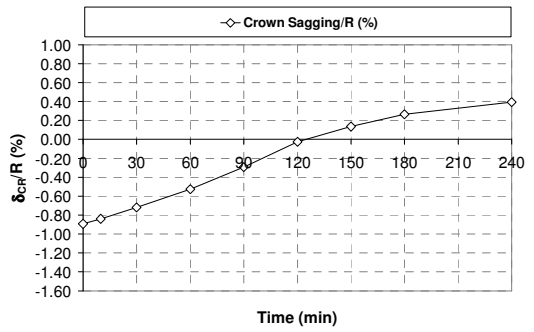
(a)



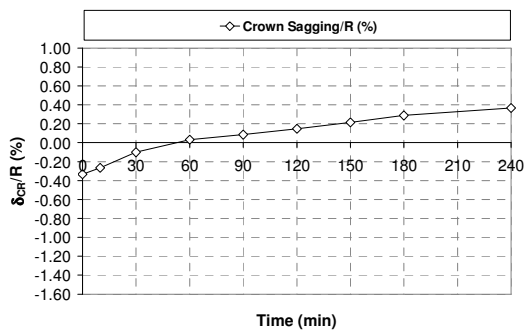
(b)



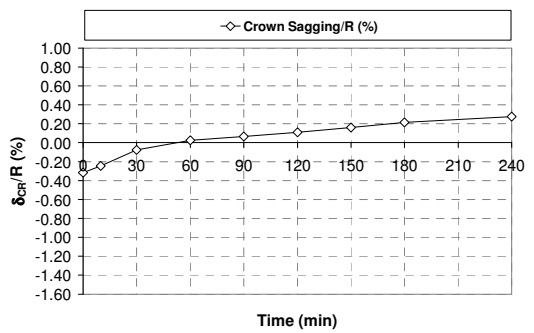
(c)



(d)

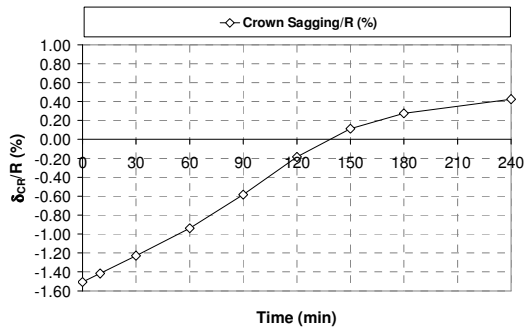


(e)

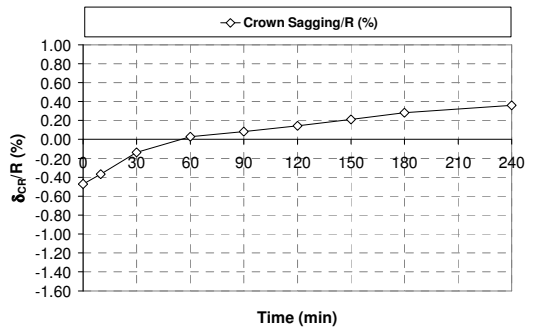


(f)

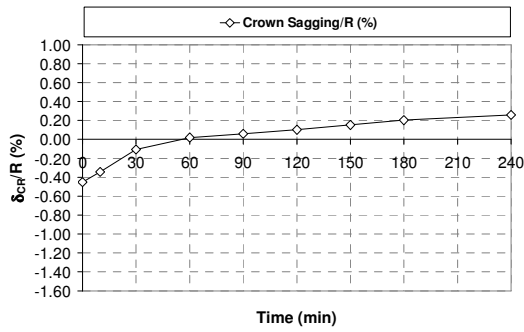
Figure G.5  $\delta_{CR}/R$ -t: (a) D3.30.010, (b) D3.30.125, (c) D3.30.240, (d) D3.36.010, (e) D3.36.125, (f) D3.36.240



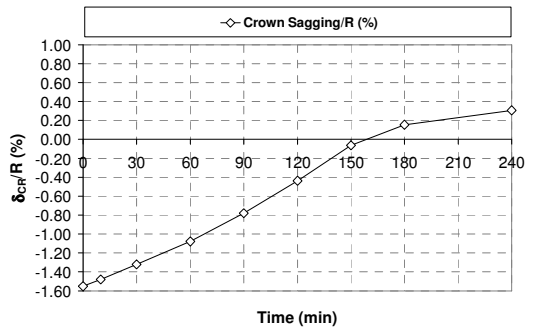
(a)



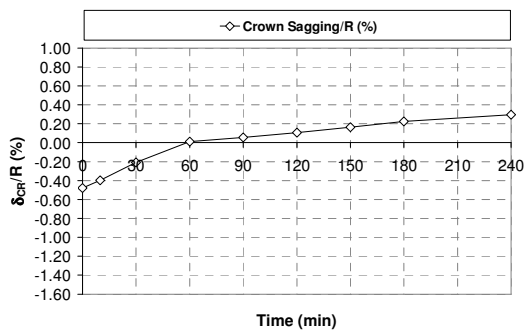
(b)



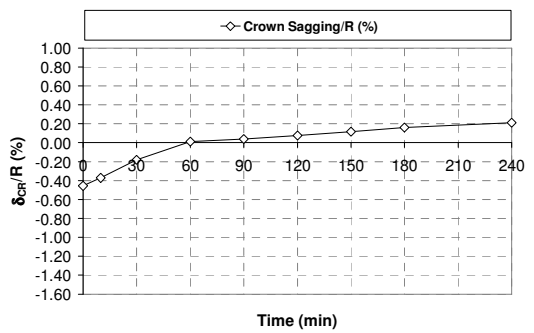
(c)



(d)



(e)

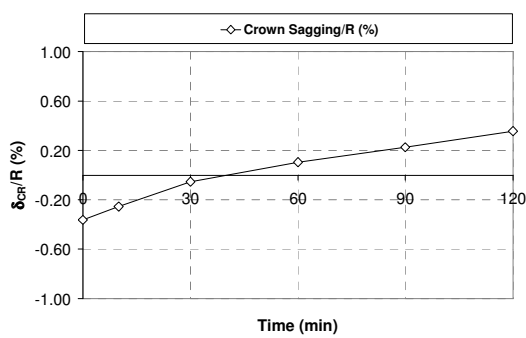


(f)

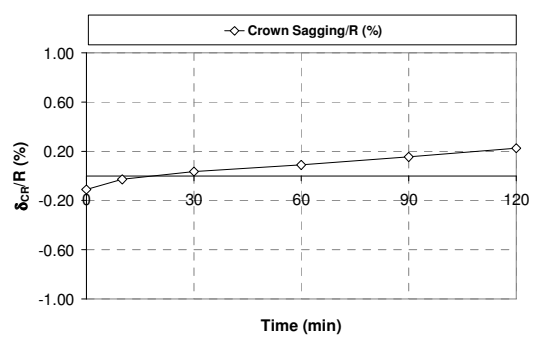
Figure G.6  $\delta_{CR}/R$ -t: (a) D4.30.010, (b) D4.30.125, (c) D4.30.240,  
(d) D4.36.010, (e) D4.36.125, (f) D4.36.240

## APPENDIX H

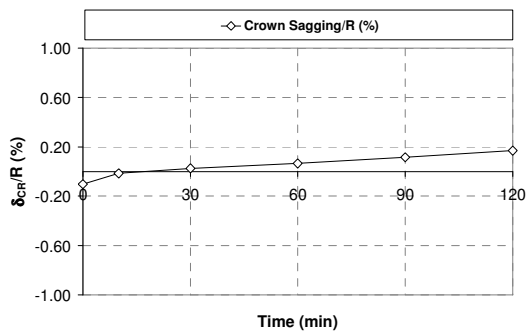
### RATIO OF CROWN DEFLECTION TO TUNNEL RADIUS DURING RWS FIRE



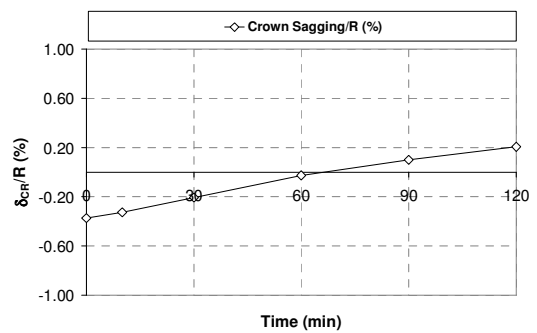
(a)



(b)

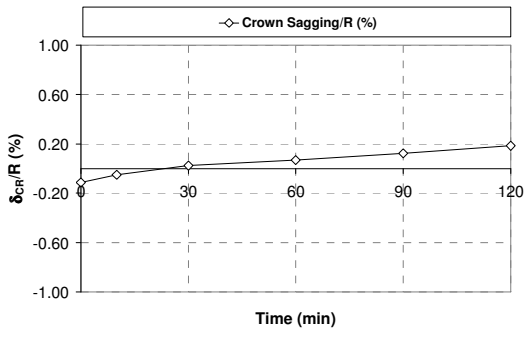


(c)

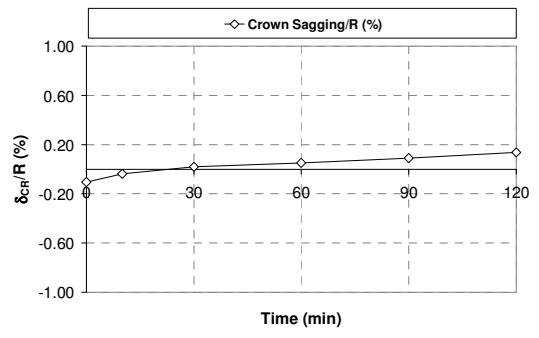


(d)

Figure H.1  $\delta_{CR}/R$ -t: (a) S3.30.010, (b) S3.30.125, (c) S3.30.240,  
(d) S3.36.010

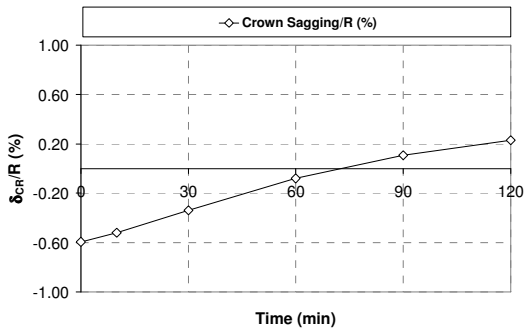


(e)

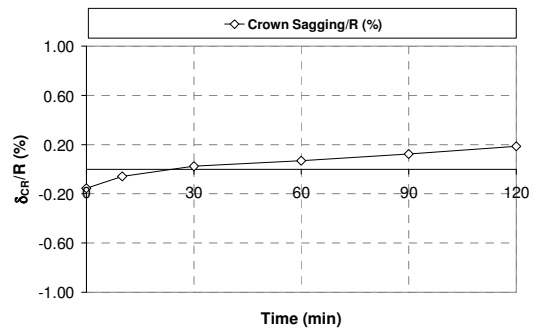


(f)

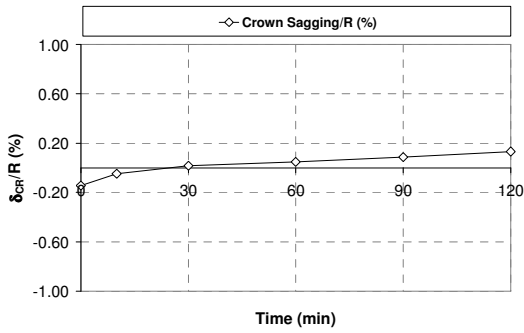
Figure H.1 (Continued)  $\delta_{CR}/R$ -t: (e) S3.36.125, (f) S3.36.240



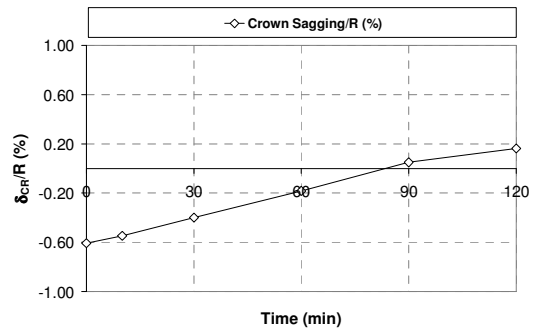
(a)



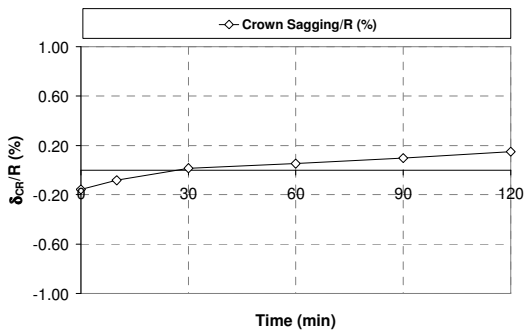
(b)



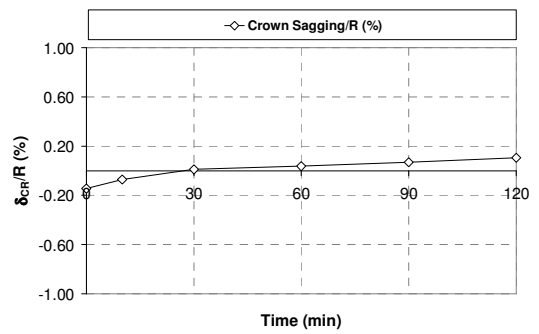
(c)



(d)

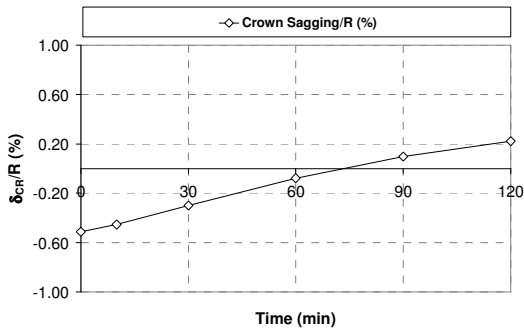


(e)

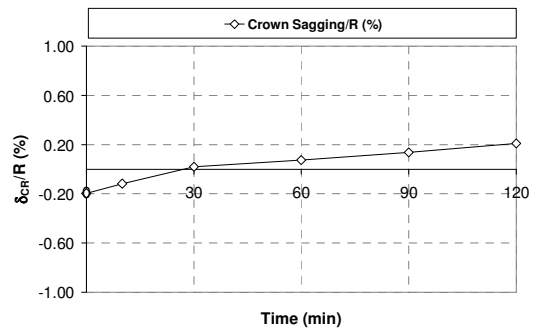


(f)

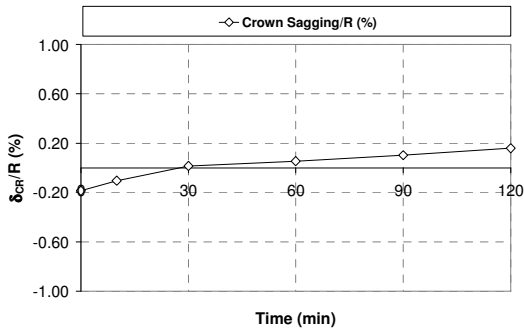
Figure H.2  $\delta_{CR}/R$ -t: (a) S4.30.010, (b) S4.30.125, (c) S4.30.240,  
(d) S4.36.010, (e) S4.36.125, (f) S4.36.240



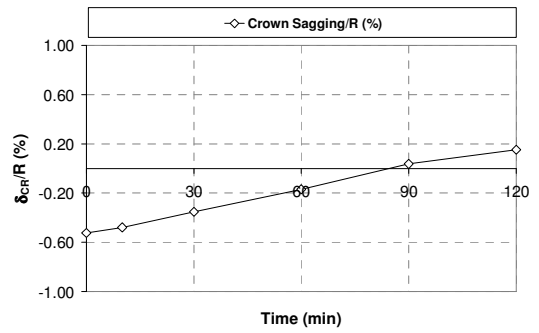
(a)



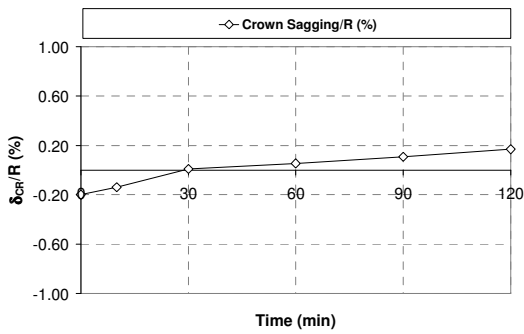
(b)



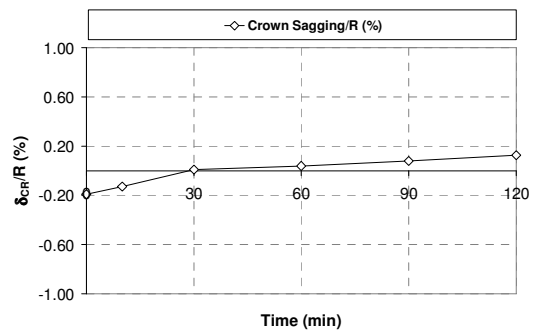
(c)



(d)

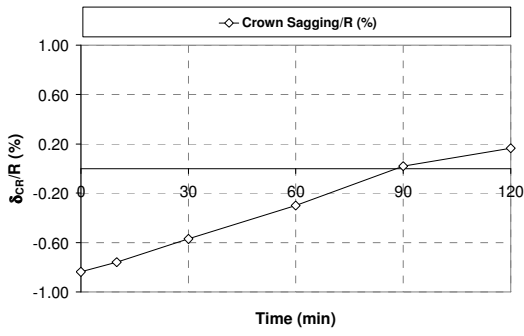


(e)

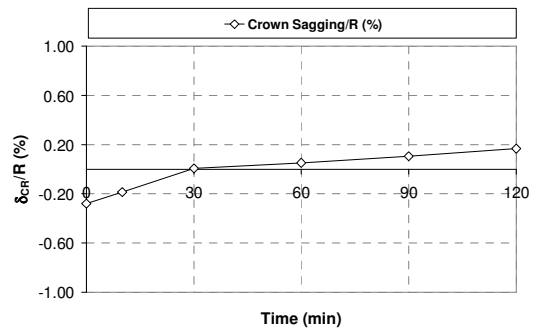


(f)

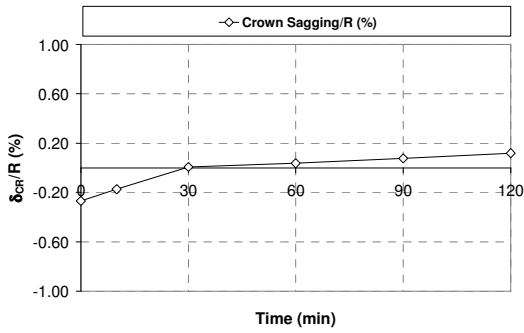
Figure H.3  $\delta_{CR}/R$ -t: (a) M3.30.010, (b) M3.30.125, (c) M3.30.240, (d) M3.36.010, (e) M3.36.125, (f) M3.36.240



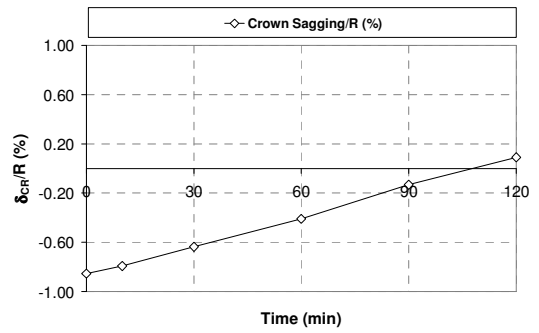
(a)



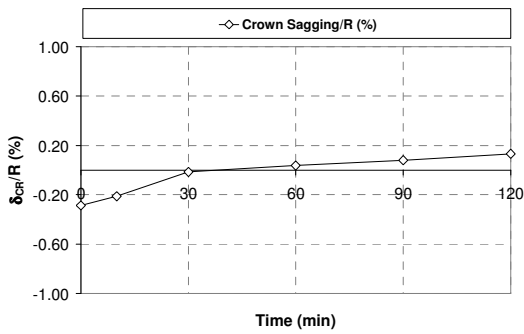
(b)



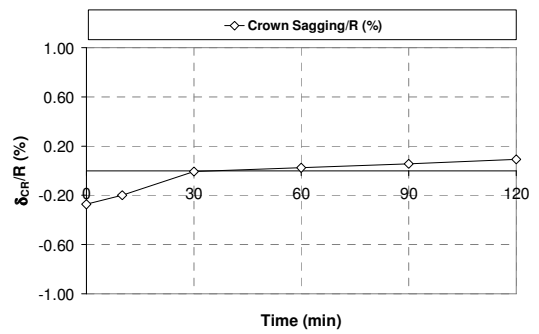
(c)



(d)

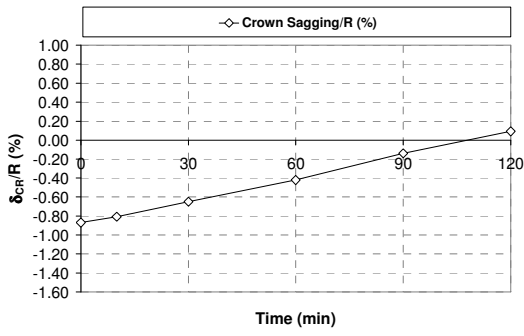


(e)

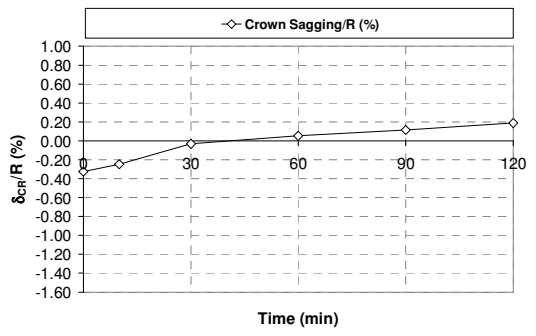


(f)

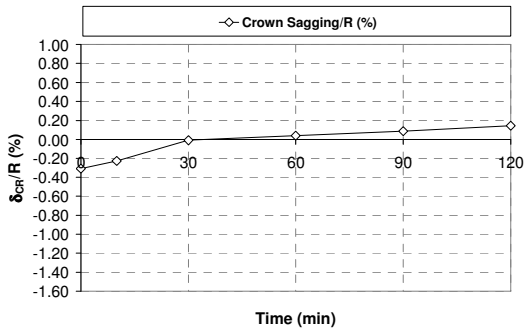
Figure H.4  $\delta_{CR}/R$ -t: (a) M4.30.010, (b) M4.30.125, (c) M4.30.240,  
(d) M4.36.010, (e) M4.36.125, (f) M4.36.240



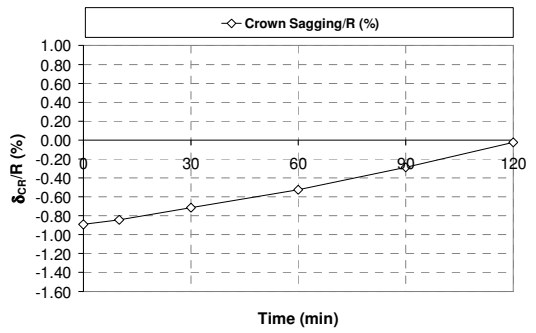
(a)



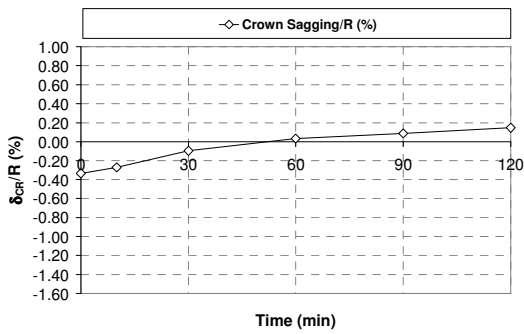
(b)



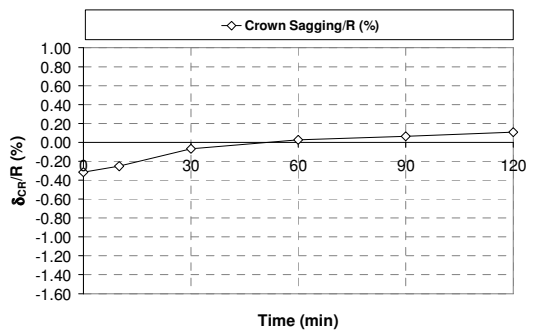
(c)



(d)

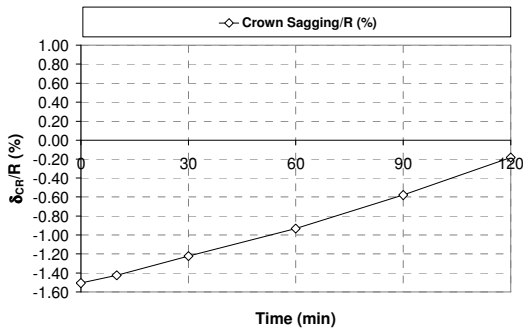


(e)

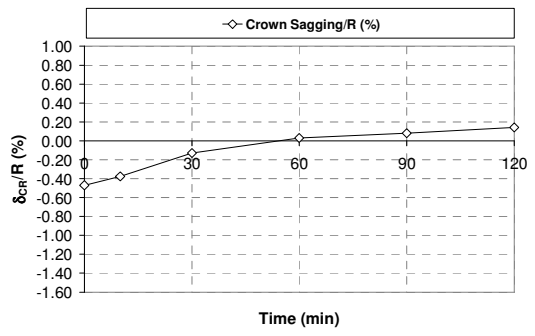


(f)

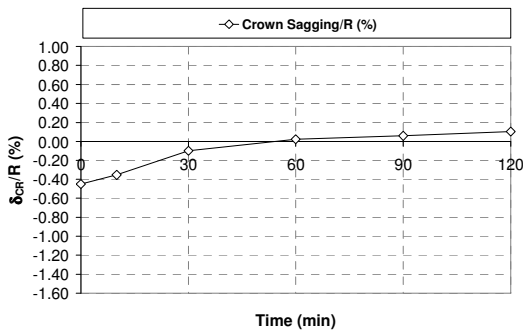
Figure H.5  $\delta_{CR}/R$ -t: (a) D3.30.010, (b) D3.30.125, (c) D3.30.240, (d) D3.36.010, (e) D3.36.125, (f) D3.36.240



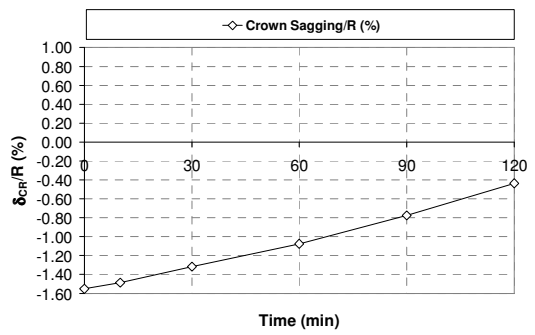
(a)



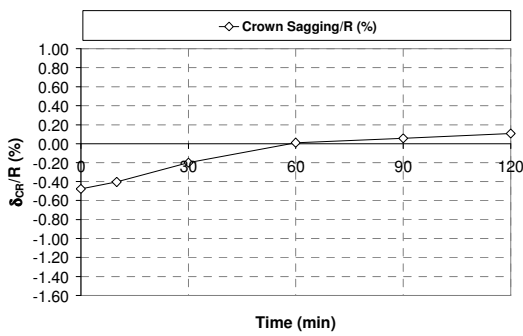
(b)



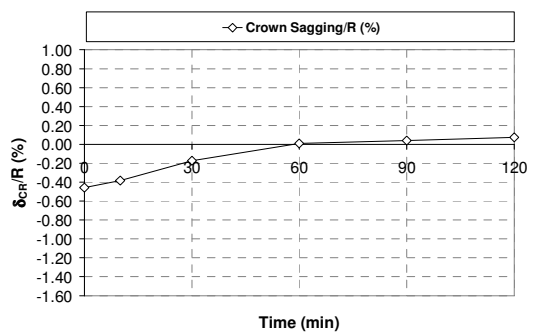
(c)



(d)



(e)



(f)

Figure H.6  $\delta_{CR}/R$ -t: (a) D4.30.010, (b) D4.30.125, (c) D4.30.240,  
 (d) D4.36.010, (e) D4.36.125, (f) D4.36.240

## **APPENDIX I**

### **COMPUTER PROGRAMS USED IN THE ANALYSES**

#### **I.1 Larsa 4D**

LARSA 4D program is typically used in construction stage and dynamic analyses of structures. It is very convenient to utilize the fire time stages with the program since material and geometric properties can be changed based on the degradation computations.

#### **I.2 Radtherm**

RADTHERM is a general heat transfer analysis program used in industry. It is very suitable to assign nonlinear behavior of thermal conductivity and specific heat of concrete using manual iterations.

#### **I.3 Firecap**

FIRECAP is a link program to transfer heat transfer analysis results into structural loads. Also the program defines degradation of concrete in terms of concrete mix design, tunnel fire, and external loads. The program can be used to determine degradation and degraded capacity at different levels of fire. The degraded capacity and increased demand is computed based on the initial strains and secondary strains obtained from structural analysis.